Synthesis, characterization and applications of silica based bio-hybrid materials

By
Archana Mishra
Enroll. No. LIFE0120 1304005

Bhabha Atomic Research Centre, Mumbai

A thesis submitted to the

Board of Studies in Life Sciences

In partial fulfillment of requirements

for the Degree of

DOCTOR OF PHILOSOPHY

of

HOMI BHABHA NATIONAL INSTITUTE

July, 2019

STATEMENT BY AUTHOR

This dissertation has been submitted in partial fulfillment of requirements for an advanced degree at Homi Bhabha National Institute (HBNI) and is deposited in the Library to be made available to borrowers under rules of the HBNI.

Brief quotations from this dissertation are allowable without special permission, provided that accurate acknowledgement of source is made. Requests for permission for extended quotation from or reproduction of this manuscript in whole or in part may be granted by the Competent Authority of HBNI when in his or her judgment the proposed use of the material is in the interests of scholarship. In all other instances, however, permission must be obtained from the author.

Archana Mishra

DECLARATION

I, hereby declare that the investigation presented in the thesis has been carried out by me. The work is original and has not been submitted earlier as a whole or in part for a degree / diploma at this or any other Institution / University.

Archana Mishra

List of Publications arising from the thesis

Publication in refereed journal:

1. Published: "An optical microplate biosensor for the detection of methyl parathion pesticide using a bio-hybrid of *Sphingomonas sp.* cells-silica nanoparticles", A. Mishra, J. Kumar, J. S. Melo, Biosensors and Bioelectronics, 2017, 87, 332–338.

2. Published: "Evaporation induced self assembled microstructures of silica nanoparticles and *Streptococcus lactis* cells as sorbent for uranium (VI)", A. Mishra, J. S. Melo, D. Sen, S. F. D'Souza, Journal of Colloid and Interface Sciences, 2014, 414, 33-40.

3. Under revision: "Preparation and application of silica nanoparticles-*Ocimum basilicum* seeds bio-hybrid for the efficient immobilization of invertase enzyme", A. Mishra, J. S. Melo, A. Agrawal, Y. Kashyap, D. Sen, Colloid and Surface B: Interfaces.

4. Manuscript under preparation: "Spray dried bio-hybrids of silica nanoparticles-sodium alginate as an efficient doxorubicin carrier", A. Mishra and J. S. Melo.

Technology arising from the thesis:

"Microplate based optical biosensor for detection of methyl parathion pesticide", A. Mishra, J. Kumar, J. S. Melo, Technology code: AB35NABTD, available on BARC website. (http://barc.gov.in/technologies/microplate/index.html)

Conferences:

1. A. Mishra and J.S. Melo, "Evaporation Induced Self Assembly Technique as an Effective Route for Synthesis of Nanosilica-Alginate Drug Carriers", presented at Interdisplinary Symposium of Material Chemistry (ISMC-2018), DAE Convention centre, Mumbai, India during 04-08 December 2018. MSD-135, p-197.
2. A. Mishra, J. Kumar and J.S. Melo, "Improved storage stability of organophosohorus hydrolase (OPH) enzyme in *Sphingomonas sp.* cells on integrating with functionalized silica nanoparticles and its application for developing a pesticide biosensor". International Conference on Material Science and Technology (ICMTech-2016), Delhi University, New Delhi, India, 2016. (www.vbripress.com/icmtech, DOI: 10.5185/icmtech.2016). (Oral presentation)
3. A. Mishra and J.S. Melo, "A facile route for synthesis of silica nanoparticles-*Ocimum bacilicum* seed bionanocomposite with improved physico-chemical properties". International Conference on Nanoscinece Nanotechnology and Advanced Materials (NANOS-2015), organized by GITAM University, Visakhapatnam, India during 14^{th}-17^{th} December 2015, OP-(A1-03), p-40. (Oral presentation)
4. A. Mishra and J. S. Melo, "Effective loading of invertase enzyme on silica nanoparticles assembled within pellicular matrix of *Ocimum bacilicum* seeds". International Conference and XI Convention of the Biotech Research Society, India, on Emerging Trends in Biotechnology (ICETB-2014), organized jointly

by the School of Environmental Sciences, Jawaharlal Nehru University, New Delhi and The Biotech Research Society, India (BRSI), JNU, New Delhi, India, November 2014. PP-IBF114, p-136.

Others:

1. "Temperature effect on the physico-chemical properties of silica based bio-hybrid composite for uranium uptake", A. Mishra and J.S. Melo, IAEA-INIS, 2013, 45, 11.
2. “A Tutorial on Biosensors”, Souvenir cum Bulletein of Indian Society for Electroanalytical Chemistry (ISEAC), J. Kumar, A. Mishra and J.S. Melo, 2018, 4(1), 32.
3. “Biodegradation of methyl parathion and its application in biosensors”, J. Kumar, A. Mishra and J.S. Melo, Austin J Environ Toxicol, 2018, 4(1), 1024.

Archana Mishra

Dedicated to my

“Father”

&

“Family”

ACKNOWLEDGEMENTS

The 6 years period of my Ph.D. has been a learning experience for me, both professionally as well as personally.

At this moment of accomplishment, first of all I would like to extend my sincere gratitude to my guide, Dr. J. S. Melo for guiding me through. I take this opportunity to thank him for his invaluable suggestions, intellectual discussions, insightful analysis and honing my scientific writing skills. I am indebted for his constant motivation and encouragement because of which I am able to complete my thesis with ease.

I would like to thank my doctoral committee members, Dr. A. K, Tyagi, Dr. B. N. Pandey and Dr. A. Ballal, for their valuable suggestions, encouragement and time during my annual report and synopsis presentation.

I would like to extend my gratitude to Dr. V. P. Venugopalan (Associate Director, BSG) and Dr. P. Suprasanna (Head, NA&BTD).

In this journey, I was fortunate to have the company of good senior colleagues and lab members: Dr. K.C. Bhainsa, Dr. Jitendra Kumar, Mr. Bhanu Prakash and Dr. A. Tripathi, sincere thanks to you all for your suggestions and discussion. Thanks to Soumya, Vishnu and Surendra for helping me in completing my experiments. Above all, they contributed to create healthy and vibrant working environment.

I would like to thank my FTD senior colleagues, Dr. M. Karani, Dr. S. Kanatt, Dr. Shashidhar, Dr. S. Jamdar, Dr. J. Tripathi and Mrs. Vanshika for their constant help and suggestions.

My sincere regards to all my teachers from my school days to BARC Training School, for their teaching and insightful guidance. I would like to thank Dr. Hema Rajaram, Dean, Life Sciences to whom I went very often for all Ph. D related paperwork and she was always obliging.

I also thank my collaborators, Dr. D. Sen and Dr. Y. Kashyap for sample characterization and insightful discussions.

My earnest thanks to all my friends, Anuradha, Manju, Pragati, Sutanwi, Aparajita, Sujay, Nishad, Saikat and Ravi for their help and support.

I would like to pay my highest regards to my parents, my sisters Vandana, Pragya, and brother Abhishek for their unconditional support and encouragement. I would like to thank my husband Vipul for his constant support and inspiration throughout my Ph. D. work and a very special thanks to my son Advik.

Besides this, many have helped me knowingly and unknowingly in the successful completion of this work. My sincere regards to each of them.

Thanks to the Almighty for giving me an opportunity and good health to peruse my Ph.D. work.

CONTENTS

		Page No.
	SUMMARY	xviii
	LIST OF FIGURES	xxi
	LIST OF TABLES	xxv
	LIST OF ABBREVIATIONS	xxvi
Chapter 1	**Introduction**	1
1.1.	Biotechnology	2
1.2.	Immobilization	2
	1.2.1. History of immobilization	2
	1.2.2. Methods of immobilization	3
	1.2.2.(a) Adsorption	3
	1.2.2.(b) Covalent Binding	3
	1.2.2.(c) Entrapment	4
	1.2.2.(d) Encapsulation	4
	1.2.2.(e) Cross-linking	5
	1.2.3. Immobilizing matrices/supports	7
	1.2.3.1. Organic supports	9
	1.2.3.1.(a) Synthetic polymers	9
	1.2.3.1.(b) Biopolymers	10
	1.2.3.2. Inorganic supports	11
1.3.	Silica based supports	12

1.3.1. Silica 12

1.3.2. Silica chemistry 13

1.3.3. Silica nanoparticles 13

1.3.4. Types of silica nanoparticles 14

1.3.4.(a) Fumed (Pyrogenic) silica 14

1.3.4.(b) Precipitated silica 15

1.3.4.(c) Silica gel 15

1.3.4.(d) Mesoporous silica 15

1.3.4.(e) Biogenic silica 16

1.4. Commercially available colloidal silica nanoparticles 16

1.5. Synthesis of silica nanoparticles 17

1.5.1. Sol-gel method 18

1.5.2. Synthesis routes of different types of silica nanoparticles 21

1.5.2.(a) Fumed (Pyrogenic) silica 21

1.5.2.(b) Precipitated silica 21

1.5.2.(c) Silica gel 22

1.5.2.(d) Mesoporous silica 22

1.5.2.(e) Biogenic silica 22

1.6. Silica based hybrid/bio-hybrid materials 23

1.7. Applications of silica nanoparticles 25

1.7.1. In enzyme immobilization 26

1.7.2. In biosensor 27

1.7.3. In heavy metal removal/remediation 29

1.7.4. In drug delivery 30

1.8. Research hypothesis 31

1.9. Objectives of the study 32

Chapter 2. Synthesis of silica nanoparticles-*Ocimum basilicum* seeds bio-hybrid for immobilization of invertase enzyme 34

2.1. Introduction 35

2.2. Materials and methods 36

2.2.1. Materials 36

2.2.2. Synthesis of seed-nano silica-enzyme bio-hybrid 36

2.2.3. Characterization 38

2.2.4. Physico-chemical studies of the free and immobilized invertase 39

2.2.5. Stability and reusability studies 40

2.2.6. Statistical analysis 40

2.2.7. Reagents 40

2.3. Results and discussion 42

2.3.1. Synthesis of seed-nano silica bio-hybrids 42

2.3.2. Characterization of the bio-hybrid 46

2.3.3. Enzyme immobilization on plain seed and bio-hybrids 57

2.3.4. Study of physico-chemical parameters 60

	2.3.5. Storage stability and reusability study	62
2.4	Conclusion	64
Chapter 3	**Synthesis of silica nanoparticles-*Sphingomonas sp.* cells bio-hybrid to detect methyl parathion pesticide**	66
3.1.	Introduction	67
3.2.	Materials and methods	68
	3.2.1. Materials	68
	3.2.2. Micro-organism, culture medium, harvesting of cells and hydrolytic activity assay	69
	3.2.3. Integration of functionalized silica nanoparticles (^{f}silica NP) with *Sphingomonas sp.*	69
	3.2.4. FTIR study	70
	3.2.5. Immobilization of bio-hybrid (*Sphingomonas sp.*-^{f}silica NP) onto microplate	70
	3.2.6. SEM study of the bio-hybrid immobilized onto microplate	71
	3.2.7. Transducer and operating system for optical detection of MP using immobilized bio-hybrid	72
	3.2.8. Calibration studies using bio-hybrid immobilized microplate	72
	3.2.9. Storage stability and reusability of bio-hybrid	72
	3.2.10. Analysis of spiked sample with developed biosensor	73

3.3.	Results and discussion	73
	3.3.1. Optimization of amount of PEI, *Sphingomonas* cells and ^{f}silica NP for synthesis of bio-hybrid	73
	3.3.2. Characterization of synthesized bio-hybrid	75
	3.3.3. Immobilization of bio-hybrid onto microplate	77
	3.3.4. SEM study of the bio-hybrid immobilized onto microplate	80
	3.3.5. Calibration studies using immobilized bio-hybrid	81
	3.3.6. Storage stability and reusability study of biosensor	82
	3.3.7. Interference study in presence of different compounds	83
	3.3.8. Analysis of spiked sample with developed biosensor	84
3.4.	Conclusion	86
Chapter 4	**Synthesis of silica nanoparticles-*Streptococcus lactis* bio-hybrid for removal of uranium (VI)**	88
4.1.	Introduction	89
4.2.	Materials and methods	90
	4.2.1. Materials	90
	4.2.2. Synthesis of non-incinerated and incinerated materials	91
	4.2.3. Characterization	93
	4.2.4. Batch adsorption experiments	93

	4.2.5. Kinetics, sorption isotherm and thermodynamic studies	94
	4.2.6. Reagents	95
4.3.	Results and discussion	96
	4.3.1. Characterization of the synthesized materials	96
	4.3.2. Removal of U (VI) by synthesized sorbents	98
	4.3.3. Effect of solution pH on U (VI) removal	104
	4.3.4. Adsorption kinetics of uranium (VI)	106
	4.3.5. Effect of initial uranium (VI) concentration on adsorption	109
	4.3.5. Adsorption isotherm study	110
	4.3.6. Thermodynamic study of U (VI) sorption	115
4.4.	Conclusion	118
Chapter 5	**Synthesis and application of silica nanoparticles-sodium alginate bio-hybrid as doxorubicin drug carrier**	119
5.1.	Introduction	120
5.2.	Materials and methods	121
	5.2.1. Materials	121
	5.2.2. Synthesis of the bio-hybrid and other drug carriers	122
	5.2.3. Characterization	122
	5.2.4. In vitro drug release profile	122
	5.2.5. Drug loading efficiency	123
	5.2.6. Cell culture	123

	5.2.7. Intracellular uptake of Dox	123
	5.2.8. Cytotoxicity assay	124
	5.2.9. Statistical analysis	125
5.3.	Results and discussion	125
	5.3.1. Characterization of drug carriers	125
	5.3.2. In-vitro Dox release study	129
	5.3.3. Cellular uptake of free and entrapped Dox	131
	5.3.4. In vitro cytotoxicity of Dox loaded bio-hybrid	133
5.4.	Conclusion	135
Chapter 6	**Future prospective**	136
	References	138

Summary

In this thesis, silica nanoparticles were associated with different bio-components in order to improve the practical applicability of the developed bio-hybrid. For association of silica NP with bio-components, two methods i.e. template assisted assembly and evaporation induced self-assembly through spray drying technique were used. In the first chapter, silica NP was assembled on the fibers of swelled *Ocimum basilicum* seeds wherein seed act as a template. Association of silica NP with seeds led to the synthesis of a fibrillar pellicular bio-hybrid support which was further used for immobilization of invertase enzyme. Enzyme immobilized on bio-hybrid Silica@PEI-seed showed fourfold higher loading of invertase enzyme and improved physico-chemical properties. This proves that using *Ocimum* seeds as template, it is possible to synthesize silica based suitable fibrillar immobilizing support with improved properties, besides the existing conventional chemical route reported earlier. In view of this, another biological component i.e. microbial cells were used as template for assembly of silica NP. Herein, silica NP was integrated with *Sphingomonas sp.* cells in order to synthesize a stable and functional bio-hybrid for its application in biosensors to detect methyl parathion pesticide. Synthesized bio-hybrid was immobilized on the 96 well microplate. Results showed an increase in the sensitivity of the biosensor and tenfold increase in storage stability. This suggests that due to presence of silica NP over the *Sphingomonas sp.* cells the leaching of enzyme which is responsible for hydrolysis of methyl parathion has been reduced. This study confirms that by coating silica NP on microbial cells (template) a stable and functional bio-hybrids can be successfully synthesized. However, for large scale application of bio-hybrid in industrial processing or for commercialization purpose, there is need to develop method/techniques which are useful for mass scale production of bio-hybrids. To achieve this, another mode for preparing bio-hybrids was devised through evaporation induced self-assembly of *Streptococcus lactis* cells and silica NP in order to synthesize a suitable sorbent for uranium (VI). Spray drying leads to the synthesis of bio-hybrids in a higher length scale which makes the separation of bio-hybrids easy once the reaction is over. It was observed that uranium sorption capacity of bio-hybrid was a sum total of uranium removal capacity by silica NP and *S. lactis* cells per se which is unique. Herein, spray drying has emerged as an efficient process for immobilizing microbial cells in silica microstructures. Besides, microbes in bio-

hybrids can also serve as another means for functionalization of silica microstructures unlike the conventional method of chemical modification. Thus, this study corroborates with the earlier template-based association between silica NP and microbial cells for synthesis of a stable and functional bio-hybrid. Spray drying also has other added advantages of being a single step process and can be used for large scale production of bio-hybrid which is required for any process development. In order to design a drug carrier, another bio-hybrid of silica NP and sodium alginate was synthesized using spray drying in the next chapter. Also spray drying can help in large scale production of drug carriers with reproducibility under good manufacturing practices (GMP) and as a dry formulation which becomes pivotal for pharmaceutical industry. It was observed that developed bio-hybrid is able to slow down the release of doxorubicin and improves its bioavailability to cancer cells. Developed bio-hybrid drug carrier has shown more killing of cancer cells than free doxorubicin. Overall, it was observed that association between silica NP and bio-components leads to the synthesis of a stable and functional bio-hybrid which improves the practical applicability of the developed bio-hybrid.

List of figures

S. No.	Title of Figures	Page No.
Chapter 1	**Introduction**	
1.1.	Immobilization of enzymes using different immobilizing techniques	5
1.2.	Main characteristics of support materials used for immobilization	7
1.3.	Chemical classification of immobilizing support	8
1.4.	Different routes for synthesis of silica nanoparticles	17
1.5.	Flow chart of sol-gel process	19
1.6.	Hydrolysis and condensation reaction of of alkoxy precursor during the sol-gel process	19-20
1.7.	Bio-hybrids	24
1.8.	Applications of silica nanoparticles	25
1.9.	Schematic presentation of the objectives of the work	33
Chapter 2	**Synthesis of silica nanoparticles-*Ocimum basilicum* seeds bio-hybrid for immobilization of invertase enzyme**	34
2.1.	Preparation process of bio-hybrids and its application	37
2.2.	Amount of silica NP loaded on plain seeds	43
2.3.	Amount of silica NP loaded on PEI treated seeds	44
2.4.	Picture of *O. basilicum* seeds, seeds soaked in water and Silica@seeds	45
2.5.	Microscopic view of the swelled seed	45
2.6.	% swelling of the seeds with increase in concentration of silica NP	46
2.7.	SAXS data for plain seeds and bio-hybrids	48
2.8.	SEM images of seed and bio-hybrids	50
2.9.	Phase contrast projections and 3D images of seed and bio-hybrids	53

2.10.	Schematic presentation of plain seed and bio-hybrids	54
2.11.	FTIR spectra	57
2.12.	Immobilized invertase enzyme on plain seeds and bio-hybrids	58
2.13.	Sorption isotherm of invertase enzyme onto bio-hybrids	60
2.14.	Effect of pH on free and immobilized invertase	61
2.15.	Temperature profiles of the free and immobilized invertase	62
2.16.	Storage stability of the free and immobilized invertase	63
2.17.	Reusability studies of immobilized invertase	64
Chapter 3	**Synthesis of silica nanoparticles-*Sphingomonas sp.* cells bio-hybrid to detect methyl parathion pesticide**	66
3.1.	Schematic presentation of hydrolysis of methyl parathion (MP) into (PNP)	68
3.2.	Schematic illustration of development of biosensor	71
3.3.	Optimization of concentration of polyethyleneimine (PEI)	74
3.4.	Optimization of ratio of cells:^{f}silica NP	75
3.5.	FTIR study	76
3.6.	Optimization of amount of bio-hybrid for immobilization	78
3.7.	Optimization of glutaraldehyde concentration for immobilization	79
3.8.	SEM micrographs	80
3.9.	Calibration study of the biosensor using MP (0.1-5 ppm)	81
3.10.	Storage stability of the developed biosensor	82
3.11.	Reusability of the developed biosensor	83
3.12.	Correlation between the spiked concentrations of MP in water and corresponding data obtained from developed biosensor	85
Chapter 4	**Synthesis of silica nanoparticles-*Streptococcus lactis* bio-hybrid for removal of uranium (VI)**	
4.1.	Synthesis process of bio-hybrid using spray dryer	92

4.2.	SEM micrographs of microstructures	98
4.3.	Removal of U (VI) by the different microstructures	99
4.4.	TGA profile of SDSM and SSSM	101
4.5.	FTIR spectra	103
4.6.	Schematic illustration of spray drying process and U (VI) sorption	104
4.7.	Effect of solution initial pH on U (VI) sorption	105
4.8.	Effect of contact time on U (VI) sorption	106
4.9.	(a) Pseudo first order kinetics and (b) Pseudo second order kinetics	108
4.10.	Adsorption effect of varying initial U (VI) concentration	110
4.11.	Adsorption isotherm of U (VI) onto SDSM by Langmuir isotherm	111
4.12.	Separation factor for adsorption of U (VI) onto SDSM	112
4.13.	Adsorption isotherm of U (VI) onto SDSM by Freundlisch isotherm	114
4.14.	Effect of temperature on U (VI) adsorption capacity of the SDSM	116
4.15.	Plot of ln K versus 1/T for the adsorption of U (VI) onto SDSM	117
Chapter 5	**Synthesis and application of silica nanoparticles-sodium alginate bio-hybrid as doxorubicin drug carrier**	
5.1.	SEM micrographs of bio-hybrid and other drug carriers	126
5.2.	Schematic presentation of interaction between silica NP and sodium alginate	127
5.3.	FTIR spectra	128
5.4.	Release profile of entrapped Dox	130
5.5.	pH dependent release profile of Dox entrapped in bio-hybrid	131
5.6.	Flow cytometry analysis of A549 cells incubated with Dox	132
5.7.	Percent positive cells with Dox expression	132
5.8.	Cell cytotoxicity study of plain bio-hybrid without Dox in	

mouse lymphocyte cells 134
5.9. In vitro cell cytotoxicity study of free and entrapped Dox 134

List of tables

S. No.	Title of tables	Page No.
Chapter 1		
1.1.	Advantages and disadvantages of different methods of immobilization	6
Chapter 2		
2.1.	SAXS analysis of plain seeds and bio-hybrids	49
2.2.	BET results of plain seed and bio-hybrids	55
Chapter 3		
3.1.	Interference study in presence of different organic compounds	84
3.2.	Biosensor measurement of MP in grape samples	86
Chapter 4		
4.1.	Pseudo-first-order and pseudo-second-order values for U(VI) sorption	109
4.2.	Isotherm constants and correlation coefficients for U(VI) sorption	114
4.3.	Comparison of uranium binding capacities of various sorbents	115
4.4.	Thermodynamic parameters of uranium (VI) sorption	117

List of abbreviations

1.	AChE	Acetylcholinesterase
2.	APTES	3-aminopropyltriethoxysilane
3.	BET	Brunauer–Emmett–Teller
4.	CFU	Colony forming unit
5.	cm^{-1}	$Centimeter^{-1}$
6.	^0C	Degree Centigrade
7.	Dox	Doxorubicin
8.	FTIR	Fourier Transform Infrared
9.	FSSAI	Food Safety and Standards Authority of India
10.	^{f}silica NP	Functionalized silica nanoparticles
11.	ΔG^0	Free energy change
12.	g/L	Gram/Liter
13.	ΔH^0	Enthalpy change
14.	KBr	Potassium bromide
15.	K	Kelvin
16.	kJ/mol	KiloJoule/mole
17.	LE	Loading efficiency
18.	mg	Milligram
19.	mg/L	Milligram/Liter
20.	µm	Micrometer
21.	µL	Microliter
22.	mm	Milimeter
23.	µg/mL	Microgram/mililitre
24.	m^2/g	$Meter^2$/gram
25.	MP	Methyl parathion
26.	µM	Micromolar
27.	MRL	Maximum residual limit
28.	MCM-41	Mobil Composition of Matter No. 41

29.	mM	Milimolar
30.	MTT	(3-(4, 5-dimethylthiazolyl-2)-2, 5-diphenyltetrazolium bromide
31.	nm	Nanometer
32.	nM	Nanomolar
33.	NP	Nanoparticles
34.	*O. basilicum*	*Ocimum basilicum*
35.	OPH	Organophosphrous hydrolase
36.	OP	Organophosphate
37.	PNP	p-nitrophenol
38.	PEI	Polyethyleneimine
39.	ppm	Parts per million
40.	q_{max}	Maximum sorption capacity
41.	Silica@seed	Silica nanoparticles loaded seed
42.	Silica@PEI-seed	Polyethyleimine treated silica nanoparticles loaded seed
43.	SBA-15	Santa Barbara Amorphous-15
44.	SAXS	Small Angle X-ray Scattering
45.	SDS	Sodium dodecyl sulfate
46.	SDSM	Spray dried doughnut shaped microstructures
47.	SEM	Scanning electron microscope
48.	*S. lactis*	*Streptococcus lactis*
49.	SSSM	Spray dried spherical shaped microstructures
50.	SRμCT	Synchrotron radiation based X-ray micro-computed tomography
51.	ΔS^0	Entropy change
52.	TEOS	Tetraethylorthosilicate
53.	TGA	Thermogravimetric analysis
54.	U(VI)	Uranium (VI)

Chapter-1

Introduction

1.1. Biotechnology

Biotechnology is defined as “the integration of natural sciences and engineering in order to achieve the application of organisms, cells, parts thereof and molecular analogues for products and services" by the European Federation of Biotechnology [1]. For the efficient utilization of biological molecules, immobilization is one of the best routes.

1.2.Immobilization

Immobilization is attachment of biomolecule with suitable support. An immobilized molecule is one whose movement in space has been restricted either completely or to a small limited region by attachment to a solid structure (suitable support) [2].

1.2.1. History of immobilization

The first scientific observation that led to the discovery of immobilized enzymes was made in 1916 wherein invertase exhibited the same activity when immobilized on charcoal [3]. This discovery led the foundation to the currently available enzyme immobilization techniques. In earlier days, it was observed that immobilization techniques had certain limitations like very low enzyme loadings in comparison to available surface area. To overcome this, extensive work was carried out during 1950-1960 to develop different methods for enzyme immobilization [4]. From 1960s, till today more than thousands of publications and patents have been published on enzyme immobilization techniques. Several industrially important enzymes like penicillin G acylase, invertase, lipases, proteases, etc. have been immobilized and applied in different large-scale bio-processes [4]. While immobilization has been studied for a number of years yet the increasing number of recent publications on immobilization shows that there is still a lot to explore in this area [5-7].

Along with enzymes many other biomolecule have also been immobilized due to their biological and biomedical applications [8]. The following are examples of some of these molecules: proteins (antibodies, antigens, cell adhesion molecules), peptides, drugs (anticancer agents, anti-thrombogenic agents, antibiotics and peptide/protein drugs), saccharides (sugars, oligosaccharides and polysaccharides), lipids (fatty acids, phospholipids, glycolipids), ligands (hormone receptors, cell surface receptors, avidin and biotin), nucleic acids (nucleotides) and micro-organism.

1.2.2. Methods of immobilization

The methods of immobilization and support material play very important role in immobilization. The methods of immobilization can be broadly divided into five types i.e. adsorption, covalent binding, entrapment, encapsulation and cross-linking [8].

1.2.2(a). Adsorption

Adsorption is the simplest method of immobilization. It involves reversible surface interactions between bio-component and support material (Fig. 1.1). The process of adsorption consists of mixing together the bio-component and support, under suitable conditions followed by incubation for a certain time period. After this, the immobilized material is recovered and washed. The first industrially used immobilized enzyme was prepared by adsorption of amino acid acylase on DEAE-cellulose [9].

1.2.2(b). Covalent binding

In case of covalent binding, formation of a covalent bond between the bio-component and support material is formed (Fig. 1.1). Covalent bonds provide the strongest linkages between bio-

component and support in comparison to other immobilization methods and minimize the leakage of bio-component from the support [10]. The bond is formed between functional groups of the support and functional groups on the surface of the bio-component. The reaction processes involve in linking a bio-component to a support are of different types like formation of a diazo linkage, formation of a peptide bond or an alkylation reaction and formation of an isourea linkage.

1.2.2(c). Entrapment

In the method of immobilization by entrapment (Fig. 1.1), the bio-components are restricted in movement by the lattice structure of a gel [11]. The porosity of the gel lattice is controlled to ensure that the structure is tight enough to prevent leakage of enzyme or cells, yet at the same time allow free movement of substrate and product. The support also acts as a barrier and protects the immobilized bio-components from microbial contamination [12] In entrapment method during ionotropic gelation, bio-component is mixed with a polyionic polymer material like carrageenan and cross-linked with the polymer using multivalent cations.

1.2.2(d). Encapsulation

Encapsulation of bio-components (Fig. 1.1) can be achieved by enveloping the biological components within various forms of semipermeable membranes [13]. It is similar to entrapment. Large biomolecule (proteins/enzymes) could not pass through the capsule, but small substrates and products can easily pass across the membrane. Ionotropic gelation of alginates has been widely used for encapsulation of enzymes and cells [14]. Menaa *et al.* have used silica-based nanoporous glasses for the encapsulation and stabilization of proteins [15-17].

1.2.2(e). Cross-linking

The cross-linking method of immobilization is support-free (Fig. 1.1) and involves joining enzyme molecules to each other to form a three-dimensional complex structure and can be achieved by chemical or physical methods [18]. Cross-linking usually involves covalent bond formation between the bio-components through a bi- or multifunctional reagent like dicarboxylic acid and glutaraldehyde. Other agents like polyethyleneimine, polystyrene sulfonates and polyamines have been also used for cross-linking the cells. Cross-linking is mostly used along with other immobilizing methods. Thus, it is rarely used as only means of immobilization because poor mechanical properties of the aggregates are its limitation.

Disadvantages and advantages of each of the immobilization methods are summarized in table 1.1.

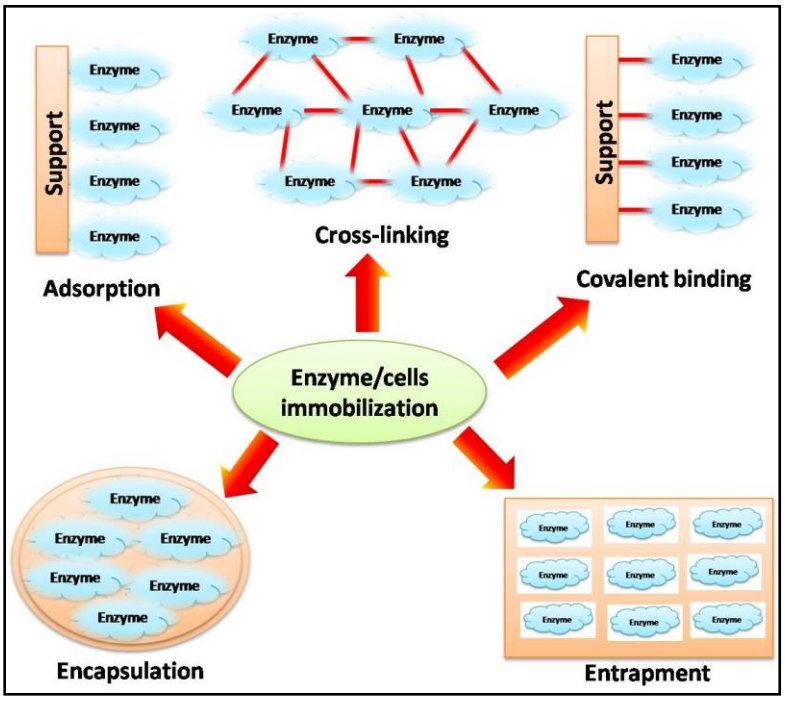

Fig. 1.1. Immobilization of enzyme using different immobilizing techniques

Table 1.1. Advantages and disadvantages of different methods of immobilization

Immobilization methods	Advantages	Disadvantages
Adsorption	• Simple and low cost • High retention of activity • No chemical changes to bio-components and support	• Leakage of immobilized bio-component • Non-specific binding
Covalent binding	• No leakage of immobilized bio-component • Increase in the stability of bio-component	• Loss in activity of bio-components • High cost
Entrapment	• Loading is very high	• Leakage of immobilized bio-component • Diffusion limitation
Encapsulation	• Possibility of co-immobilization	
Cross linking	• Immobilization is support free • Cross-linking between the same bio-components stabilizes the bio-components	• Harshness of reagents towards bio-components • Bio-components may become partially/fully inactive if cross-linking reagent reacts with active site

1.2.3. Immobilizing matrices/supports

The term support is usually referred to a solid insoluble matrix. A variety of matrices have been used as support materials for immobilization [19]. To use a support for immobilization, a range of fundamental properties are required, which are listed (Fig. 1.2) as follows [20]:

a. Support should be widely available and can be obtained from a reliable commercial source

b. Support should have abundance of functional groups which can be easily functionalized

c. Support should have high surface area

d. Support should have high affinity for target molecule

c. Support should offer high mechanical and chemical stability

d. Support material should be biocompatible and user friendly

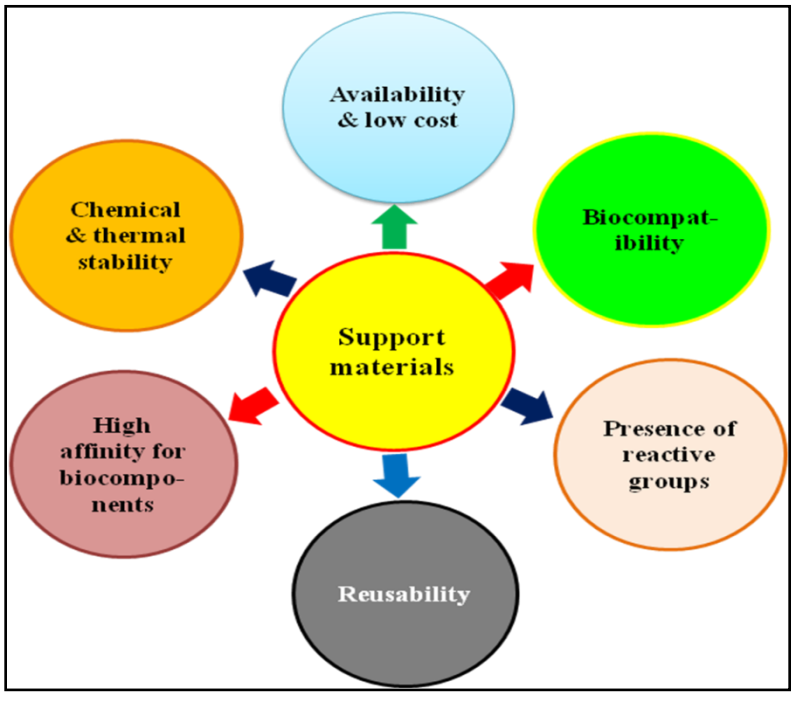

Fig.1.2. Main characteristics of support materials used for immobilization

The properties of immobilized bio-components are governed by the properties of both the bio-component and the support material. The interaction between these two decides specific chemical, biochemical and kinetic properties of an immobilized bio-component. The supports on which bio-components such as enzymes, microbes, antibodies, antigens, etc will be immobilized are of great interest. Supports for immobilization can be classified according to their chemical composition as organic and inorganic supports (Fig. 1.3). The former can be further classified into natural and synthetic matrices. In inorganic supports, the focus is more on silica based materials among silica based materials silica nanoparticles have gained a lot of popularity.

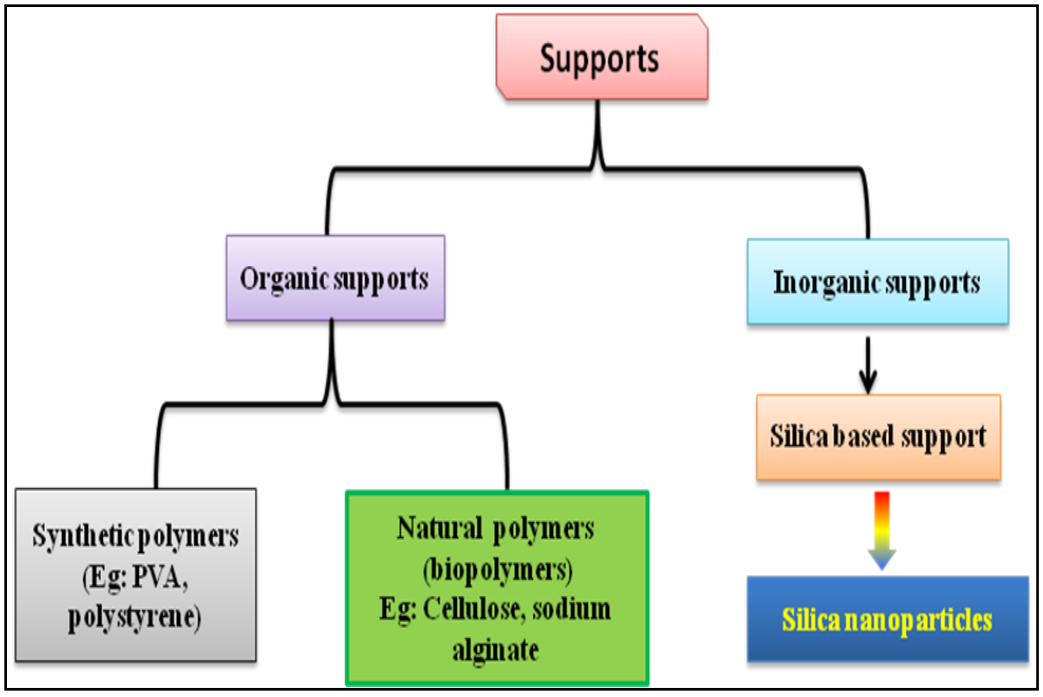

Fig. 1.3. Chemical classification of immobilizing supports

1.2.3.1. Organic supports

Organic support materials can be divided into two main groups: synthetic polymers and biopolymers.

1.2.3.1(a). Synthetic polymers

The greatest advantage of synthetic polymers as support materials is that the monomers that build the polymeric chain can be selected according to the requirement and process in which the immobilized matrix will be used [21]. The chemical structure and properties of the synthetic polymer is determined by the type and quantity of the monomers. A very wide range of functional groups (for example, amine, carbonyl, carboxyl, hydroxyl, epoxy and diol groups, as well as strongly hydrophobic alkyl groups) may be observed in the structure of polymers [22]. These groups facilitate effective enzyme binding and also functionalization of the polymer surface. The type and quantity of functional groups determine the hydrophobic/hydrophilic character of the matrix and therefore its ability to form polar or hydrophobic interactions with the bio-component [23].

Various synthetic polymers have been used for enzyme immobilization. For example, *a*-amylase was immobilized on polyaniline while tyrosinase was immobilized on polyamide 66 (Nylon 66) [24-25]. In another study, lipase was immobilized by covalent binding on polystyrene microspheres [26]. Glucose oxidase was immobilized on amino- and carboxyl-plasma-activated polypropylene film [27]. Commercially available ion exchange resins have also been used for the immobilization of enzyme [28]. However, the limitation of synthetic polymer is that the synthesis of a synthetic polymer with the desired properties and functional groups is usually a

costly, time-consuming process and generates chemical wastes which cause environmental pollution.

1.2.3.1(b). Biopolymers

Biopolymers are an alternative to the synthetic polymers as support for immobilization of bio-component. Biopolymers are polymers of natural origin. Examples of biopolymers are cellulose, chitosan, alginate, pectin etc., which are used for immobilization [29-33]. Properties like biocompatibility, non-toxicity, biodegradability to harmless products and affinity towards proteins make them suitable support for bio-components. The biocompatibility and natural origin aspect of biopolymers minimizes their negative impact on the structure and properties of bio-components which further helps to maintain the catalytic activities of the immobilized bio-components. Along with this, the availability of functional groups in bio-polymers (mainly hydroxyl but also amine and carbonyl moieties) enables direct reaction between the bio-component and biopolymer [34]. Another important aspect is biopolymers are easy to obtain which makes them inexpensive and reduces the costs associated with the immobilization process [35].

Examples of biopolymer used as immobilizing support

(i) Cellulose: Cellulose is the most abundant natural polymer which has been widely used to immobilize various enzymes like penicillin G acylase, α-amylase, tyrosinase, lipase and β-galactosidase [29, 36-39].

(ii) Chitosan: is one of the most frequently used biopolymer for enzyme immobilization. Shi *et al*. used chitosan microspheres for the immobilization of nuclease [30]. In another study, glucose isomerase was adsorbed in macroporous chitosan beads [40]. Chitosan has been used in

combination with alginate where chitosan-coated enzymes had less leaching effect compared to alginate owing to the physical and ionic interactions between the enzyme and support [32].

(iii) Alginate: The remarkable ability of gelation of alginate which is responsible for the creation of capsules makes it a suitable immobilizing support [41]. However, their utilization in immobilization is restricted due to the relatively low mechanical stability of alginate gels and diffusional limitations in the transport of the substrates and products. [31]. Betigeri and Neau immobilized lipase in calcium alginate beads and showed high immobilization yields [32]. The products showed good catalytic activity retention however, their reusability was poor because of leaching of the enzyme from the support.

(iv) Pectin: Pectin along with 0.2–0.7 % glycerol acts as plasticizer to reduce brittleness of support and was used for immobilization of papain [33]. Pectin–chitin and pectin–calcium alginate supports have enhanced thermal and denaturant resistance and catalytic properties of entrapped enzymes due to the formation of high stable polyelectrolyte complexes between the enzyme and the pectin-coated support [42-43].

1.2.3.2. Inorganic supports

Inorganic supports are widely considered the material of choice for immobilization since the thermal and mechanical stability of inorganic supports are generally higher. These are resistant to microbial attack because inorganic materials are not substrates for bacterial/fungal growth. Two main characteristics which distinguish inorganic supports from organic are rigidity and porosity. Organic materials can also be obtained with strictly controlled porosity but they are usually very sensitive to pressure or pH or in many cases to both. On the other hand, the typical stiffness of the inorganic supports ensures the invariance of pore diameter/pore volume, which guarantees

constant volume and shape to the support itself. Among inorganic supports, inorganic oxides are of more importance.

Inorganic Oxides

In previous studies, titanium, aluminium and zirconium oxides have been used for the immobilization of many enzymes, for example lipase, urease and α-amylase [44-46]. These supports are known for their high stability, mechanical resistance and good sorption capacity. Moreover, these materials are inert under various reaction conditions, which facilitate their application as supports for various classes of enzymes. However, the biocompatibility, availability and ease to functionalization makes silica one of the most frequently used inorganic support materials for immobilization. Its high thermal, chemical resistance and good mechanical properties make it a suitable material for many practical applications. Silica offers good sorption properties due to its high surface area and porous structure. These properties allow effective bio-component attachment and reduces diffusional limitations. The presence of many silanol groups on the surface of silica facilitates bio-component attachment and favors its functionalization with surface modifying agents like 3-aminopropyltriethoxysilane (APTES) [47].

1.3.Silica based supports

1.3.1. Silica

Silicates are the most common component of the Earth's surface. One form of silicate is known as silica (general chemical formula SiO_2 or $SiO_2.xH_2O$) which is most commonly found in nature and also in various living organisms. SiO_2 exists in two main forms crystalline and amorphous [48]. Quartz and cristobalite are two mains crystalline forms of silica.

1.3.2. Silica chemistry

Silica surfaces arise from dehydration of hydrated silica preparations ("silicic acids") or from grinding bulky silica [48]. As the temperature rises, water elimination takes place followed by condensation of silanol (Si–OH) which produces siloxane bridges Si–O–Si and at ~ 1300 ^{0}C, usually all silanol groups are eliminated [49]. Generally, two main groups i.e. silanols (Si–OH) and siloxanes (Si–O–Si) are present on the surface of silica. Silanols are acidic and makes silica surfaces negatively charged in a wide range of pH, and act as hydrogen donors in hydrogen bonding [50]. Hydrated silica act as an acidic oxide when it is exposed to basic solutions and therefore it shows a tendency to go into solution: OH^- ions gradually break siloxane bridges and a solution containing alkaline silicates is obtained [51]. The reaction is slow for quartz however it is fast for amorphous silica. A layer of silanol groups is present on the surface of silica along with siloxane. Due to presence of high number of siloxane motifs, some silica shows hydrophobic property [52]. Because of presence of both hydrophobic and hydrophilic sites on silica surface and the properties like weakly acidic and high tendency to take part in hydrogen bonding, silica shows higher adsorption properties. This adsorption property of silica plays very important role in the immobilization of bio-components.

1.3.3. Silica nanoparticles

Silica has been extensively used throughout history due to its accessibility and ease of recovery to manufacture glass, ceramics and silicones. Recently, colloidal silica has gained popularity in materials science as nano- and microparticle [53]. The reason behind wide applicability of colloidal silica in research is due to the unique properties which they possess like high surface

area, high colloidal stability, low toxicity, biocompatibility, well known surface chemistry, optical transparency and chemical and thermal stability [54**].**

Colloidal silica has a wide range of applications like catalytic supports [55-57], biosensor supports [58-61], drug carriers [62-66], antifouling coatings [67-68] and additives to paints/lacquers/coatings [69-70]. Because of large number of applications, colloidal silica production has become a significant industry. For a wide range of applications, commercially available colloidal silica is used because naturally available mineral silica is contaminated with various metal ions and not suitable for use in the scientific research and industrial applications [71]. Also, mineral silica offers less surface area (with a few exceptions) and exists in crystalline form which is damaging to health. Thus, for most of the applications chemically synthesized colloidal silica is preferred.

1.3.4. Types of silica nanoparticles

1.3.4 (a). Fumed (Pyrogenic) silica

Fumed silica has commercial uses as additive to modulate rheological properties, polisher, flowing aid and even as dental filler [72]. Fumed silica is also used for the production of silicone rubber for medical applications because of the high purity (>99.8 wt % SiO_2), low moisture content and transparency [73]. Fumed silica is used as a reinforcing agent, particularly in concrete because of its fine particle size (7−40 nm after milling of the aggregates) offering a high degree of reinforcement and the ability to accelerate hydration for ultrahigh performance concrete [74]. However, because of its high cost and less number of surface silanol groups in comparison to precipitated silica (synthesized via liquid methods), fumed silica has limited application [74-75].

1.3.4 (b). Precipitated silica

The precipitated silica are currently used in a wide variety of applications which include acting as reinforcing agents for rubber manufacture, catalytic supports and flow regulators [76-80].

1.3.4 (c). Silica gel

Silica gel is an amorphous and porous form of silicon dioxide (silica), consisting of an irregular tridimensional framework of alternating silicon and oxygen atoms with nanometer-scale pores. The pores may contain water or some other liquids or may be filled by gas or vacuum. In the latter case, the material is properly called silica xerogel. Silica gel have high specific surface area and adsorbs water readily thus it is useful as desiccant (drying agent). Silica gel is used as food additive (approved by the FDA as generally recognized as safe (GRAS)), as humidity indicator (blue/orange silica gel) and in domestic water filters.

1.3.4 (d). Mesoporous silica

Mesoporous silica is a mesoporous form of silica and has gained a lot of popularity in nanotechnology. The most common types of mesoporous nanoparticles are MCM-41 and SBA-15 [81]. Mesoporous silica nanoparticles (MSNs) were independently synthesized in 1990 by researchers in Japan and later on produced at Mobil Corporation laboratories and named Mobil Composition of Matter (or Mobil Crystalline Materials, MCM) [82-84].

Later on, silica nanoparticles with much larger (4.6 to 30 nanometer) pores were produced at the University of California, Santa Barbara (12) and named Santa Barbara Amorphous type material (SBA-15). [85] Mesoporous silica nanoparticles have many applications in medicine, biosensors, imaging and thermal energy storage [86-87].

1.3.4 (e). Biogenic silica

Biogenic silica is formed through the process of biosilication. Biosilication is the formation of silica using biological components. This process has received significant attention wherein diatoms and siliceous marine sponges have been used for synthesis of silica [88-92]. Diatoms (unicellular organisms) cell wall contains biosilica. A number of specialized proteins (silaffins, silacidins and cinguliums) are also known to be responsible for synthesis of biogenic silica. Silaffins are polypeptides rich in lysine and serine residues with a high degree of post-translation modification [91]. Sponges are the other major biosilica producing organism and silicatein isoforms have been identified in siliceous sponge species which play role in synthesis of biosilica [93].

1.4.Commercially available colloidal silica nanoparticles

One of the well known and widely used commercially available colloidal silica is supplied by brand name LUDOX® colloidal silica. LUDOX® colloidal silica is aqueous dispersions of silica nanoparticles in the low nanometer size range with narrow particle size distribution. LUDOX supplies different variants of colloidal silica which makes LUDOX® colloidal silica an excellent choice for applications in the field of food, catalysis, pharmaceutical, paint industry and material science.

In India, commercially available colloidal silica nanoparticle is supplied by Visa chemical industries. They supply various grades of colloidal silica in the nm size range. They also supply a number of nano-sols containing modified silica and blended with other metals (lithium/aluminum) in different pH range which finds application in paint, lacquer and textile industry.

1.5.Synthesis of silica nanoparticles

For the synthesis of silica nanoparticles, different methods have been developed. The main synthesis processes are presented in Fig. 1.4.

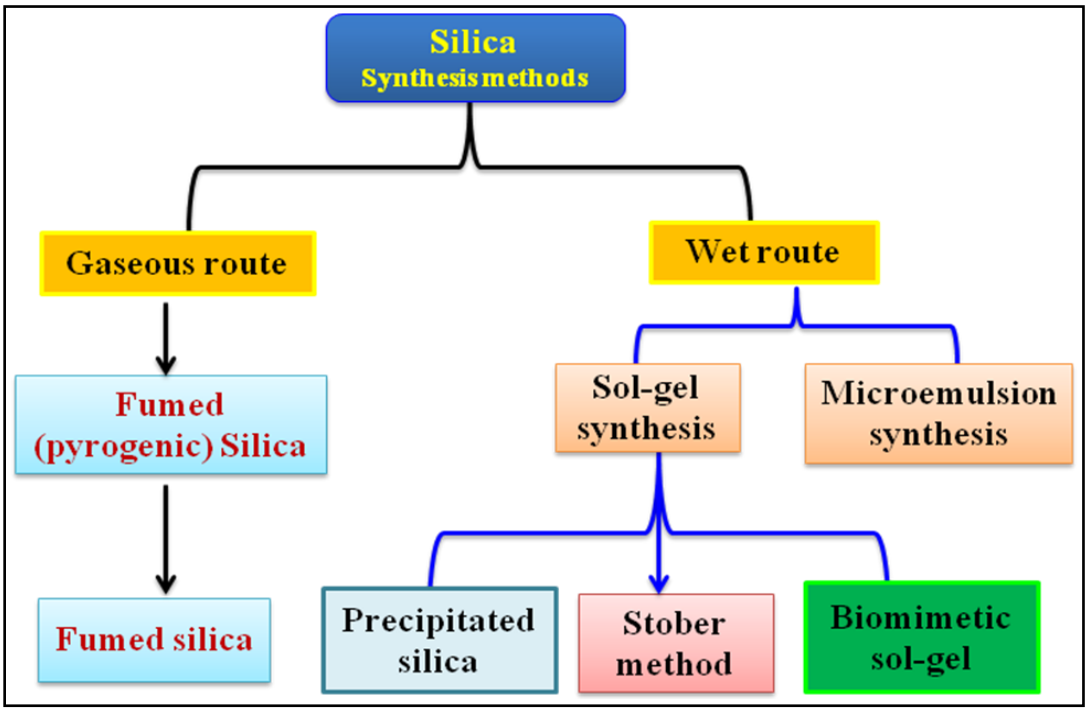

Fig. 1.4. Different routes for synthesis of silica nanoparticles

Various methods that have been used to obtain silica particles can be categorized into two main approaches i.e. top-down and bottom-up. Top-down is reducing the dimension of the original size (physical approach). Bottom-up or chemical approach involves a common route used to produce silica nanoparticles from atomic or molecular scale. Some of the widely used methods to synthesize silica nanoparticles are flame synthesis, reverse microemulsion and sol-gel process [54]. Out of these, sol-gel process is widely used to produce pure silica particles due to its ability

to control the particle size, size distribution and morphology through systematic monitoring of reaction parameters.

1.5.1. Sol-gel method

The sol-gel process is widely used to synthesize silica, glass and ceramic materials due to its ability to form pure and homogenous products. The role of the sol-gel method has been studied since the mid of 1800's. However, Ebelman and Graham during their studies on silica gels observed that tetraethyl orthosilicate, $Si(OC_2H_5)_4$, underwent hydrolysis in acidic conditions to form SiO_2, in a glass-like form [94]. Sol-gel chemistry is a process of transformation of liquid (colloidal) sol phase to a solid gel phase. The process involves hydrolysis and condensation of metal alkoxides ($Si(OR)_4$) such as tetraethylorthosilicate (TEOS, $Si(OC_2H_5)_4$) or inorganic salts such as sodium silicate (Na_2SiO_3) in the presence of acid (HCl) or base (NH_3) as catalyst [95]. The hydrolysis and condensation of the metal alkoxide leads to the formation of a colloidal phase, consisting of relatively higher molecular weight polymeric intermediates, which is known as the sol phase. The intermediates undergo polycondensation reactions and lead to the formation of three dimensional gel material. A general flow chart for sol-gel process which leads to the production silica using silicon alkoxides ($Si(OR)_4$) is shown in Fig. 1.5.

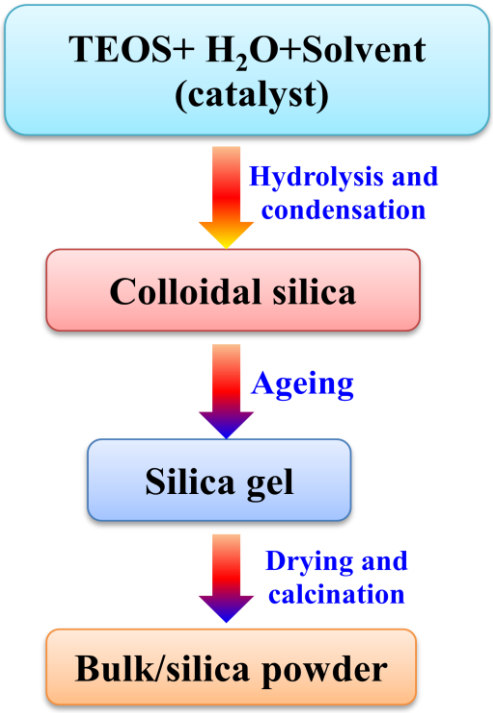

Fig. 1.5. Flow chart of sol-gel process

The reactions involved for the synthesis of silica using alkoxisilane in the sol-gel process can be written as follows (Fig. 1.6),

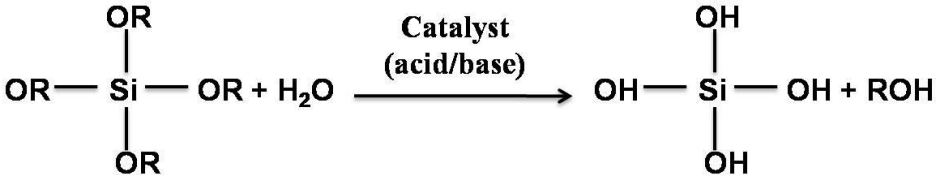

(a) Hydrolysis of alkoxisilane to silanol

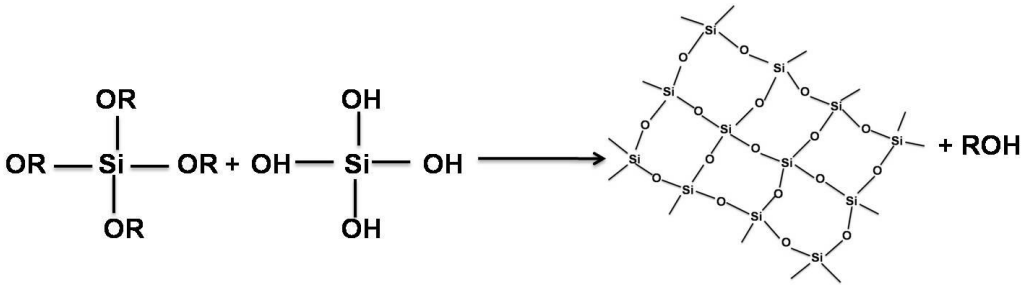

(b) Alcohol condensation: reaction between silanol and alkoxisilane

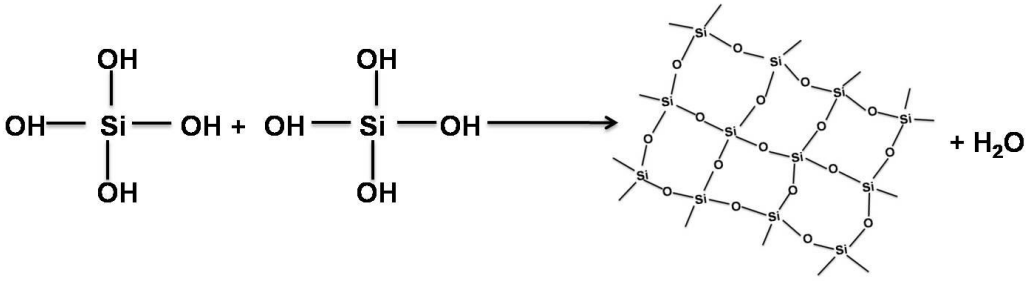

(c) Water condensation: reaction between silanols

Fig. 1.6. Hydrolysis and condensation reaction of of alkoxy precursor during the sol-gel process

The hydrolysis of alkoxysilane forms silanol groups. The condensation/polymerization between the silanol groups or between silanol groups and alkoxy groups forms siloxane bridges (Si–O–Si) that form entire silica structure. The rate of hydrolysis of the alkoxysilane is high at acidic as well as basic pH [96-97]. Under both reaction conditions, hydrolysis proceeds via nucleophilic substitution reactions [98]. In acid catalyzed reaction, entangled linear or randomly branched chains are generated in the silicate sol. Upon gelation (i.e., when the reaction system lost it fluidity), silicate gel or eventually silica monolith is produced. Base catalyzed hydrolysis results in the formation of a network consisting of discrete, highly branched clusters [99]. At basic pH, colloidal silica or weakly crosslinked clusters are formed.

In 1968, a pioneering work was carried out by Stober *et al*. and controlled synthesis of spherical and monodispersed silica particles was reported [100] by the hydrolysis and condensation of alkoxysilanes in presence of ammonia as catalyst (basic condition). Following that many others have reported the synthesis of silica nanoparticles. The main advantage of Stober method is the

ability to form monodispersed spherical silica particles compared to the acid-catalyzed systems which usually results in gel structures.

1.5.2. Synthesis route of different types of silica nanoparticles

1.5.2 (a). Fumed silica

For the synthesis of fumed silica, volatile liquid silicon tetrachloride is used as the feed [101]. The silicon tetrachloride is vaporized in a hydrogen and oxygen flame at temperatures >1000 °C [102-103]. The reaction proceeds via condensation polymerization and/or oxidation of the $SiCl_4$ feed stock (Eq. 1.).

$$2H_{2(g)} + O_{2(g)} + SiCl_{4(g)} \longrightarrow SiO_{2(s)} + 4HCl_{(g)} \quad (1)$$

The silica product forms as molten silica nuclei, which grow as the reaction continues into molten, spherical, nonporous "subparticles" (7−40 nm diameter, 2.2 g/cm^3 density). High temperature fusion and partial sintering of these "subparticles" result in their agglomeration into larger, mesoporous silica aggregates with a higher specific surface area (BET, 50−380 m^2/g) and wider size distribution [102-103]. Control of particle size, size distribution and surface area may be achieved by varying the concentration of reactants, flame temperature and retention time.

1.5.2 (b). Precipitated silica

Precipitated silica (synthesized from sodium silicate) has the largest share of the global specialty silica market [104-105]**.** Commercial precipitated silica is generally produced in a batch or semi batch process from sodium silicate and sulfuric acid as per Eq. 2.

$$Na_2Si_3O_7 + H_2SO_4 \rightarrow 3SiO_2 + Na_2SO_4 + H_2O \quad (2)$$

As the reaction is over, the precipitate is filtered, washed, dried and milled to the size range appropriate for the application [105].

The precipitated silica method is highly cost-effective and with continued improvements has even approached the purity obtained by the fumed silica synthesis route. However, the harsh conditions required for precipitated silica synthesis is a bottle neck of this method of synthesis.

1.5.2 (c). Silica gel

For synthesis of silica gel, an aqueous solution of sodium silicate is acidified to produce a gelatinous precipitate followed by washing and dehydration [106].

1.5.2 (d). Mesoporous silica

Mesoporous particles were synthesized using sol-gel method or spay drying [95, 107]. Mesoporous silica nanoparticles were synthesized by using tetraethyl orthosilicate with a template. This results in the synthesis of nano-sized spheres or rods that are filled with a regular arrangement of pores. The template can be removed by using various methods like washing with a solvent adjusted to the proper pH [108].

1.5.2 (e). Biogenic silica

Synthesis of the biogenic silica which is required for diatom's cell walls is performed in a specialized silica deposition vesicle (SDV) wherein highly controlled acidic environment is maintained [109-111]. A number of coprecipitating organic molecules like long chain polyamines (LCPAs), specialized proteins (silaffins, silacidins and cinguliums) and saccharides (e.g., chitin) are believed to be responsible for synthesis of biogenic silica also.

1.6. Silica based hybrid/bio-hybrid materials

According to International Union of Pure and Applied Chemistry (IUPAC), "a hybrid material is a mixture of inorganic components and organic components, or both types of component and the components usually interpenetrate on scale of less than 1 μm" [112]. The combination of silica nanoparticles with organic materials results in the development of silica based hybrid materials [113]. A number of articles on silica based hybrids have been published wherein silica nanoparticles have emerged as suitable inorganic component [114-117]. Silica nanoparticles offer a number of advantages like wide availability, high surface area, ease to functionalization, biocompatibility, resistance towards microbes, biodegradability and high thermal, mechanical, chemical stability. These properties make silica a suitable inorganic component for the synthesis of hybrid materials and its application as a suitable support. From last decade "bio-hybrid" has gained attention wherein the organic component of hybrids is replaced with biological component (protein/microbes). Biological component acts as functional unit and inorganic component acts as structural unit in the bio-hybrid (Fig. 1.7). Silica based bio-hybrids are gaining popularity as advanced material due to their selective and improved applicability in the field of catalysis, biosensing, food, bioremediation and pharmaceuticals. Bio-hybrid materials exhibit dual functionality like hybrid materials which comes from inorganic and biological components. Associations of biological components with silica nanoparticles have opened a window of interest because of their immense potential applications.

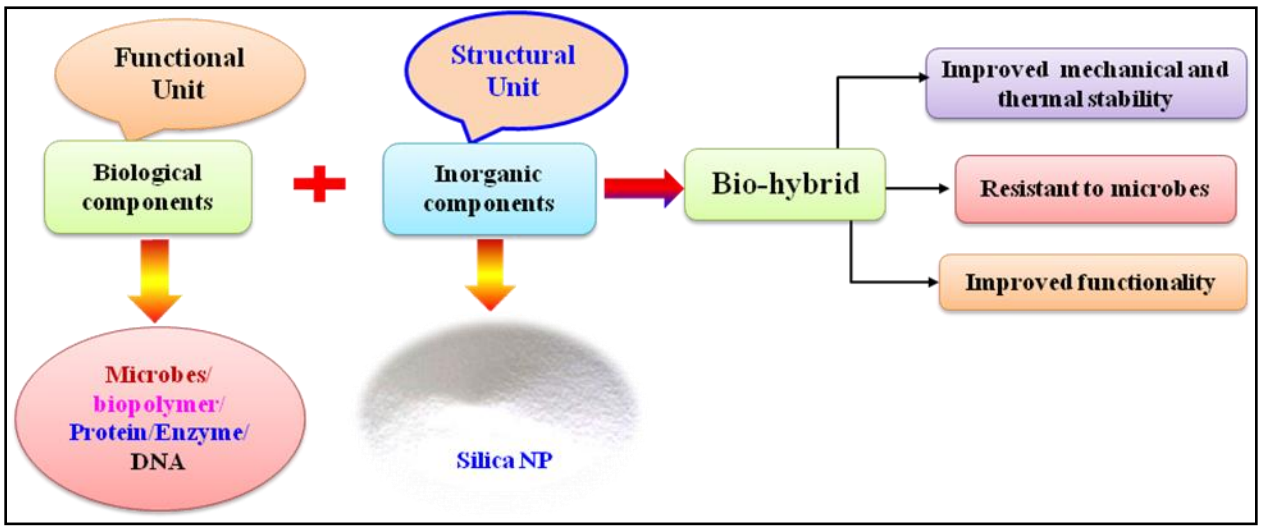

Fig. 1.7. Two components of bio-hybrids

Synthesis of hybrids/bio-hybrids by sol-gel method

There are other methods also available for synthesis of hybrids/bio-hybrids however, sol-gel method has been widely used [116-118]. Because of its mild reaction conditions and compatibility with a wide variety of solvents, it could efficiently combine silica (inorganic oxide) with an organic phase/bio-component. The development of a number of novel polymeric-silica hybrid materials with good performance has been reported using sol-gel process [119]. Also there are many reports wherein biological components enzymes and microbes have been associated with silica through sol-gel process [120-122].

However, production of alcohol as byproduct during the sol-gel process limits its application when biological components are involved. Thus, there is a need to find out suitable methods for associating bio-components with silica nanoparticles to develop bio-hybrids and improve the practical applicability of associated bio-components.

1.7. Applications of silica nanoparticles

Morphology-controlled nanomaterials such as silica play a crucial role in the development of technologies and find applications in the field of bioprocessing, environment and health. In recent years, significant interest has been observed in the synthesis of silica nanoparticles based materials with various sizes, shapes, morphologies and functional properties. These materials have gained popularity because of their advanced features and applied in various fields. In this chapter, the applications of silica nanoparticles in four major areas i.e. bioprocessing, biosensor, remediation and drug delivery are discussed (Fig. 1.8).

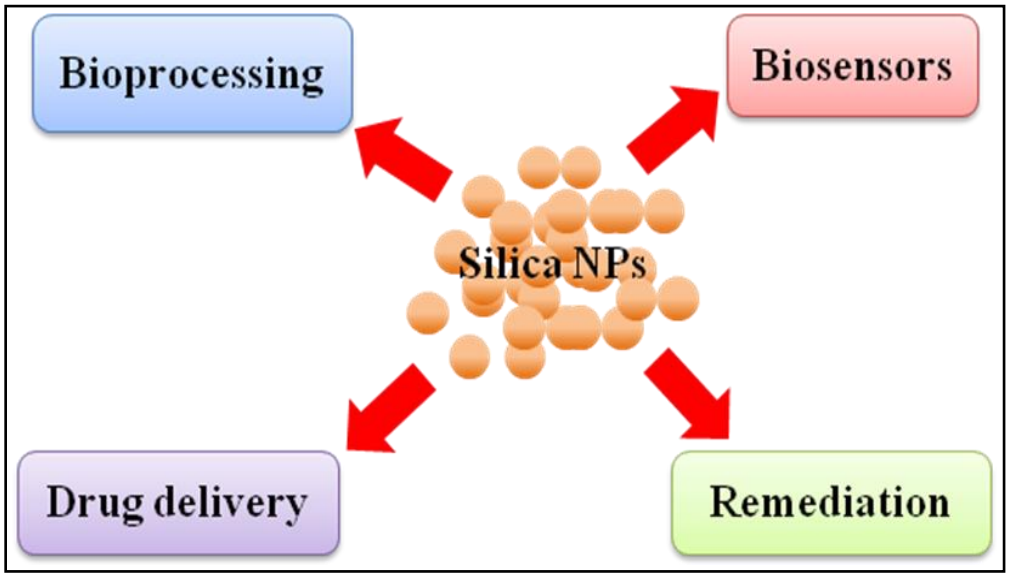

Fig. 1.8. Applications of silica nanoparticles

1.7.1. In enzyme immobilization

Among various immobilizing supports/carriers available in the field of enzyme technology, silica based supports stand out because of its peculiar features. Silica based materials have been successfully used for immobilization of enzymes [55-57, 123]. Balkus *et al*. used MCM-41 for immobilization of lysozyme and emphasized the importance of silica pore size to encapsulate the enzyme [124]. The limitation is, encapsulation of larger biomolecules is not possible in MCM-41 [125]. However, SBA-15 with larger pore sizes (5–30 nm) have possibilities to immobilize larger proteins [126]. Sun *et al*. showed very fast lysozyme adsorption by enlarging the conventional SBA-15 pore [127]. Fabrication of silica hollow spheres was reported by Liu *et al*. which exhibited a high adsorption capacity (up to 536 mg g^{-1}) and very rapid (<5 min to reach equilibrium) lysozyme immobilization. This study revealed that mesoporous silica hollow spheres with rugged surfaces can increase the enzyme adsorption rate during the adsorption process [128].

Presence of functional groups on the surface of supporting material improves the enzyme-support binding and further reduces the chances of leakage of immobilized enzymes. Lei *et al*. showed that enzymes immobilized within functionalized mesoporous silica had improved activity compared to free enzymes [129]. Chong *et al*. proved that the activity of immobilized penicillin G acylase (PGA) within vinyl-functionalized mesoporous silica support was higher than free PGA [130]. These results showed that enzymes immobilized on functionalized mesoporous silica can perform better which further proves that functionalization of silica is very crucial when the support is going to be used for immobilization purpose.

In this regard, the importance of organic functionalization of silica based material for enzyme immobilization was also studied. Vinyl functionalized silica demonstrated a high performance in enzyme immobilization and enzyme activity as well as enzyme stability [123]. Vinyl organosilane introduced hydrophobicity to the silica surface, which increased the silica surface's affinity against the proteins (BSA and cellulase enzyme). The vinyl mesoporous silicas were able to maintain the enzyme activity. In contrast, amine functionalized mesoporous silica (APTES) showed the highest adsorption amount however the activity of immobilized cellulose was very less. The reason could be that the amine functionalization induced electrostatic interactions between the amine terminal groups of mesoporous silica and carboxylic group of the enzyme's active sites [130]. One pot synthesis method was also explored for immobilizing enzymes (fumarase, trypsin, lipase and PLE). Herein, enzymes were entrapped in the matrix during the synthesis process of mesoporous silica [131]. The results showed that immobilized enzymes had high activity and stability and can be used for immobilization of other enzymes also.

As discussed above, these reports suggest that for efficient immobilization of enzymes and to maintain the activity and stability of immobilized enzyme, functionalized silica based supports are most suitable. Here again, the small pore size, synthesis and functionalization of mesoporous silica are bottleneck for its application as immobilizing support.

1.7.2. In biosensors

Enzymes immobilized onto/within silica have also gained popularity for its application in the field of biosensors and bioreactors [58-61,132-134]. Yeast spores and microbes have also been recently immobilized within silica [135-139] and it was observed that their enzymatic activity was retained. Ponamoreva *et al*. have synthesized yeast-based self-organized hybrid bio-silica

sol–gels for the design of biosensors [138]. It was observed that methylotrophic yeast cells of *P. angusta* BKM Y-2559 encapsulated in silica matrix maintain their activity in the presence of the alcohol formed during the sol–gel process. The immobilized cells works efficiently under stress conditions (in the presence of heavy metals or exposure to UV radiation) which allows them to be used in the development of amperometric biosensors for the determination of methanol in sewage systems. These biosensors also have shown the ability to remain active even after exposure to UV irradiation. Diana Yu *et al.* have encapsulated genetically engineered *Moraxella* spp. cells using sol-gel technique for the detection of organophosphates [139].

Methyl parathion (MP) was used as insecticide in agriculture. However, it causes harm to human health also. In this regard, microbial cells with organophosphorous hydrolase (OPH) enzyme which are able to hydrolyze MP into an optically detectable product p-nitrophenol (PNP), were immobilized on to various supports and used as biosensor to detect MP [140-144]. Studies from our laboratory have shown that *Flavobacterium sp.* expressing OPH enzyme when immobilized on glass fiber filters could detect MP in the range of 1-20 ppm [142]. In another study, when *Sphingomonas sp.* cells were immobilized on surface of microplate wells directly or with the help of inner epidermis of onion bulb scales, it showed the same detection range of MP (1-20 ppm) and further displayed a storage stability of only 18 and 32 days, respectively [143-144]. However, the low sensitivity and storage stability in the previous studies was a matter of concern. Thus, the challenge was to improve the sensitivity (up to 0.1 ppm) which is in the range of MRL value for methyl parathion in food commodities as well as to enhance the storage stability. Improved storage stability of biosensors is crucial for many practical/routine applications in different fields and to avoid the time consuming preparation of a fresh biosensor.

1.7.3. In heavy metal removal/remediation

Mesoporous silica and nanosize silica i.e. silica gel and silica particles have been widely used for the removal of toxic metals due to their remarkable characteristics, their large surface area, ease of functionalization, high adsorption capacity, excellent mechanical resistance, non-swelling behavior and excellent stability [145-150]. In 1997, hybrid mesoporous silica were used for removal of heavy metal by the groups of Feng and Mercier and Pinnavaia [151-152]. Wherein, synthesized mercaptopropyl-funtionalized mesoporous silica showed exceptional binding affinity toward Hg (II).

In other reports also, functionalized mesoporous materials (propylthiol-modified MCM-41 and HMS silica) were used for adsorption of heavy metals from wastewater [153-154]. Among different variants of silica, SBA-15 attracted much attention for water treatment applications [155]. The reason behind high demand of SBA-15 is its huge surface area (600-1000 m^2/g), narrow pore size distribution, large and controlled pore diameter (5-30 nm), which facilitate metal ions diffusion to the internal pore structure, resulting in fast adsorption kinetics [156]. Furthermore, it is considered hydrothermally stable because of its thick walls, about 4 nm in comparison to 1 nm for MCM-41 [154]. The advanced features of SBA-15 make it a promising support however, to improve its performance as adsorbent functionalization is pivotal. Organically functionalized mesostructured silica has received extensive attention as promising sorbents for the removal of heavy metal ions and hazardous chemicals [155, 157-161]. Michard *et al.* and others studied sorption and speciation of uranyl using different forms of silica i.e. silica gel, silica particles and amorphous silica [145-149].

Despite the numerous studies and interesting results, functionalization of mesoporous silica is still not applicable in real environment. There are two main bottlenecks, first is to design suitable mesoporous materials with high adsorption capacity to be applied for large volumes of discharges (e.g., continuous process column) and second is synthesis of high selectivity adsorbents with high stability and effective recyclability. Thus, there is need to devise low cost methods to functionalize silica based support with improved functionality which further increase the adsorption capacity.

1.7.4. In drug delivery

Silica NPs are suitable candidates for improved drug delivery systems because of their intrinsic characteristics like hydrophilicity, biocompatibility and nontoxicity, as well as the excellent protection they provide to encapsulated/entrapped drugs **[**162]. Vallet-Regí *et al*. introduced for the first time MCM-41 as a drug delivery system in 2001, following that, a lot of work has been carried out wherein mesoporous silica nanoparticles were applied as drug carrier for cancer treatment [62-66, 163-168]. In a study, it was reported that after the NPs are efficiently taken up by tumor cells, irradiation of the photosensitizing drug entrapped in the NPs results in efficient generation of singlet oxygen, which, in turn, causes significant cancer cell damage [169]. Interestingly, the discovery that mammalian cells take up and internalize mesoporous silica NPs without cytotoxic effects opened the door to the use of silica nanoparticles as a drug delivery system [170]. Surface modification/functionalization of the silica nanoparticles allow the release of loaded drug on specific cells or receptors. Yang *et al*. have synthesized pH-responsive mesoporous silica nanoparticles for controlled drug delivery systems for cancer treatment [171].

Tian *et al.* have developed polymeric mesoporous silica nanoparticles as a pH-responsive switch to control doxorubicin intracellular delivery [172].

For application of drug carriers in industry, there is need to produce the drug carriers in large scale under Good Manufacturing Practices (GMP) conditions with reproducibility and low cost. In this regard, the scaling up of the synthesis of mesoporous silica nanoparticles is a tedious job because mesoporous silica nanoparticles are often developed in the lab in small quantity [173]. Again to maintain reproducibility on the synthesis of mesoporous silica nanoparticles at small scale is relatively easy but at the larger scale is very difficult to control. Small pores (e.g., 2–3 nm) of developed mesoporous drug carriers also limit their application. The poor penetration capability of nanosystems within the tumor mass is one of the major issues which hamper the diffusion of nanocarriers [173]. Therefore, there is need to increase the penetration rate of mesoporous silica nanoparticles into tumor masses. Another bottleneck is regarding their potential toxicity and immunogenicity, which depend on the surface functionalization of mesoporous silica nanoparticles.

Thus, there is need to devise a suitable method for the synthesis of drug carriers in large scale with reproducibility as well as its functionalization through suitable biopolymers which will improve the bioavailability of loaded drug with less immunogenicity. The bio-components used for the design of the bio-hybrid drug carriers also have an impact on cellular uptake.

1.8. Research hypothesis

As reviewed above, the requirement for silica based materials with advanced properties is continuously increasing. The efficiency of mesoporous silica for various applications is mainly

due to their porous structure which allows molecules to disperse on their large internal surfaces. However, need of functionalization, small pore sizes and limited accessibility of the surface inside the pores which causes mass-transport issues are the bottlenecks. Thus, it is necessary to overcome the limitations of mesoporous silica. In this regard, by integrating the bio-component of interest with silica nanoparticles using a suitable method, new 'bio-hybrid' materials can be obtained. Developed bio-hybrids can be applied for different applications such as bioprocessing, biosensing, bioremediation and drug delivery. This integration of silica nanoparticles with bio-component will no doubt lead to new functional materials, improved sensing materials and new drug delivery vehicles which will have far-reaching impact in biotechnology.

The hypothesis of this work is to develop methods for the association of bio-components and silica nanoparticles with an objective to improve the practical applicability of the associated biomolecule. This thesis deals with the synthesis of four different bio-hybrid materials using two different routes (i.e. template (biocomponent) dependent route assembly and evaporation induced self assembly route) which find applications in four different fields i.e., catalysis, biosensor, bioremediation and drug delivery.

1.9. The specific objectives of the study are (Fig 1.9):

1. Synthesis of silica nanoparticles-*Ocimum basilicum* seeds bio-hybrid for immobilization of invertase enzyme
2. Synthesis of silica nanoparticles-*Sphingomonas sp.* cells bio-hybrid to detect methyl parathion pesticide
3. Synthesis of silica nanoparticles-*Streptococcus lactis* bio-hybrid for removal of uranium (VI)

4. Synthesis and application of silica nanoparticles-sodium alginate bio-hybrid as doxorubicin drug carrier

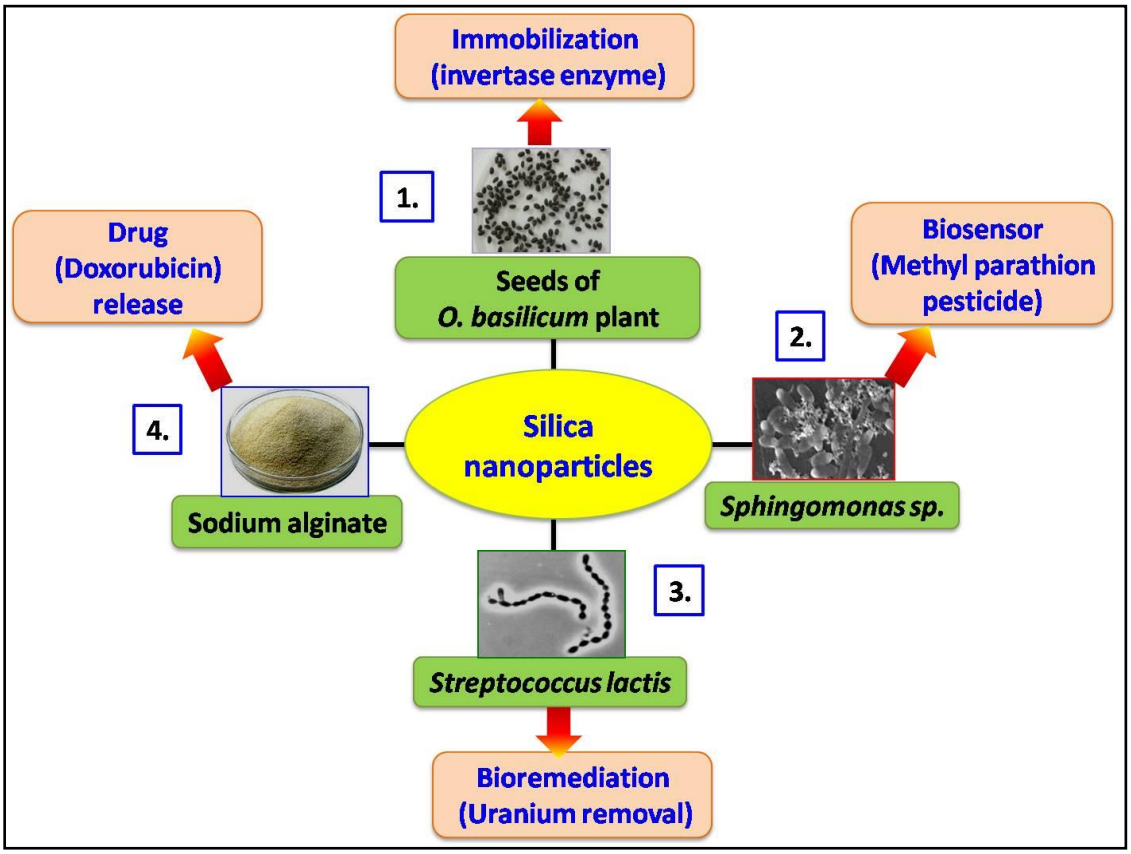

Fig.1.9. Schematic presentation of the objectives of the work

Chapter-2

Synthesis of silica nanoparticles-*Ocimum basilicum* seeds bio-hybrid for immobilization of invertase enzyme

2.1.Introduction

An immobilizing support should be stable, relatively cheap, environmentally benign and exhibit a high capacity for enzyme binding without affecting the activity of enzyme. As discussed in Chapter 1, a number of organic as well as inorganic supports were used for immobilization of enzyme however, each one have its own advantages and disadvantages. One such natural organic immobilizing support is *Ocimum basilicum* seeds (Indian name sabja) [174-177]. Seeds when stepped in water impart a fibrous structure.

Different inorganic nanoparticles (silica being the most common) have been used for the synthesis of higher length scale (nano/micro) materials and applied for immobilization [178-183]. Some authors have shown that fibrous silica structures can overcome limitations of mass diffusion [180]. Still, there is no study which shows the use of fibrous–pellicular structures of biological origin for assembly of silica nanoparticles and its application for enzyme immobilization. In this context, it is of interest to develop a recoverable, reusable, fibrous pellicular biocompatible support which is easier to synthesize in the laboratory at low cost and is also environment friendly.

To achieve this, *O. basilicum* seeds were used as template for the assembly of silica nanoparticles and two different approaches were followed for synthesis of seed-nano silica bio-hybrids. Seeds (biological origin) along with silica nanoparticles (inorganic component) can provide benefits which are specific to the individual components and thus help in enzyme immobilization. Herein, all the steps involved in the synthesis and characterization have been described. To the best of our knowledge, seed-nano silica bio-hybrid with this type of fibrous

pellicular morphology is first-of-its-type. In order to study the potential of the synthesized novel bio-hybrid as an immobilizing matrix, it was used for immobilization of invertase (EC 3.2.1.26) enzyme, which is one of the extensively used enzymes for the production of invert sugar syrup and has applications in food industry [184].

2.2.Materials and methods

2.2.1. Materials

O. basilicum seeds (locally known as Sabja) were purchased from the local market. Silica nanoparticles (silica NP) colloidal dispersion (~15 nm) was obtained from VISA Chemicals, Mumbai, India. Invertase (β-D-fructofuranoside fructohydrolase, EC 3.2.1.26) produced from baker's yeast, *Saccharomyces cerevisiae*, was obtained from Sigma Chemical Company (USA). Sucrose was obtained from Thomas Baker, Mumbai. Di-nitrosalicylic acid was obtained from Merck Ltd, Mumbai. Sodium acetate and sodium phosphate monobasic and dibasic were purchased from Thomas Baker, Chemicals, Mumbai. All chemicals were of analytical grade. Deionized water was used for all reactions and treatment processes.

2.2.2. Synthesis of seed-nano silica-enzyme bio-hybrid

2.2.2(a). Assembling silica nanoparticles (silica NP) on *O. basilicum* seeds

Two different methods were followed for assembling silica NP on *O. basilicum* seeds. In the first approach, 100 mg dry seeds were added to different concentrations of colloidal silica (1%-10% v/v) and agitated for 3.5 h at 150 rpm. Seeds were then filtered, properly washed with water to remove any loosely bound silica and further indicated as Silica@seeds. In the other approach, 100 mg seeds were first treated with (0.01%) polyethyleneimine (PEI) for 30 min. After washing

with water, the PEI treated seeds were suspended in different concentrations of colloidal silica solution (1% -10% v/v) for 3.5 h with constant shaking at 150 rpm. Seeds were filtered, washed properly and named as Silica@PEI-seeds.

2.2.2(b). Invertase immobilization

For the immobilization of enzyme**,** 100 mg each of immobilizing support (seed, Silica@seeds and Silica@PEI-seeds) was suspended in an aqueous solution of acetate buffer (100 mM, pH 4.5) containing different concentrations of invertase enzyme (1-5 mg/mL) at 4 ^{0}C for 12 h with intermittent shaking. Matrix was filtered out using a sieve and the supernatant was retained. The immobilized support was washed three times with 100 mM acetate buffer (pH 4.5) and then stored in the same buffer at 4 ^{0}C till further use. The amount of invertase present on support (immobilized invertase), as well as in the supernatant (unbound invertase), was determined by the enzyme assay using dinitrosalicylic acid reagent as described below. Fig. 2.1, shows the overall preparation process of bio-hybrids and its application for immobilization of invertase enzyme.

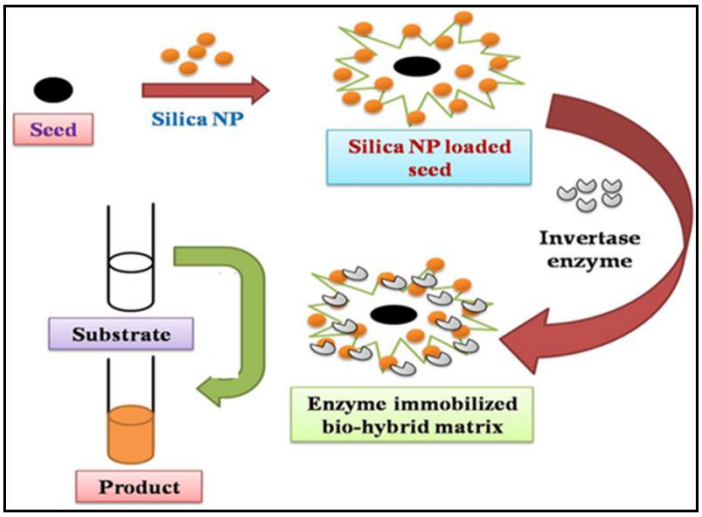

Fig. 2.1. Preparation process of bio-hybrids and its application for immobilization of enzyme

2.2.3. Characterization

2.2.3.1. Scanning Electron Microscope (SEM) protocol

A scanning electron microscope (PEMTRON) was used to characterize the plain seed (control) and silica nanoparticles loaded seeds. For SEM study, seeds were placed on a carbon tape with gentle pressing, mounted on the stub and coated with gold (Au) using a sputter coater. The stubs were fitted on the stage of the SEM and further used for SEM analysis.

2.2.3.2. Fourier Transform Infra-red (FTIR) protocol

For FTIR analysis, samples were placed on KBr filled groove of the sample holder and after appropriate background correction with KBr powder, the spectrum of the samples were measured in a diffused reflectance mode using Jasco FT-IR 600 plus spectrometer. All spectra were recorded over 4000-400 cm^{-1} range with a resolution of 4 cm^{-1}.

2.2.3.3. Small Angle X-ray Scattering (SAXS) study

Small-angle X-ray scattering (SAXS) measurements were carried out using a laboratory based small-angle X-ray scattering facility with micro-focused Cu-K_α source. The scattering intensity was recorded as a function of wave vector transfer q ($=4\pi\sin\theta/\lambda$, where 2θ is the scattering angle and λ is the wavelength of the incident radiation) in the range of 0.1 to 2.2 nm^{-1}. The real space dimension 'd' is inversely proportional to the wave vector transfer q, i.e. $d \approx 2\pi/q$. Thus, it is evident that SAXS data in the present q range provide information in the length scale of approximately 2-60 nm.

2.2.3.4. Micro-computed tomography analysis

Synchrotron radiation based X-ray micro-computed tomography (SRμCT) was used to characterize micro-structure and morphological changes in the lyophilized swelled seeds

(control) and synthesized bio-hybrids. The experiments were conducted at X-ray imaging beam-line at Indus-2 Synchrotron source, RRCAT, Indore India. In SRμCT experiments, the samples were fixed on the rotation stage using a centrally fitted sample holder and data was collected by rotating the sample about its axis through 180^0 with an angular step of 0.2^0. X-ray of energy 10 keV was selected and total 900 projections were collected with a data acquisition time of 600 ms for each projection. The effective pixel size of the projection image was 4.5μm.

2.2.3.5. Brunauer–Emmett–Teller (BET) analysis

BET analysis of the control and bio-hybrids were carried out at University of Pune using Quantachrome Instrument v3.01 (Autosorb iQ) by outsourcing. For BET analysis, sufficient amount of sample was added to the test tube. Sample containing test tube was placed in the flowing-gas degassing unit for the time depending on the nature of sample. After this, the test tube was removed from the oven and allowed to cool for 5 min. Dried and degassed sample was placed in the instrument for further analysis.

2.2.4. Physico-chemical studies of the free and immobilized invertase

The effect of pH on the invertase activity in the free and immobilized form was determined in the pH range of 2.0–9.0 using 100 mM acetate buffer (pH 3.0–5.0), 100 mM phosphate buffer (pH 6.0–8.0), and 100 mM bicarbonate buffer (pH 9.0) at 25 ^{0}C. Hydrolytic activity for the free and immobilized enzyme was determined.

The effect of temperature on enzyme activity was measured by determining the activity of the enzyme in free and immobilized form at temperatures ranging from 15 ^{0}C to 75 ^{0}C at their respective optimum pH.

2.2.5. Stability and reusability studies

To determine the storage stability, the immobilized enzyme was stored in acetate buffer (100 mM, pH 5.0) for a period of up to 60 days at 4 ^{0}C and hydrolytic activity was measured.

Reusability of immobilized enzyme was also investigated by measuring its activity on repeated use. After each reaction, the immobilized enzyme was recovered, washed with buffer and then used in the next hydrolytic reaction and compared with the first run (activity defined as 100%).

2.2.6. Statistical analysis

All experiments were carried out in triplicate and the mean values with ± standard deviation were plotted.

2.2.7. Reagents

Sodium acetate buffer (pH-4.5): sodium acetate solution (200 mM) was prepared by adding 16.41 g of sodium acetate powder in 1 L distilled water. A 200 mM concentration acetic acid was prepared by adding 11.55 mL acetic acid solution in 1 L distilled water. For the preparation of 100 mM sodium acetate buffer (pH-4.5), sodium acetate solution (200 mM) and acetic acid solution (200 mM) was mixed in 1:1. As per requirement, sodium acetate buffer was diluted and used.

Sucrose solution (25%): sucrose powder (25 g) was dissolved in 100 mL of (100 mM) sodium acetate buffer and used.

Glucose solution (1mg/ml): 100 mg glucose powder was added in 100 mL distilled water and used for preparing standard graph.

DNSA reagent:

(a) 2N NaOH: 80g NaOH pellets were dissolved in 1 L distilled water.

(b) *Sodium potassium tartarate*: 150 g sodium potassium tartarate was dissolved in 250 mL.

(c) *DNSA Reagent*: 5g DNSA was dissolved in 100 of 2N NaOH solution and slowly 250 mL of sodium potassium tartarate prepared above was added and final solution volume was made 500 mL.

DNSA protocol for quantification of invertase activity

1. In the tube, 2 mL acetate buffer, 2 mL sucrose (25%) and 1 mL free/immobilized enzyme was added and incubated for 5 min at RT. A blank was also prepared which contains 2 mL acetate buffer, 2 mL sucrose (25%) and 1 mL of distilled water.
2. The reaction was stopped by adding 1 drop NaOH and tube was placed in boiling water bath for 10 min.
3. From the above solution, appropriate aliquot was taken and diluted to 2 mL solution further 2 mL DNSA reagent was added and placed in boiling water bath for 10 min. In another tube, 2 mL distilled water and 2 mL DNSA reagent was used as reagent blank.
4. Tubes were allowed to cool and 20 mL distilled water was added.
5. The solution was mixed well and the absorbance of sample was measured at 540 nm using JASCO V-530 UV/VIS Spectrophotometer.
6. The absorbance against different concentrations of glucose was plotted to get a standard calibration graph.
7. The concentration of unknown samples was determined using standard calibration graph.

Calculation for enzyme activity:

From standard calibration graph, it was observed that 0.1 O.D. corresponds to 0.375 mg of reducing sugar.

0.1 O.D. = 0.375 mg of reducing sugar

Y O.D. = (0.375/0.1)*Y mg of reducing sugar

Y O.D. = Z mg of reducing sugar

Enzyme activity = (Z/reaction time)*(reaction volume/amount of sample taken for DNSA)*(Total volume of enzyme/amount of enzyme used for reaction)

Enzyme activity = S mg reducing sugar formed

Enzyme (Units) = (S/360)*1000 μmoles of reducing sugar formed

Calculation for enzyme immobilized on seeds:

Enzyme (Units) = [(Z/reaction time)*(reaction volume/amount of sample taken for DNSA)*(Total weight of enzyme immobilized seeds/weight of enzyme immobilized seeds used for reaction)]/360*1000

Relative activity = (activity of sample of interest/ activity of the control sample)*100

2.3. Results and discussion

2.3.1. Synthesis of seed-nano silica bio-hybrids

Fig. 2.2, shows the loading of silica NP on plain seeds. Results indicate that seeds having a fibrous –pellicular outer structure are able to bind silica on its surface. However, as the concentration of silica was increased from 5% to 10%, not much variation in the loading of silica was observed which suggests that saturation was achieved at 5% silica concentration.

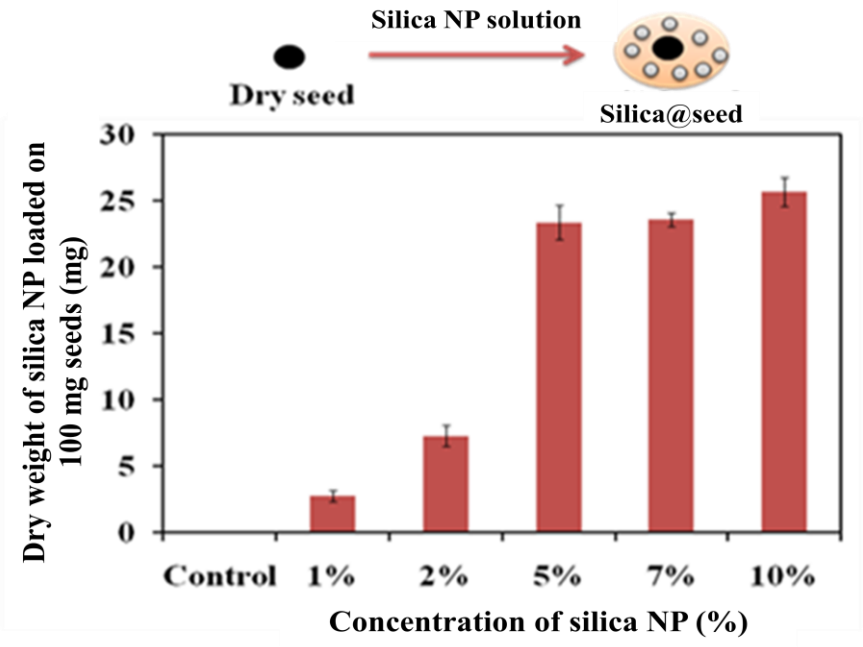

Fig. 2.2. Amount of silica nanoparticles loaded on plain seeds using different concentrations of silica NP (1%-10%). (Experimental conditions: initial weight of seed: 100 mg, volume of silica nanoparticles solution: 20 ml, agitation time: 3.5 h, temperature: 25 ^{0}C)

However, when PEI treated seeds were used the amount of silica NP loaded was half for Silica@PEI-seeds in comparison to the Silica@seeds at 5% silica NP concentration (Fig. 2.3). Thus, PEI treatment could not increase the loading of silica NP on the seeds may be because of steric hindrance caused by PEI. In both the approaches, loading of silica NP was found to be optimal when the concentration of silica NP used was 5%. So, in further studies 5% silica NP was used for the synthesis of nano silica-seed bio-hybrids.

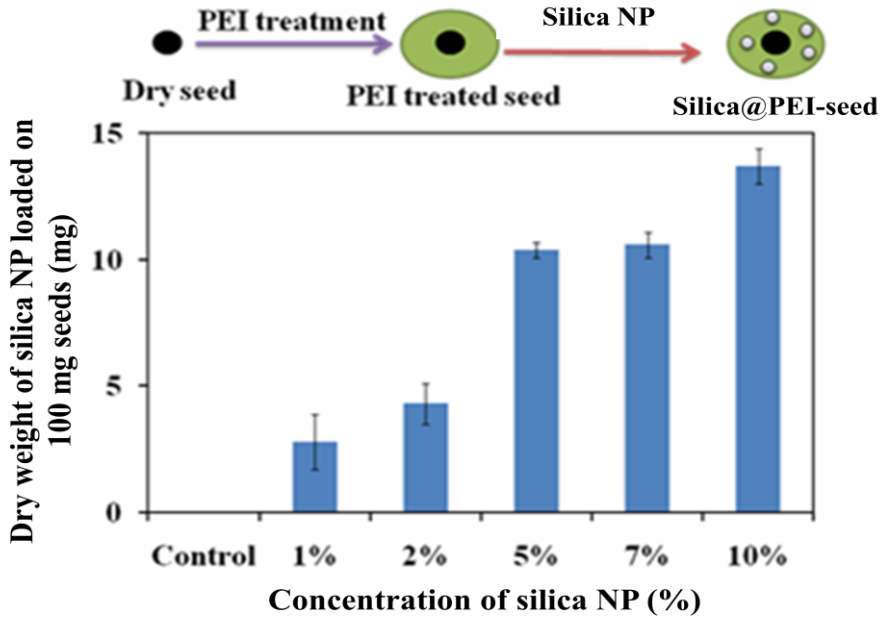

Fig. 2.3. Amount of silica nanoparticles loaded on PEI treated seeds using different concentrations of silica NP (1%-10%). (Experimental conditions: initial weight of seed: 100 mg, volume of silica nanoparticles solution: 20 ml, agitation time: 3.5 h, temperature: 25 ^{0}C)

Fig. 2.4, is a representation of dry *Ocimum basilicum* seeds, seeds when stepped in water and in a suspension of silica NP (Silica@seeds). *O. basilicum* seeds swell fairly quickly (10-15 min) when stepped in water. Swollen seeds have hydro-gel like outer coat and an inner black hard core. In the case of Silica@seeds, it was observed that the outer coat of seeds was opaque in relation to seeds swelled in water. The mucilaginous outer layer is a pectinous matrix, consisting of considerable amount of unesterified galacturonic acid with a large capacity for hydration [176]. Due to its high absorption capacity, seeds are having a natural gel-mesoporosity which can absorb organic/polymeric molecules or inorganic particulates that are dispersed or dissolved in water [177].

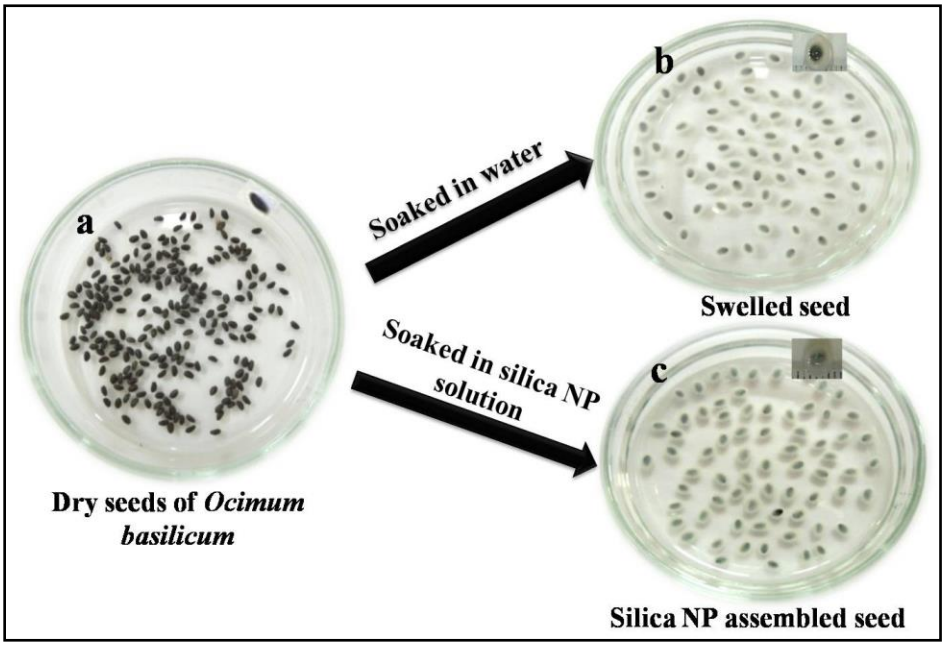

Fig. 2.4. Picture of *Ocimum basilicum* seeds, seeds soaked in water and seeds soaked in 5% silica NP.

Fig. 2.5, is a microscopic view of the seed swelled in water. The protruding fibrillar structures on the seed surface can be seen.

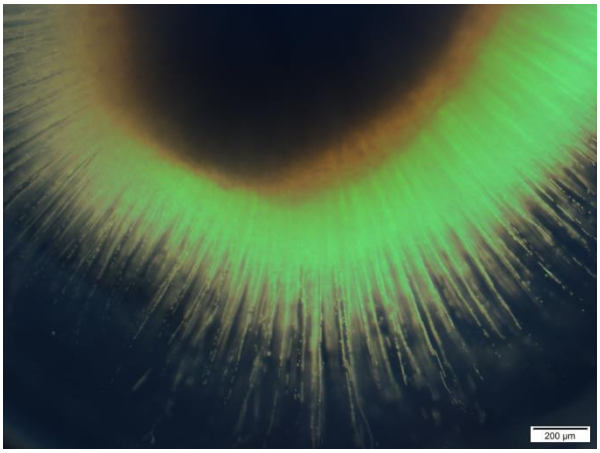

Fig. 2.5. Microscopic view of the swelled seed.

Swelling behavior of seeds in water and in a suspension of silica NP was studied. It was observed that seeds showed the highest swelling capacity in water whereas with increasing concentrations of silica NP the swelling capacity decreased (Fig. 2.6). The lower swelling degree at higher concentration of silica NP could be due to presence of silica NP which causes closer packing of the fibrillar structures on the seed surface and further leads to lower absorption of water [185].

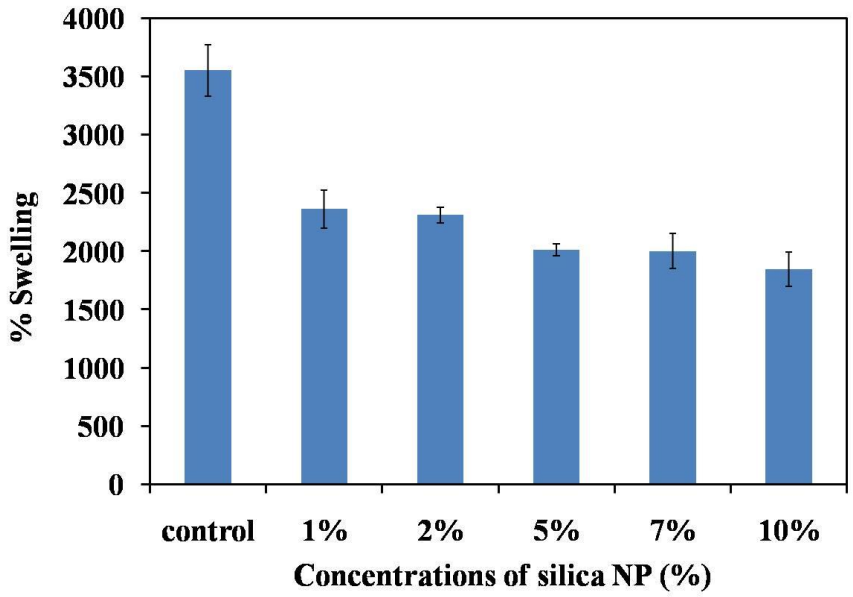

Fig. 2.6. Variation in % swelling of the seeds with increase in concentration of silica NP (1%-10%).

2.3.2. Characterization of bio-hybrid materials

To study the surface morphology and internal structure of silica nanoparticles assembled bio-hybrids a number of techniques were used.

2.3.2.1. Small angle X-ray scattering

To gain insight into the deposition/assembly of silica NP, SAXS was carried out. Variation of scattering intensity with wave-vector transfer (q) for the plain seed and developed bio-hybrids is plotted in Fig. 2.7. It is discernible from the Fig. 2.7, that the scattering profile from the plain seeds typically shows a power law scattering. The following form of the scattering was considered

$$I_1(q) = C_0 + C_1 q^{-\alpha} \qquad (3)$$

Here, C_0, C_1 and α are q independent parameters, which were estimated by fitting the model to the scattering profile. For the hybrid samples, the total scattering was assumed to be the cumulative contributions from the seed and the correlated silica NP.

$$I_{total}(q) = I_1(q) + I_2(q) \qquad (4)$$

Here, $I_2(q)$ is the scattering contributions from the correlated particles. Under local mono-disperse approximations [186],

$$I_2(q) = C_2 \int P_{NP}(q,r) D_{NP}(r) V^2_{NP}(r) S(q,R) dr \qquad (5)$$

Here, C_2 is a q independent scale factor and depends on number density of silica NP and scattering contrast, $P_{NP}(q,r)$ represents the form factor of a spherical particle of radius r, $V_{NP}(r)$ represents the volume of the spherical particle, S(q,r) is the interparticle structure factor that appears due to the correlation among the dense assembly of the silica NP and contains the information about the local volume fraction of silica NP. A hard sphere type of interparticle

interaction was considered in the present case. $D_{NP}(r)$ is the size distribution of the silica NP and was considered as Log-normal of the form

$$D(r)=\frac{1}{r\sigma\sqrt{2\pi}}e^{-\ln\left(r/\mu\right)^2/2\sigma^2} \qquad (6)$$

Values of different parameters {α, C_0, C_1, C_2, σ and M (nm)} were estimated from fitting of the scattering model (Eq. 4) to the scattering data (Fig. 2.7) and the parameters are tabulated in table 2.1, which indicates that although the local volume fraction of silica NP remained nearly similar for the two cases, the amount of absorbed silica in Silica@PEI-seeds is significantly less than that in Silica@seeds. This is evident from the significantly higher value of the ratio (C_2 /C_1) for the Silica@seeds as compared to Silica@PEI-seeds. The value for the estimated local volume fraction corresponds to the value of random jamming process.

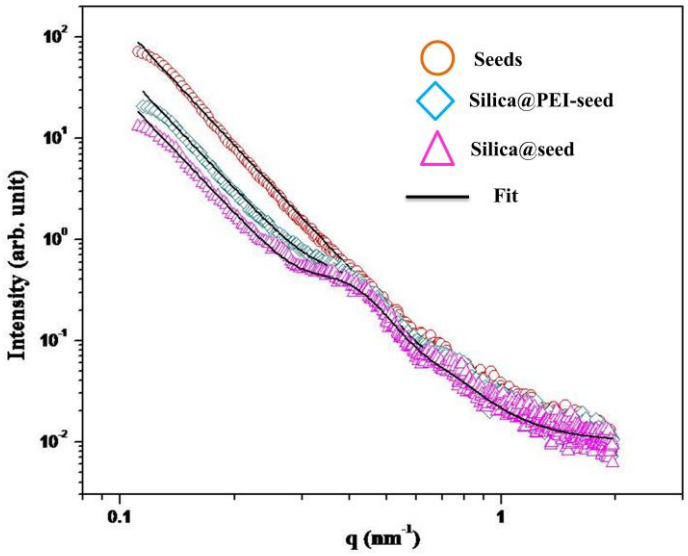

Fig. 2.7. SAXS data for plain seeds and synthesized bio-hybrids (Silica@seeds and Silica@PEI-seeds).

Table 2.1. SAXS analysis of plain seeds and bio-hybrids.

Materials	α	C_0	C_1	C_2	C_2/C_1	σ	M (nm)	Local volume fraction of silica NP
Seed	4.04	0.011	0.013	-	-	-	-	-
Silica@seeds	4.0	0.01	0.0028	1.5×10^{-6}	535.7×10^{-6}	0.21	7.46	0.64
Silica@PEI-seeds	4.0	0.01	0.005	1.378×10^{-6}	275.6×10^{-6}	0.21	7.46	0.64

2.3.2.2. SEM analysis

Fig. 2.8, depict the SEM micrographs of plain seeds, Silica@seeds and Silica@PEI-seeds after lyophilization. In the case of seeds swelled in water (control) due to the lyophilization, fibrils appear aggregated with a microporous surface [Fig. 2.8(i)]. Fig. 2.8(ii), clearly indicates dense loading of silica NP on the Silica@seeds surface. Whereas in case of Silica@PEI-seeds [Fig. 2.8(iii)] there is less deposition of silica NP in relation to Silica@seeds. This correlates with the earlier observations of lower binding of silica NP on Silica@PEI-seeds. In an earlier study, Biswal *et al*. also showed environmental SEM images of the plain seeds and seeds loaded with Fe_3O_4 nanoparticles, the micrographs reveal empty and filled pores respectively [177]. Thus, our

observations are in agreement with the previous study and prove that silica NP can be loaded into the micro-porous cavities of the seed during the swelling process.

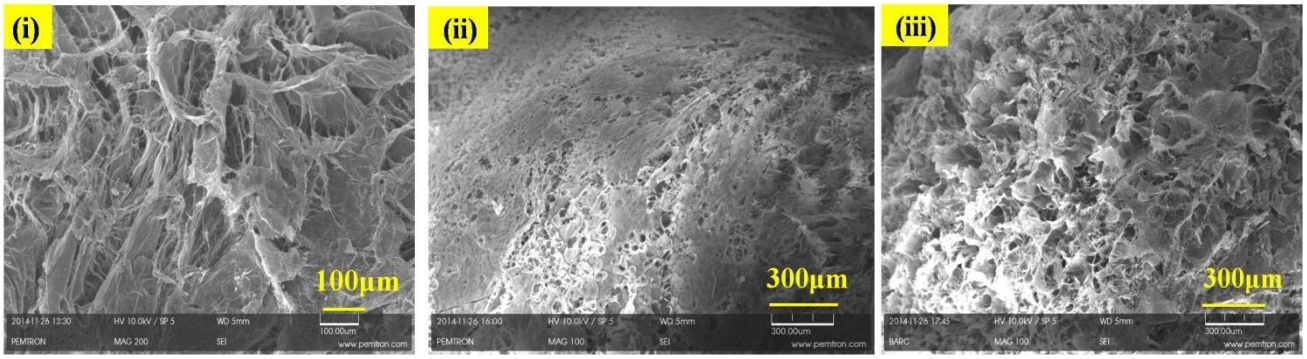

Fig. 2.8. SEM images of lyophilized *O. basilicum* seed after swelling in water 3(i), Silica@seeds 3(ii) and Silica@PEI-seeds 3(iii).

2.3.2.3. Synchrotron radiation based X-ray micro-computed tomography (SRµCT)

Synchrotron radiation based X-ray micro-computed tomography (SRµCT) technique was used to study the internal structure and morphological changes in the lyophilized swelled seeds and synthesized bio-hybrids. In this 3D imaging technique, a highly collimated X-ray beam of selected energy is passed through the samples and several radiographic projections are collected on an X-ray area detector, while the sample is rotated about its axis through 180^0. These projections are further used to computationally generate a series of 2D cross-sectional slice images of the sample. SRµCT slice images show the spatially resolved map of the sample's X-ray attenuation co-efficient which in turn depends on effective density and composition of the sample. When these slices are stacked together and volume rendered, they can provide three dimensional view of the internal structure, morphology and local density distribution of sample. Phase contrast projection images gives an overall (global) distribution of structure and density in

the sample whereas SRμCT images give local structure/density variation which is more detailed and clear.

Fig. 2.9, show the phase contrast projection images (a-c), SRμCT slice images (d-f) and 3D volume images (g-i) of plain seeds (a, d, g), Silica@seeds (b, e, h) and Silica@PEI-seeds (c, f, i). Phase contrast projection images identify three different regions in the seed i.e. (R1) the core, (R2) the core proximity with fiber roots and (R3) the outer fibrous region in all the samples. We are interested mainly in the fibrous regions (R2) and (R3), because assembly of silica nanoparticles in this region is going to affect the morphology of fibres. The image darkness at a given pixel in the radiography projection images is proportional to line integral of X-ray attenuation coefficient of the sample along the line of beam propagation. Visualization of fibers in these images depends on their thickness, number density and effective atomic number. Phase contrast image of plain seed shows that the image darkness decreases from core to outer region because of decreased absorption in the fibers, indicating a decreased fiber number density from core to outer region which is confirmed with the similar observations in optical microscopy image (Fig. 2.5). In Silica@seeds samples, image darkness is higher in (R2) as compared to (R3) possibly due to deposition of silica NP. In case of Silica@PEI-seeds samples, the darkness is very high on the outer region (R3) of fibres and gradually decreases towards the core. This suggests that the deposition of appears to be mostly on the outer region. If we compare, SRμCT slice images (d, e, f), plain seed shows fibers originating from the core and going nearly radially outwards. The fiber number density and image intensity also decreases (from 150 to 60) as one moves from core to outer region which confirms the reduction in fiber density. For Silica@seed, the effective image intensity is high (in the range 230-100) as compared to plain seed indicating

increased attenuation due to deposition of silica NP. Here, fibres appear to be entangled with each other causing appearance of foam like structure. Further, there is also presence of a thin shell on the outermost region of Silica@seeds possibly due to silica NP present on the edges of fibres which come together during the process of lyophilization. This observation was confirmed by SEM micrographs also wherein the surface of Silica@seeds looks fully packed with silica NP. On the other hand, in the Silica@PEI-seeds, the image intensity values is higher (255-200) in the outer region and lower (40-60) near the core, this indicates that there is localized deposition of silica NP which is more prominent in the outer region. In this also, the fibers appear to be entangled and they form foam like structure, wherein the cell size is even smaller than Silica@seeds. The physical appearance of the lyophilized plain seeds and bio-hybrids also supports this result because plain seeds are the largest one followed by Silica@seeds and Silica@PEI-seeds. These observations are also in correlation with the SEM images which show the surface porosity is highest in plain seeds and it decreases significantly in Silica@seeds due to more deposition of silica NP and decreases partially in Silica@PEI-seeds due to less amount of silica NP deposited. Based on these observations, a schematic picture of plain seeds, Silica@seeds and Silica@PEI-seeds was prepared which explains the loading of silica NP on both the bio-hybrids (Fig. 2.10). In Fig. 2.10, in the case of Silica@seeds, silica NP assembly leads to the synthesis of a compact structure. However, ordered assembly of silica nanoparticles created spacing between the fibres in Silica@PEI-seeds.

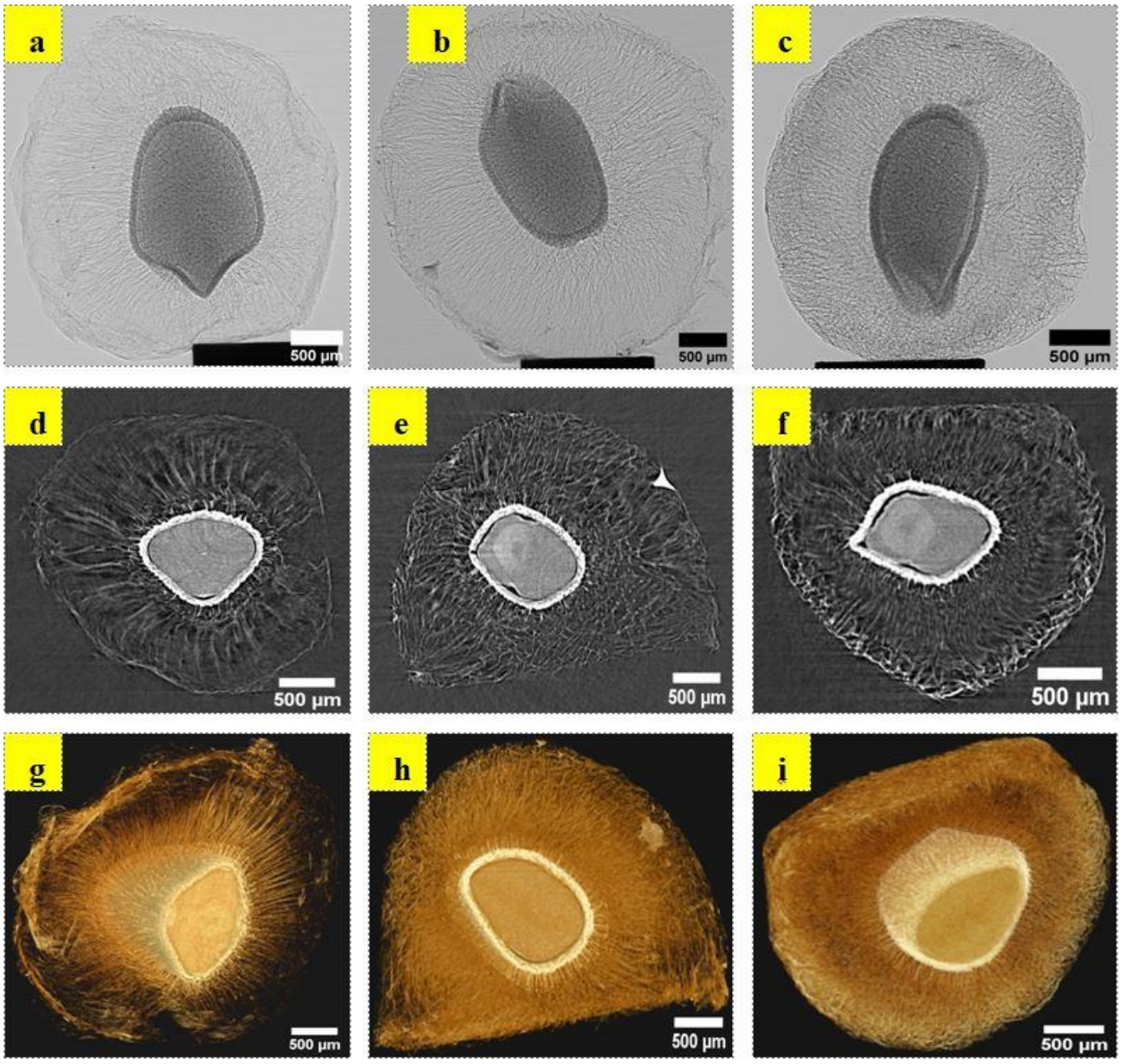

Fig. 2.9. Phase contrast projections (a-c), SRμCT slice(d-e) and 3D images(g-f) of plain seeds (a, d, g), Silica@seeds (b, e, h)and (iii) Silica@PEI-seeds (c, f, i).

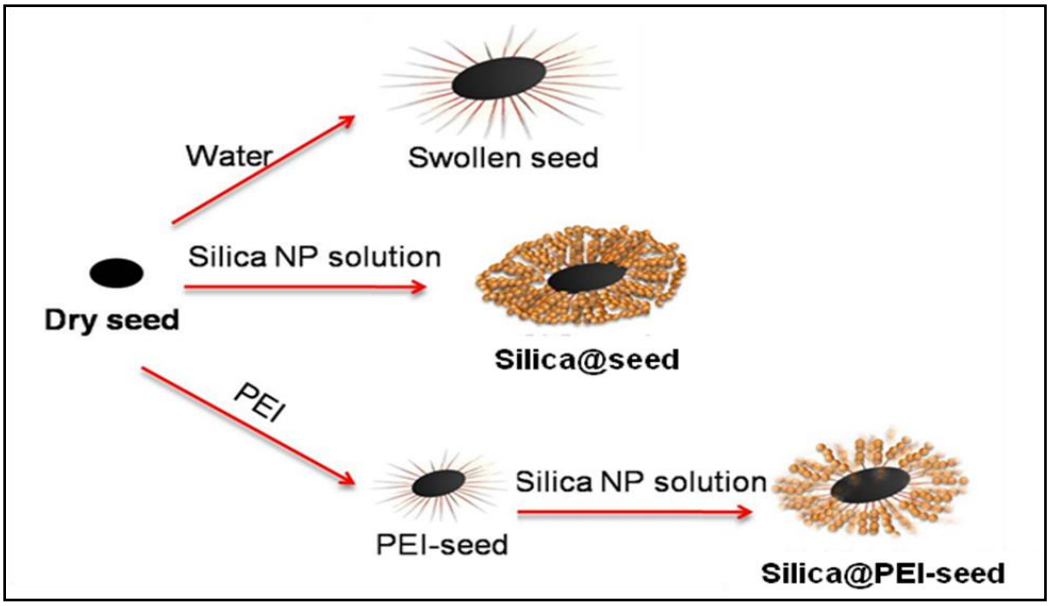

Fig. 2.10. Schematic representation of plain seed, Silica@seed and Silica@PEI-seed.

2.3.2.4. BET analysis

The BET results indicate that the surface area of the three supports increased in the order of plain seed < Silica@seeds < Silica@PEI-seeds (Table 2.2). It is apparent that incorporation of silica NP increased the surface area of the seeds. Although, Silica@seeds have higher loading of silica NP unlike Silica@PEI-seeds the surface area was higher in Silica@PEI-seeds. A plausible explanation could be that in the case of Silica@PEI-seeds, there was ordered assembly of NP on the outer surface of fiber because fibers are positively charged. In Silica@PEI-seeds, seeds were first stepped in PEI solution (which imparts positive charge to fibrillar structures) followed by stepping in silica NP solution. Positive charge on fibrillar structures helps in assembly of negatively charged silica NP on fibrillar structures in ordered manner. Because of assembly of nanoparticles in an ordered way on fibrillar structures, the increase in surface area is higher than the Silica@seeds (Fig. 2.10).

Table 2.2. BET results of plain seed and bio-hybrids.

	Seed	Silica@seed	Silica@PEI-seed
Surface area (m^2/g)	6.1	10.0	23.4

2.3.2.5. FTIR analysis

To elucidate the interaction between the seeds and silica NP, FTIR spectra of silica NP, plain seeds, Silica@seeds and Silica@PEI-seeds were recorded (Fig. 2.11). The FTIR spectra of the silica NP showed absorption peaks arising from asymmetric vibration of Si-O-Si (1090 cm^{-1}), asymmetric vibration of Si-OH (950 cm^{-1}), symmetric vibration of Si-O-Si (795 cm^{-1}) and the peak at 1635 cm^{-1} is due to scissor bending vibration of molecular water [183]. The peaks in the range from 3200 to 3600 cm^{-1} are attributed to silanol stretch and absorbed water on the surface. The main characteristic peaks observed for plain seeds were as follows: in the high wavenumber domain, spectra of the seeds display a peak at ~3283 cm^{-1} which can be assigned to the ν(OH) stretching of the polymer hydroxyl groups [185]. The peaks at 1745 cm^{-1} and 1650 cm^{-1} correspond to C=O stretching of esterified carboxylic groups (-$COOCH_3$) and free carboxylic groups (-COOH), respectively [187]. The peaks at 1384 cm^{-1} corresponds to in plane CH_3 asymmetric bending. The peaks at 1239 cm^{-1} and 1161 cm^{-1} corresponds to methylester COC groups stretching and COC stretching, respectively. Stretching and bending of COH ring was observed at peak 1098 cm^{-1} while peak at 705 cm^{-1} is assigned to the pyranoid ring.

In Silica@seeds, there is shift in the peak of seed from 3283 cm^{-1} to 3290 cm^{-1} which could be due to presence of silanol group of silica NP. The peaks present in seeds at 1239 cm^{-1} and 1161 cm^{-1} have disappeared in Silica@seeds, this may be due to the involvement of methylester COC

groups and COC groups in binding with silica NP. The symmetrical stretching vibrations of Si-O-Si bands are not visible in spectra of Silica@seeds due to overlapping with peaks of COC bonds corresponding to the pectin chains in seeds, while the asymmetric vibration of Si-O-Si band is shifted to 796 cm^{-1} [185]. The peak at 950 cm^{-1} which is assigned to Si-OH stretching has disappeared, may be because of involvement of silanol (Si-OH) groups for binding to the seeds. There is shift in the peak from 705 cm^{-1} to 683 cm^{-1} in silica assembled seeds. Overall there is involvement of hydroxyl, methylester COC groups stretching, COC stretching groups of seeds and silanol group of silica NP in Silica@seeds.

In case of Silica@PEI-seeds, the peak which is present in seeds at 3282 cm^{-1} is shifted to higher wavenumber at 3289 cm^{-1} and broadening of peak was observed. This could be due to presence of silanol groups of silica NP and amino groups of PEI because the seeds were treated with PEI before loading of silica nanoparticles. The peak which is present at 1384 cm^{-1} in seeds was shifted to 1391 cm^{-1}, this may be because seeds were treated with PEI. There is shift in the peak from 1745 cm^{-1} to 1742 cm^{-1}, this could be due to the involvement of C=O group interacting with PEI and silica NP because in Silica@seeds no shift was observed. However, the shift in peak at 1651 cm^{-1} shows the involvement of COO^{-} groups with silica NP and same shift was observed in Silica@seed. The peaks present in seeds at 1239 cm^{-1} and 1161 cm^{-1} have disappeared in Silica@PEI-seeds same as Silica@seeds. Again in Silica@PEI-seeds, the symmetrical stretching vibrations of Si-O-Si bands are not visible due to overlapping with peaks of COC bonds corresponding to the pectin chains of the seeds, while the asymmetric vibration of Si-O-Si band is shifted from 801 cm^{-1} to 794 cm^{-1}. Here again, the peak at 950 cm^{-1} which is assigned to Si-OH stretching has disappeared as in Silica@seeds which shows the involvement

of silanol groups. Overall, in Silica@PEI-seeds hydroxyl, carbonyl, methylester COC groups, COC stretching groups of seed, amino of PEI and silanol group of silica NP are involved in assembly of silica NP on PEI treated seeds.

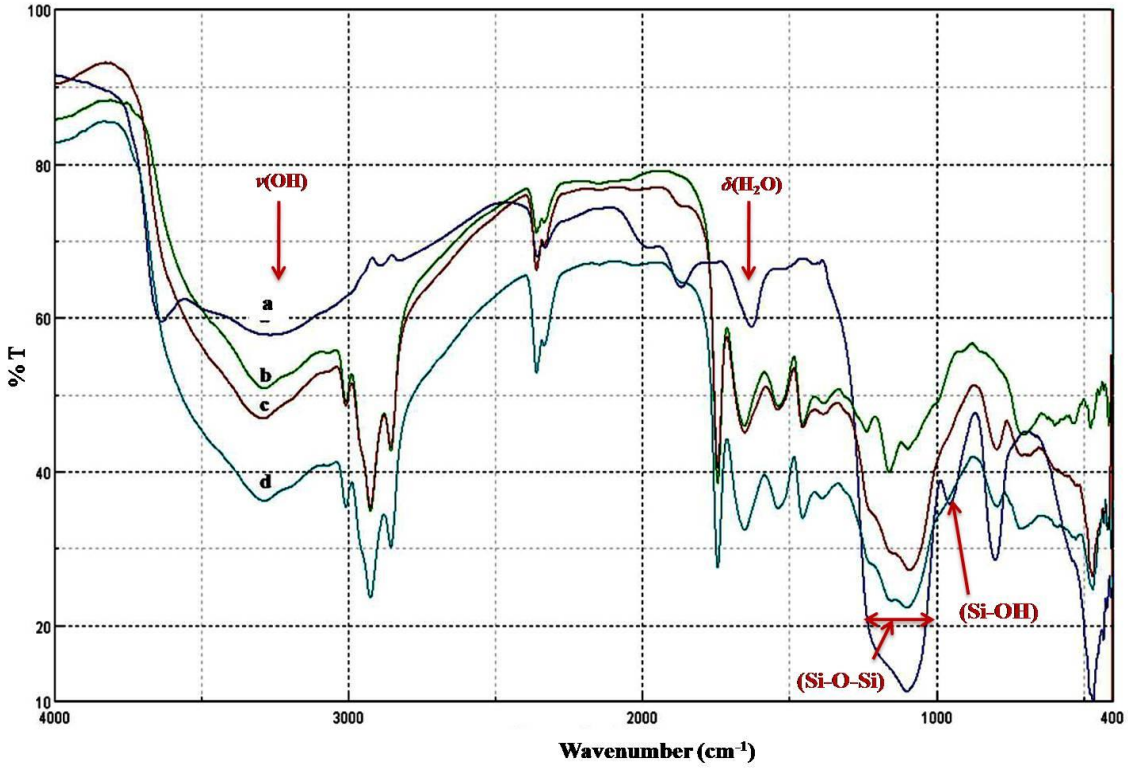

Fig. 2.11. FTIR spectra: (a) Silica, (b) *O. basilicum* seeds, (c) Silica@seeds and (d) Silica@PEI-seeds.

2.3.3. Enzyme immobilization on plain seed and bio-hybrids

The immobilization of enzymes is generally performed to improve the stability and function of enzymes as well as immobilization also helps in easy recovery of both product and enzyme. Mesoporous silica is the most commonly used support for enzyme immobilization [188-189]. However, due to certain limitations like mass transfer, there is constant need for developing a suitable silica NP based material for its application in enzyme immobilization. In this direction,

to assess the applicability of the synthesized bio-hybrids (Silica@seeds and Silica@PEI-seeds) as immobilizing support, these were used for immobilization of invertase enzyme.

Immobilization of invertase enzyme on plain seeds, Silica@seeds and Silica@PEI-seeds was performed for 12 h to achieve the maximum binding of enzyme (Fig. 2.12.). As shown in Fig. 2.12, initially there is an increase in the binding of enzyme with increase in enzyme concentration and thereafter a plateau was reached in all the supports. Silica@PEI-seeds showed highest enzyme loading followed by Silica@seeds and plain seeds. Higher binding of enzyme in Silica@PEI-seeds indicates that the support is providing favorable environment for enzyme immobilization. A possible reason could be the morphology of the Silica@PEI-seeds (the way silica has assembled). Enzyme immobilization involves a multistep process, in which first enzyme molecules are adsorbed on the readily available sites of the support (which takes short time) and with increase in enzyme concentration more enzyme molecules are further adsorbed on inner surfaces (which takes a longer time) till equilibrium is reached [190].

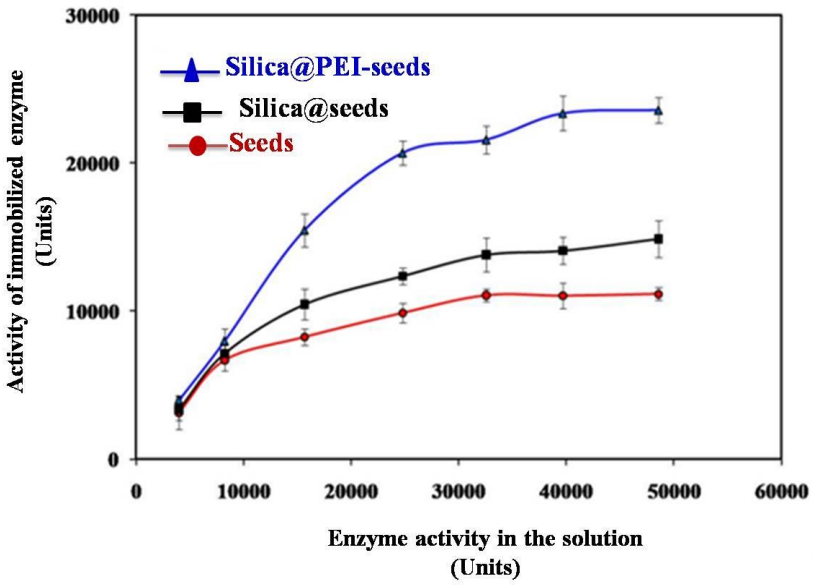

Fig. 2.12. Immobilized invertase enzyme on plain seeds, Silica@seeds and Silica@PEI-seeds.

To understand the adsorption process of invertase enzyme onto the bio-hybrids, two classical isotherms models (Langmuir and Freundlich which are widely used) were applied. In the Langmuir model, it is assumed that all the sorption sites of the sorbent have an identical binding energy and each site binds to only a single sorbate (enzyme molecule) [183]. The linearized Langmuir isotherm is given as:

$$C_e / q_e = 1/(q_m K_L) + C_e / q_m \quad (7)$$

where, q_e is the equilibrium adsorption capacity of adsorbent in mg (enzyme)/g(sorbent), C_e is the equilibrium concentration of enzyme in mg/L, q_m is the maximum amount of enzyme adsorbed in mg/g and K_L is the Langmuir constant [183].

On the contrary, the Freundlich model is based on a reversible heterogeneous sorption process since it does not restrict to monolayer sorption capacity [191]. The linearized Freundlich isotherm is given as:

$$\log q_e = \log K_F + 1/n \log C_e \quad (8)$$

where, q_e is the equilibrium sorption capacity of the sorbent in mg/g, C_e is the equilibrium concentration of enzyme in mg/L, K_F [(mg/g)/(mg/L)$^{1/n}$] is the constant related to the adsorption capacity of the sorbent, and n is the constant related to the sorption intensity [183].

In case of synthesized bio-hybrids Silica@seeds and Silica@PEI-seeds, the correlation coefficient values for Langmuir are 0.855 and 0.696, respectively while the correlation coefficient values for Freundlich isotherm was 0.971 and 0.955, respectively. The correlation coefficient values shows goodness of fit to Freundlich isotherm compared to Langmuir isotherm for both the bio-hybrids (Fig. 2.13). This proves that the developed supports are offering multilayer adsorption of invertase enzyme.

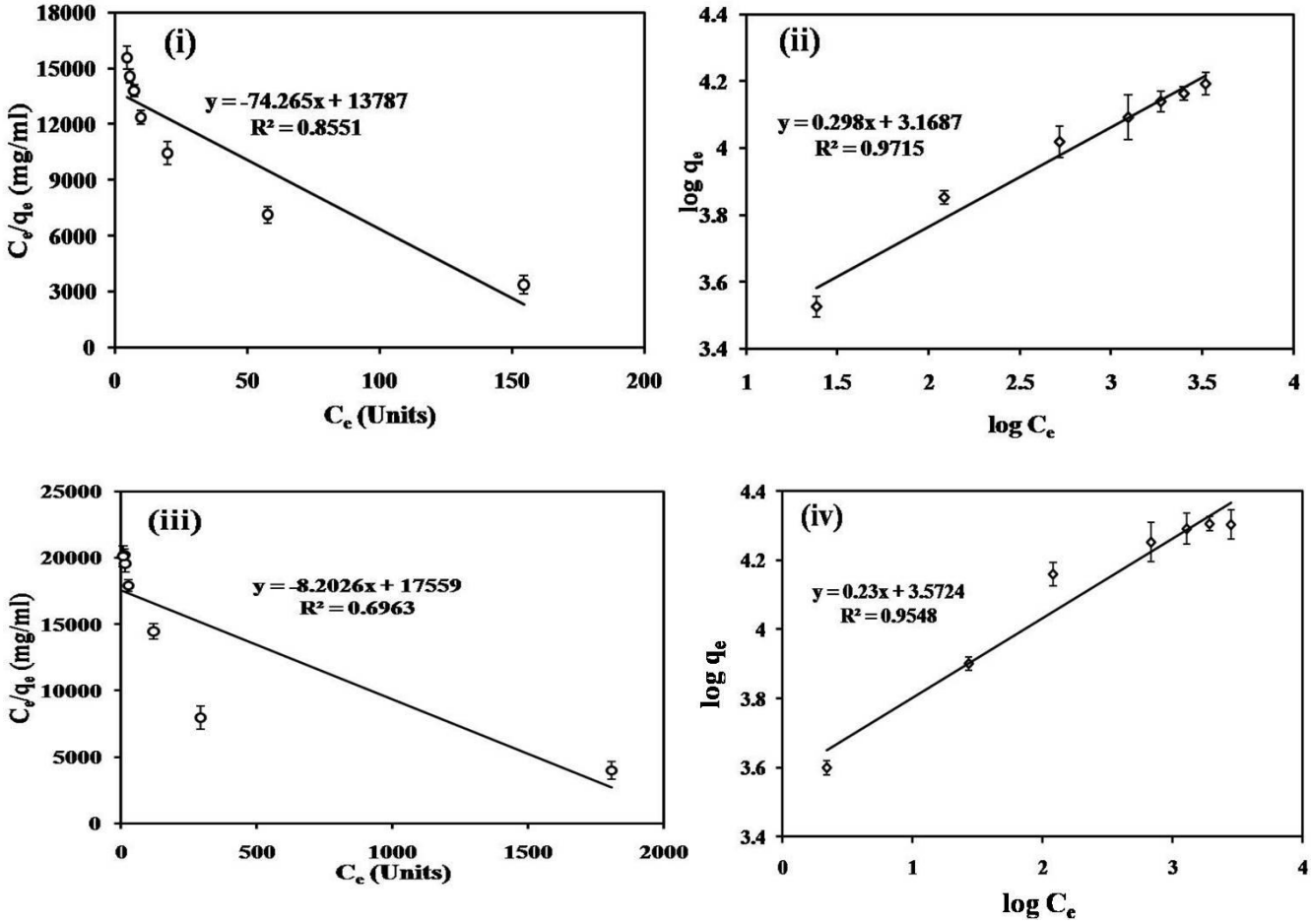

Fig 2.13. Sorption isotherm of invertase enzyme onto bio-hybrids Silica@seeds and Silica@PEI-seeds (i and iii) by Langmuir isotherm and (ii and iv) Freundlich isotherm.

2.3.4. Study of physico-chemical parameters of free and immobilized invertase enzyme

The effect of pH on the activity of the free and immobilized invertase for sucrose hydrolysis is presented in Fig. 2.14. There was no change in the optimum pH for the free and immobilized enzyme was observed. Fig. 2.14, shows the same optimum pH of 4.5 for the free and

immobilized invertase which indicates that the immobilizing support is providing a favorable environment to the enzyme. In earlier studies, wherein invertase was immobilized on poly(hydroxyethyl methacrylate-coglycidyl methacrylate) and jute fabric using polyethyleneimine, a similar trend was obtained [192-193]. In other studies also wherein enzymes were immobilized on polymeric matrices no shift in optimal pH was observed [194-195].

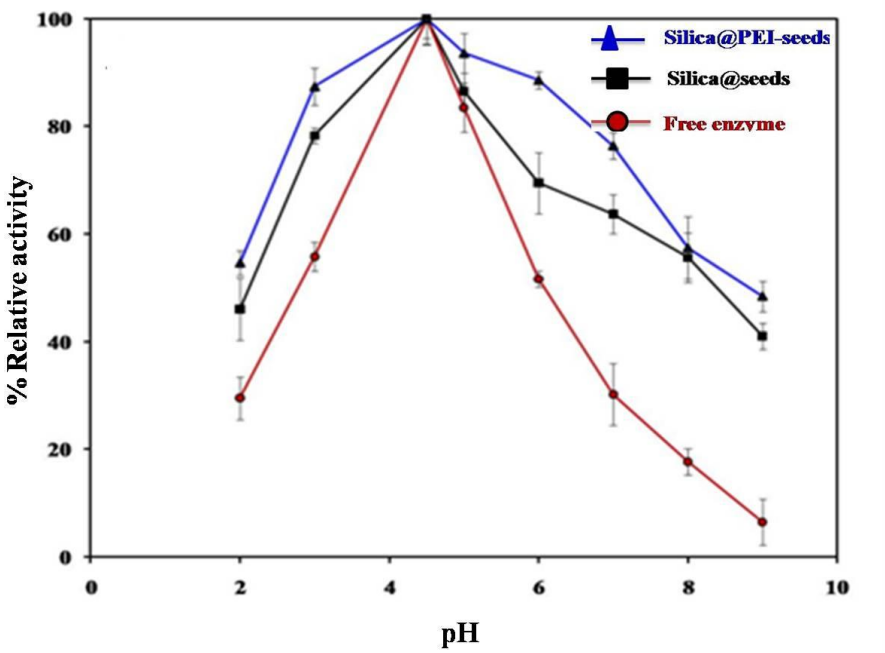

Fig. 2.14. Effect of pH on free and immobilized invertase.

The effect of temperature on free and immobilized invertase was determined by measuring the hydrolysis of sucrose at temperatures ranging from 15 to 75 ^{0}C. As seen in Fig. 2.15, there was no change in the optimum temperature of invertase after immobilization. The optimum temperature for free and immobilized invertase was 55 ^{0}C, however the temperature profile of immobilized invertase was broader in comparison to free enzyme. The broader temperature

profile of immobilized invertase is probably a result of enhanced thermal stability. In earlier studies also, immobilized invertase has shown higher thermal stability compared to the free form [193, 196]. Arica *et al*. have reported that hydrogel carriers such as carboxymethylcellulose and poly(2-hydroxyethyl methacrylate) provide a protective microenvironment for enzymes which yield higher stability [196-197].

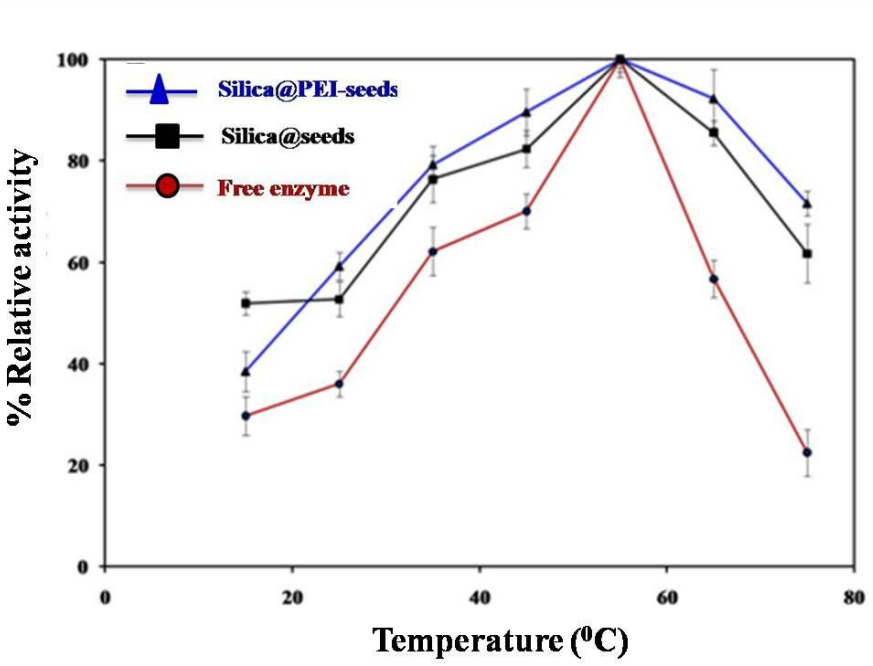

Fig. 2.15. Temperature profiles of the free and immobilized invertase.

2.3.5. Storage stability and reusability study of immobilized invertase enzyme

As shown in Fig. 2.16, the activity of the immobilized invertase on Silica@seeds and Silica@PEI-seeds was about 45% and 78% respectively after 60 days of storage at 4 ^{0}C. The free enzyme (in buffer) lost all its activity in 25 days. In previous studies, invertase immobilized on PVAL microspheres and pHEMA-GMA membrane retained 62% activity after 28 days at 4 ^{0}C

and retained 78% of initial activity after 35 days of storage, respectively while the free enzyme, in both the studies, lost all its activity [198-199].

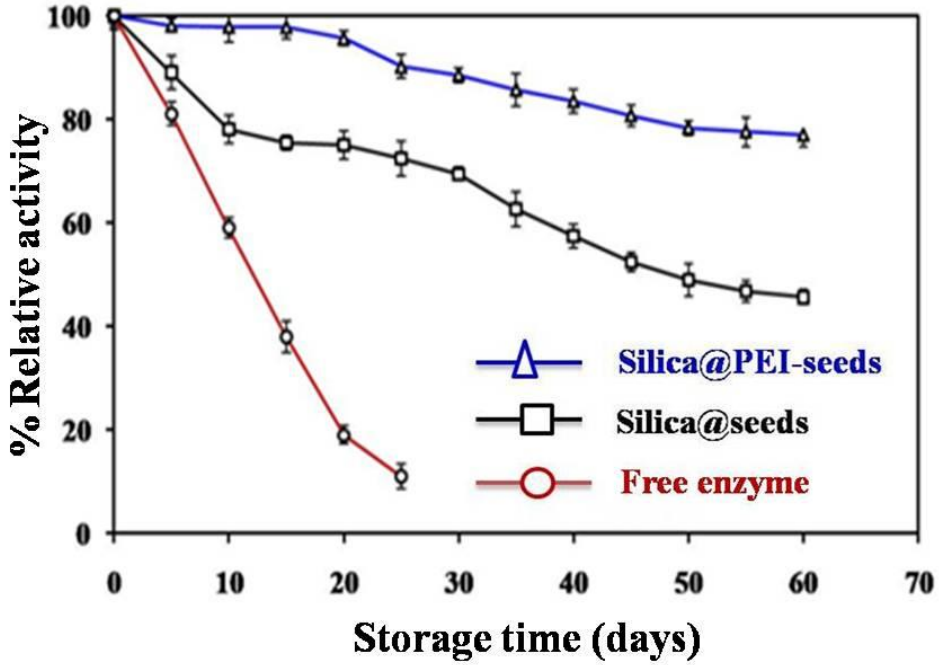

Fig. 2.16. Storage stability of the free and immobilized invertase.

The reusability of immobilized invertase is important to determine the economic viability of a system. The immobilized invertase on Silica@seeds and Silica@PEI-seeds was successively reused up to ten cycles (Fig. 2.17). After eight cycles of reuse, Silica@seeds and Silica@PEI-seeds showed 54% and 82% activity. The decrease in the activity could be due to desorption of enzyme from the support during washing [200]. Based on these results, it is proved that Silica@PEI-seeds has emerged as promising silica based immobilizing support for invertase enzyme.

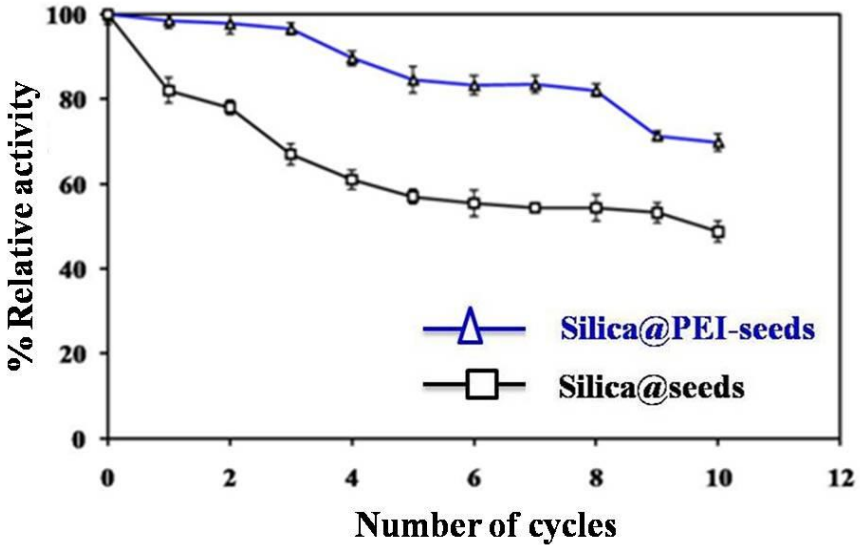

Fig. 2.17. Reusability studies of immobilized invertase

2.4. Conclusion

In this study, we reported for the first time assembly of silica NP on the *O. basilicum* seeds which led to the synthesis of two different forms of bio-hybrids (Silica@seeds and Silica@PEI-seeds). Bio-hybrids were further used for immobilization of industrially applicable invertase enzyme. Presence of silica NP increases the surface area of the bio-hybrids and provides a favored microenvironment for immobilizing enzyme molecule which results in enhanced enzyme loading, improved physico-chemical properties and higher storage stability. Of the two forms of bio-hybrids developed, Silica@PEI-seeds emerged as the best immobilizing support. Herein, seeds were used as template for assembly of silica NP and this work has led to the development of a simple and efficient way for synthesis of silica based fibrillar pellicular support. In this regard, another important biological component i.e. a microbial cell (*Sphingomonas sp.*) was

used as a template for assembly of silica NP and developed bio-hybrid was used for developing a biosensor to detect methyl parathion pesticide in the next chapter.

Chapter-3

Synthesis of silica nanoparticles-*Sphingomonas sp.* cells bio-hybrid to detect methyl parathion pesticide

3.1. Introduction

Methyl parathion (MP) is an organophosphate (OP) compound which is used as insecticide in agriculture. However, it is harmful to human health also as it causes acetylcholinesterase inhibition. It is banned in developed countries; however it was still used as a restricted insecticide in India till August 2018. Although methyl parathion was not recommended for fruits, vegetables and spices, still there are reports which show the presence of pesticide in vegetables and spices probably because methyl parathion is cheaper than the other currently recommended pesticides. The FAO/WHO Codex Alimentarius Commission and Food Safety and Standards Authority of India (FSSAI) have recommended the Maximum Residue Limits (MRLs) in several food commodities in the range between 0.1-1 ppm [201-203]. Therefore, there is an urgent need to develop a method that is sensitive, reliable, and able to monitor a large number of MP samples simultaneously and economically feasible.

A number of methods have been developed for detection of MP/OP wherein most of the studies for the detection of MP/OP are based on the use of acetylcholinesterase (AChE) and organophosphorus hydrolase (OPH) [204-207]. Among these, OPH based methods have advantages wherein OPH enzyme hydrolyzes MP into an optically detectable colored product p-nitrophenol (PNP) (Fig. 3.1) which can be detected by electrochemical or colorimetric methods and further used to develop a biosensor for detection of MP [143-144, 208]. In this direction, microbial cells with OPH enzyme were immobilized on to different supports and associated with optical transducer for MP detection [140-144]. However, the low sensitivity and storage stability with respect to what has been reported till date is a matter of concern. Thus, the challenge is to

improve the sensitivity (up to 0.1 ppm) which is in the range of MRL value for MP in food commodities as well as to enhance the storage stability.

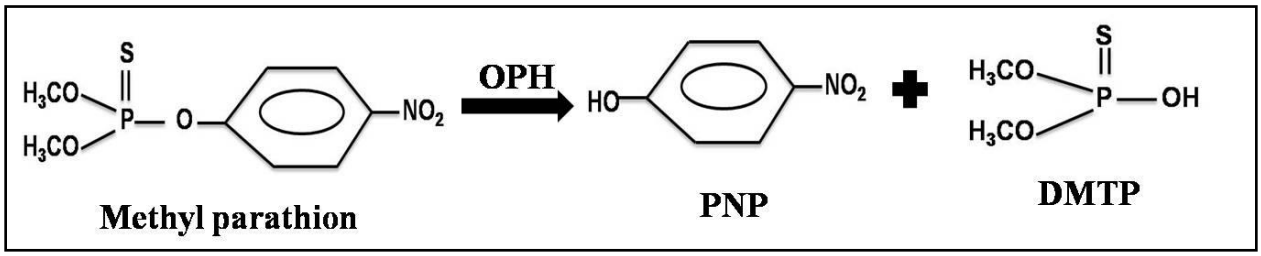

Fig. 3.1. Schematic presentation of hydrolysis of MP into p-nitrophenol (PNP)

Thus, silica NPs were integrated with *Sphingomonas sp.* cells to design a more sensitive and stable optical microbial biosensor for the detection of MP. Microbial cells integrated with silica NP were immobilized on the microplate well surface and further used for detecting multiple samples of MP on a single platform.

3.2. Materials and methods

3.2.1. Materials

Methyl parathion (*O*,*O*-dimethyl *O*-4-nitrophenyl phosphorothionate) purity, 98.5% analytical grade was purchased from Dr. Ehrenstorfer Schorfers Augsburg, Germany. Colloidal silica nanoparticle (~15 nm) was obtained from VISA Chemicals, Mumbai, India. Polyethyleneimine (PEI), average $M_w \sim 7.5\times10^5$) was purchased from Sigma Chemical Co., MO, USA. Microplate (96 wells) used for immobilization were procured from BD Flacon (USA). All other analytical grade chemicals were purchased from Sisco Research Laboratory, Mumbai, India.

3.2.2. Micro-organism, culture medium, harvesting of cells and hydrolytic activity assay

Sphingomonas sp. JK1 culture (MTCC8489) was available in our laboratory. *Sphingomonas sp.* JK1 was first cultivated in modified Wakimoto media (consist of 15 g sucrose; 5 g peptone; 2 g $Na_2HPO_4 \cdot 12H_2O$; 0.5 g $Ca(NO_3)_2 \cdot 4H_2O$; and 0.5 g $FeSO_4 \cdot 7H_2O$ in 1 L milli Q water) for overnight at 30 ^{0}C. After this, 1/100th volume from the overnight grown culture was sub-cultured in Luria broth (200 mL) and grown for 48 h at 30 ^{0}C on a rotary shaker at 150 rpm till absorbance of 2.2 at λ_{max} 600 nm was achieved for optimum MP hydrolytic activity [143]. Cells were harvested by centrifugation at 5000×*g* for 10 min and washed three times with 50 mM phosphate buffer (pH 8.0). Finally, the pellet was resuspended in 1/10th volume in phosphate buffer (pH 8.0) and stored at 4 ^{0}C. Microbial OPH activity of the cells was measured by adding 50 µL of whole cell suspension in 1 mL of 50 ppm MP and production of PNP was determined by measuring absorbance at λ_{max} 410 nm (ε_{410} = 16,500 M^{-1} cm^{-1} for PNP) [143].

3.2.3. Integration of functionalized silica nanoparticles (^{f}silica NP) with *Sphingomonas sp.*

(a) Optimization of polyethyleneimine (PEI) concentrations for functionalization of silica NP

Silica NP solution (0.1% v/v) was treated with varying concentrations (0.001-0.1 % v/v) of PEI solution for 30 min with stirring at 150 rpm on incubator shaker. After this, suspension was centrifuged and washed properly to remove unbound PEI. ^{f}Silica NP were suspended in distilled water.

(b) Optimization of ratio of *Sphingomonas* cells: ^{f}silica NP

Different ratios of *Sphingomonas* cells to ^{f}silica NP (1:3, 1:2, 3:4, 1:1, 4:3 and 2:1) was mixed together and incubated for overnight with stirring at 30 ^{0}C. After this, cells bound with ^{f}silica NP were separated by centrifugation, washed thoroughly with phosphate buffer (pH 8.0) and used further. A 100 µL of harvested cell suspension contains ~2 x 10^{9} CFU.

3.2.4. FTIR study

Samples (silica NP, ^{f}silica NP, *Sphingomonas sp.* cells and bio-hybrid of *Sphingomonas sp.*-^{f}silica NP) were air dried at RT. Dried samples were mixed with KBr powder in the ratio of 1:20 and ground finely using a mortar and pestle. FTIR analysis was carried out as described in Section 2.2.3.2.

3.2.5. Immobilization of bio-hybrid (*Sphingomonas sp.*-^{f}silica NP) onto microplate

Various concentrations of bio-hybrid (10-60 µL) were immobilized onto the interior surface of the wells of microplate (96 well) and then air dried for 1 h at room temperature. After washing the wells, immobilized bio-hybrid was cross-linked with different concentrations (0.5-5%) of glutaraldehyde. Immobilized wells were washed with buffer and microplate was stored at 4 ^{0}C until use. The production of PNP was determined by measuring absorbance at λ_{max} 410 nm. The overall process of synthesis and immobilization of bio-hybrid is shown in Fig. 3.2.

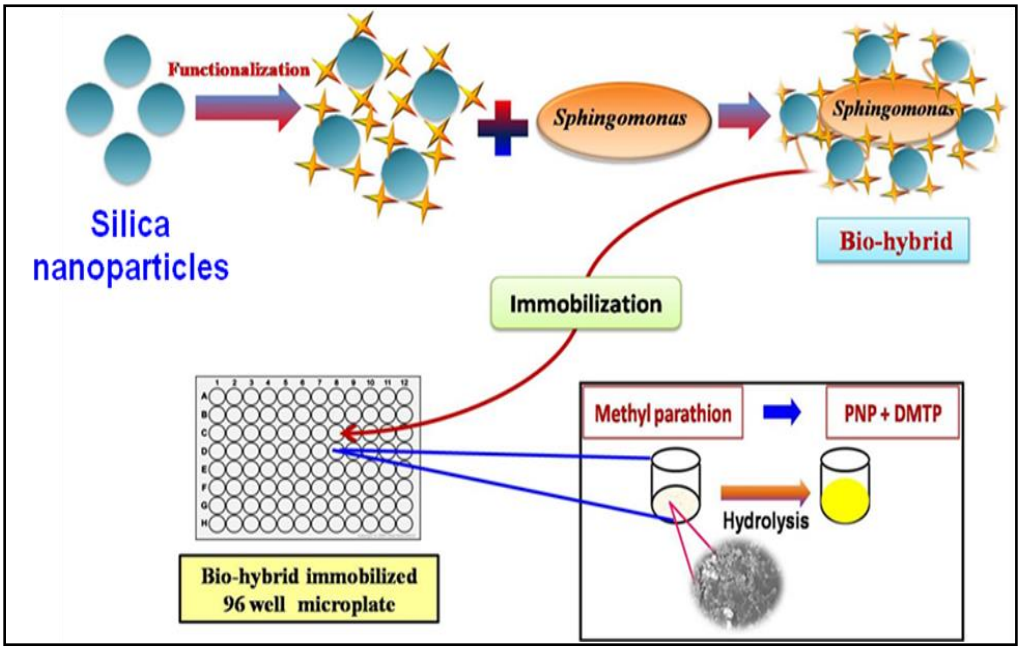

Fig. 3.2. Schematic presentation of development of whole cell based biosensor.

3.2.6. SEM study of the bio-hybrid immobilized onto microplate

For this study, the inner bottom surface of the microplate well was cut carefully and removed. On this surface, *Sphingomonas sp.* cells and bio-hybrid were immobilized separately (as discussed earlier). The well surface where *Sphingomonas sp.* cells were immobilized served as the control. Scanning electron microscope (PEMTRON) was employed to observe the surface morphology of the wells of microplate after immobilization of *Sphingomonas sp.* cells and bio-hybrid. For SEM study, well of the microplate was mounted on stubs and coated with gold (Au) using a sputter coater. The SEM micrographs of the immobilized well were acquired at magnification of 6000X.

3.2.7. Transducer and operating system for optical detection of MP using immobilized bio-hybrid

Multi detection microplate reader (MDMR) from Bioteck (SynergyTM HT) was used for optical detection of MP. It consists of a xenon flash light source in conjunction with the photomultiplier tube (PMT) detector which helped to make time-resolved measurements. This reader works in a wavelength range from 200–999 nm with an increment of 1 nm. The transducer was optical and microplate reader was completely controlled via KC4TM PC software [143, 209]. For the analysis of MP, sample was added into the bio-hybrid immobilized wells and formation of PNP was measured at 410 nm. The difference in absorbance between the initial and final reading corresponds to the amount of PNP formed.

3.2.8. Calibration studies using bio-hybrid immobilized microplate

Bio-hybrid immobilized microplate (stored at 4 ^{0}C) was integrated with the optical microplate reader. It was calibrated using MP concentration ranging from 0.1 to 5.0 ppm in phosphate buffers (pH 8.0) at room temperature for 5 min and the formation of PNP was measured on optical microplate reader at 410 nm. All experiments were carried out with phosphate buffer (pH 8.0) at room temperature in triplicates.

3.2.9. Storage stability and reusability of bio-hybrid

Immobilized bio-hybrid was stored at 4 ^{0}C and the storage stability of immobilized bio-hybrid was determined for a period of 200 days using 1 ppm of MP and PNP was detected at regular interval. Reusability of the immobilized bio-hybrid (stored at 4 ^{0}C) was also studied using 1 ppm

of MP. After each reaction, the hydrolyzed MP was removed; immobilized bio-hybrid was washed with buffer and fresh samples of MP were analyzed up to 10 cycles.

3.2.10. Analysis of spiked sample with developed biosensor

For real sample analysis, water sample was spiked with different concentrations of MP (0.2, 0.4, 0.5, 0.6, 0.8 and 1 ppm) and then subjected to quantification using bio-hybrid immobilized optical microplate biosensor.

In another study, 50 g of grapes were spiked with different concentrations of MP, adsorbed MP was extracted in phosphate buffer and the same was used for detection of MP on the developed microplate based biosensor.

3.3. Results and discussion

3.3.1. Optimization of amount of PEI, *Sphingomonas* cells and ^{f}silica NP for synthesis of bio-hybrid

A number of combinations were tried out for optimizing the integration of *Sphingomonas sp.* cells with ^{f}silica NP and quantified in terms of maximum MP hydrolysis or PNP formed. Different concentrations of PEI (0.001-0.1%) for functionalization of silica NP were tested for maximum formation of PNP (Fig. 3.3). It was observed that 0.01% PEI is able to functionalize 0.1% silica NP.

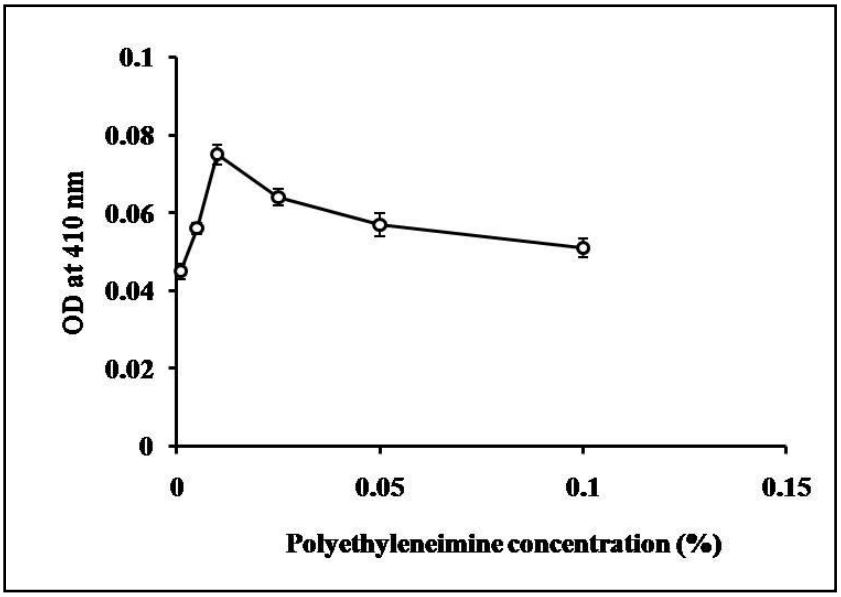

Fig. 3.3. Optimization of concentration of polyethyleneimine (PEI)

Results of optimization of ratio of cells to ^{f}silica NP are shown in Fig. 3.4. As shown in Fig. 3.4, it was observed that 1:2 ratio of cells to ^{f}silica NP showed maximum hydrolysis of MP and on further increase in the ratio there is no increase in PNP formation. A possible explanation could be that an optimum concentration of ^{f}silica NP is required for binding on the cell surface and to cover the whole surface of cell. However, at lower ratio of 1:3, the amount of ^{f}silica NP may not be sufficient to cover the overall surface of cells. Therefore, for further study, 1:2 ratio of cells to ^{f}silica NP was used.

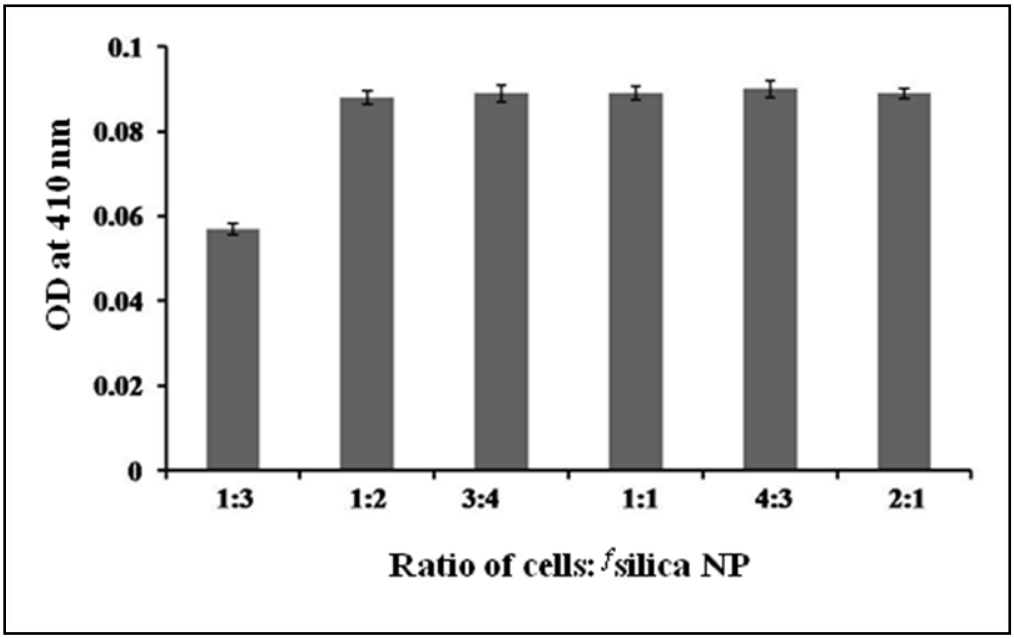

Fig. 3.4. Optimization of ratio of cells:^{f}silica NP

3.3.2. Characterization of synthesized bio-hybrid through FTIR study

FTIR spectra of silica NP, ^{f}silica NP, *Sphingomonas sp.* cells and bio-hybrid of *Sphingomonas sp-*^{f}silica NP was recorded as shown in Fig. 3.5. FTIR spectra of the silica NP showed peaks at 1109 cm^{-1}, 956 cm^{-1}, 800 cm^{-1} corresponding to the asymmetric vibration of Si-O-Si, asymmetric vibration of Si-OH and symmetric vibration of (Si-O-Si) groups, respectively [183]. After functionalization of silica NP with PEI new peaks appears at 3500-3200 cm^{-1} which are assigned to the NH stretch and OH stretch and peak at 1464 cm^{-1} assigned to stretching vibration of $-CH_2$ and $-CH_3$ functional groups which confirms the functionalization of silica NP. Spectra of *Sphingomonas* cells showed peak at 3500-3200 cm^{-1} which are assigned to the NH stretch and OH stretch. The peak at 1395 cm^{-1} was characteristic of C=O symmetric stretching of the COO^{-} group of biomolecules. A peak at ~1654 cm^{-1} and ~1530 cm^{-1} corresponds to amide I and amide II, respectively that characterizes the presence of protein [183]. Stretching vibration of $-CH_2$ and

-CH_3 groups were detected at 1400-1460 cm^{-1}. Peak at ~1240 cm^{-1} is due to the -C-O stretching and C-O-H asymmetric stretching of -COOH group. After integration of cells with ^{f}silica NP the bio-hybrid showed the peaks at 3500-3200 cm^{-1}, 2929 cm^{-1}, 2357 cm^{-1}, 1652 cm^{-1}, 1534 cm^{-1}, 1454 cm^{-1}, 1390 cm^{-1}, 1105 cm^{-1} and 798 cm^{-1}. Peaks of cells and ^{f}silica NP were present in the spectra of bio-hybrid of *Sphingomonas sp.*-^{f}silica NP. The disappearance of peak at 1240 cm^{-1} and changes in the region 1380-1400 cm^{-1} suggests the role of carboxylic group for integration with ^{f}silica NP. Peak at ~ 950 cm^{-1} present in ^{f}silica NP was missing in spectra of bio-hybrid which shows involvement of silanol (Si-OH) groups in the integration of silica NP with PEI. The presence of peaks due to ^{f}silica NP and cells in the bio-hybrid supports the fact of integration of cells with silica NP.

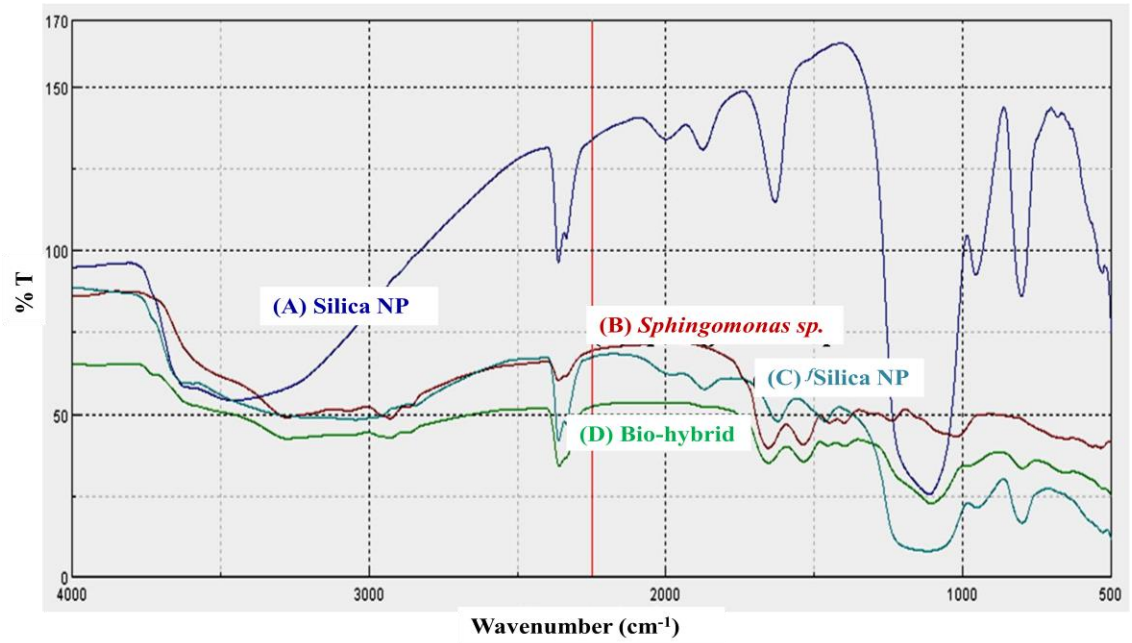

Fig. 3.5. FTIR study of (A) silica nanoparticles (silica NP), (B) ^{f}silica NP, (C) *Sphingomonas sp.* cells and (D) bio-hybrid of *Sphingomonas sp.*-^{f}silica NP

3.3.3. Immobilization of bio-hybrid onto microplate

Immobilization of microorganisms on a suitable support or the transducer plays a very pivotal role in the development of a biosensor. A number of methods such as adsorption, adsorption followed by cross-linking, covalent attachment and layer-by-layer (LbL) approach etc. have been extensively applied for the immobilization of microbial cells/enzymes [143-144, 175, 200, 205, 210-213]. Microbial cells and enzyme were immobilized onto the well surface of microplate by adsorption followed by cross-linking and used for developing biosensors [143-144, 209]. In the present study, microplate made up of polystyrene was used for the immobilization of bio-hybrid component. In previous studies, microplate has emerged as a suitable support for immobilization because the microplate are vacuum gas plasma treated and in the process, highly energetic oxygen ions are generated, which then oxidize and get grafted onto the surface of polystyrene chains [209, 214]. Because of this the interior surface of wells are negatively charged and are suitable for immobilization of positively charged biomolecules on interior surface of the microplate. Herein, cells integrated with ^{f}silica NP are positively charged due to PEI and easily get adsorbed on negatively charged interior surface of wells of microplate. The advantages of microplate based assays are the requirement of small sample volumes and simultaneous analysis of multiple samples on a single platform. Another important aspect is response time which is only 5 min for the measurement of multiple samples on single platform. This is the first report where *Sphingomonas sp*. cells were integrated with ^{f}silica NP and further immobilized onto polystyrene microplate and used for optical biosensor application.

(a) Optimization of amount of bio-hybrid for immobilization onto microplate

One of the important study is to optimization of amount of bio-hybrid immobilized onto surface of wells due to availability of limited space on the bottom surface of the wells (diameter = 5.7 mm; area = 25.74 mm^2) of microplate. Thus, to understand the effect of bio-hybrid loading, different amounts of bio-hybrid were used for immobilization and PNP formation was measured. Different amount of bio-hybrid from 10 to 60 µL was immobilized (Fig. 3.6). However, maximum formation of PNP was observed at 40 µL of bio-hybrid. Further increase beyond 40 µL, causes no increase in PNP formation which may be due to leaching of excess cells during washing. This shows that on the limited space at the bottom of the well, 40 µL of bio-hybrid can be immobilized to get best signal for detection. Therefore, 40 µL of bio-hybrid was used for the subsequent experiments.

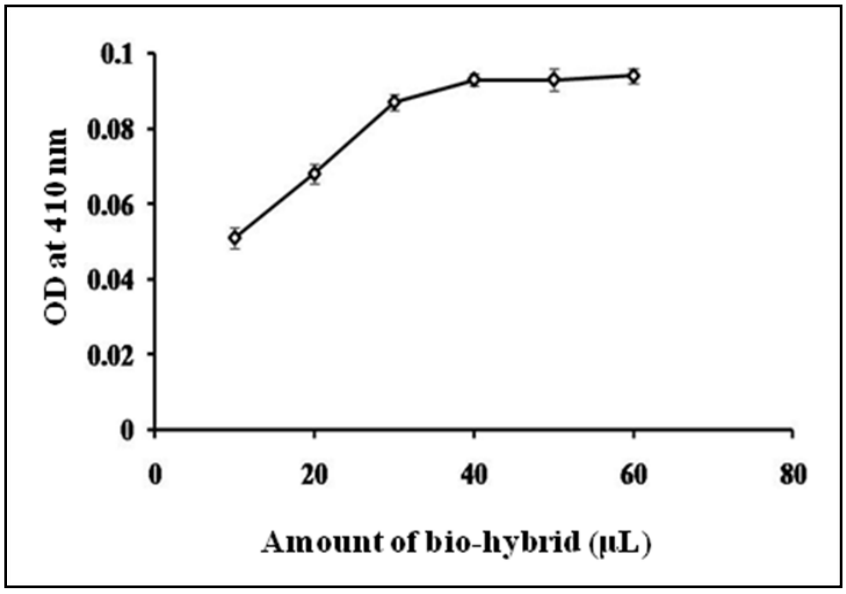

Fig. 3.6. Optimization of amount of bio-hybrid for immobilization

(b) Optimization of glutaraldehyde (GA) concentration for immobilization

Different concentrations of glutaraldehyde (0.5%-5% (v/v)) were used for the cross-linking of bio-hybrid onto the microplate wells as shown in Fig. 3.7. A 2% glutaraldehyde concentration was found optimum for cross-linking of bio-hybrid on the microplate. Further increase in glutaraldehyde concentration led to decrease in formation of PNP as shown in Fig. 3.7. This work is in agreement of previous results [143]. Glutaraldehyde is a well known cross-linking agent as well as a protein denaturing agent; excess glutaraldehyde may have an adverse effect on microbial enzyme which causes decrease in PNP formation.

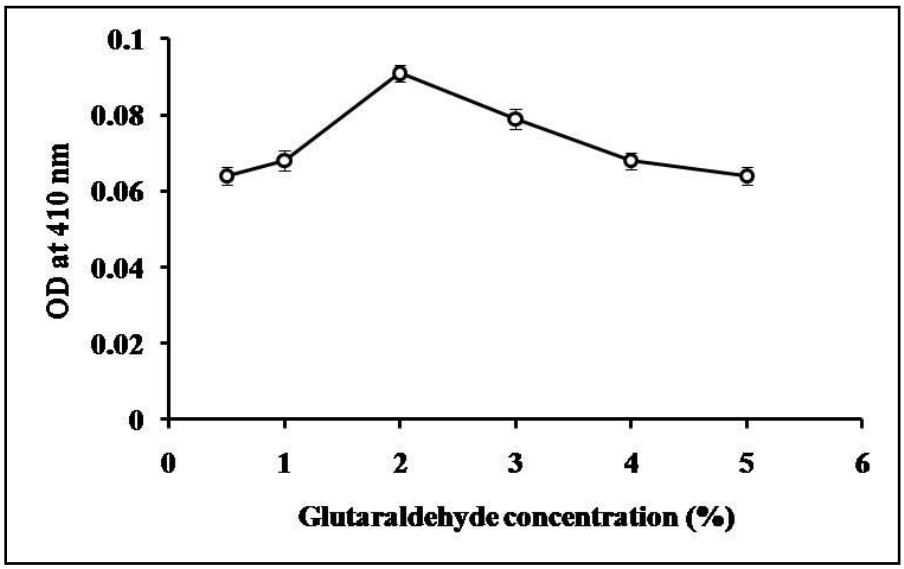

Fig. 3.7. Optimization of glutaraldehyde concentration for immobilization of bio-hybrid

3.3.4. SEM study of the bio-hybrid immobilized onto microplate

SEM analysis was carried out to observe the changes in the surface characteristics of wells after immobilizing *Sphingomonas sp.* cells and bio-hybrid. In Fig. 3.8., SEM image of wells immobilized with cells and bio-hybrid is shown. In the micrograph of cells immobilized onto surface of well, only bacterial cells were observed which were cross-linked (Fig. 3.8a) while in case of bio-hybrid immobilized well, cells were embedded in silica (Fig. 3.8b). One can see in Fig. 3.8a., there are less number of cells when plain cells were immobilized while the number of cells were much higher when bio-hybrid was immobilized (Fig. 3.8b.). Better binding was observed in case of bio-hybrid immobilized onto wells which may be because the bio-hybrid is positively charged and surface of well is negatively charged. However, in case of plain cells which were immobilized on wells, the cells and surface of wells both are negatively charged and limited binding was seen due to the cross-linking. SEM micrographs confirm the immobilization of bacterial cells and bio-hybrid onto the wells of microplate.

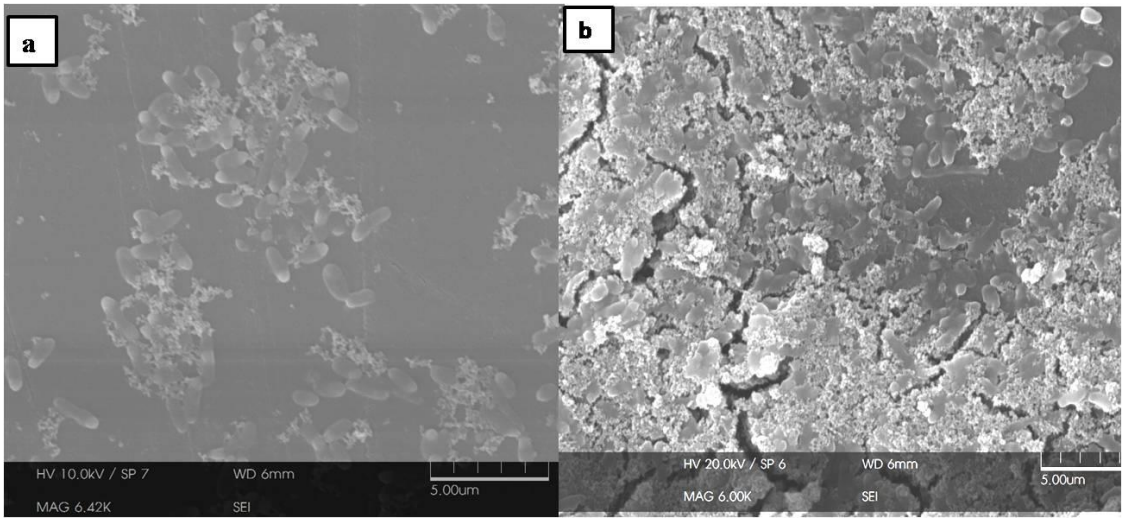

Fig. 3.8. SEM micrographs of (a) *Sphingomonas sp.* cells and (b) bio-hybrid of *Sphingomonas sp.*[f]silica NP immobilized on microplate

3.3.5. Calibration studies using immobilized bio-hybrid onto microplate

Different (0.1-5 ppm) concentrations of MP were used for calibration study of developed biosensor (Fig. 3.9). From calibration plot, a linear range (with linear regression equation, y = 0.0443x + 0.0387, r^2 = 0.997) was achieved between 0.1-1 ppm which shows the detection range of the biosensor. Therefore, developed biosensor is able to detect 0.1-1 ppm of MP and this observation is better than our earlier reports [142-144]. The developed biosensor has potential to analyze multiple samples of MP in the range of 0.1-1 ppm which lies in the MRL value as per FAO/WHO Codex Alimentarius Commission and FSSAI recommendation.

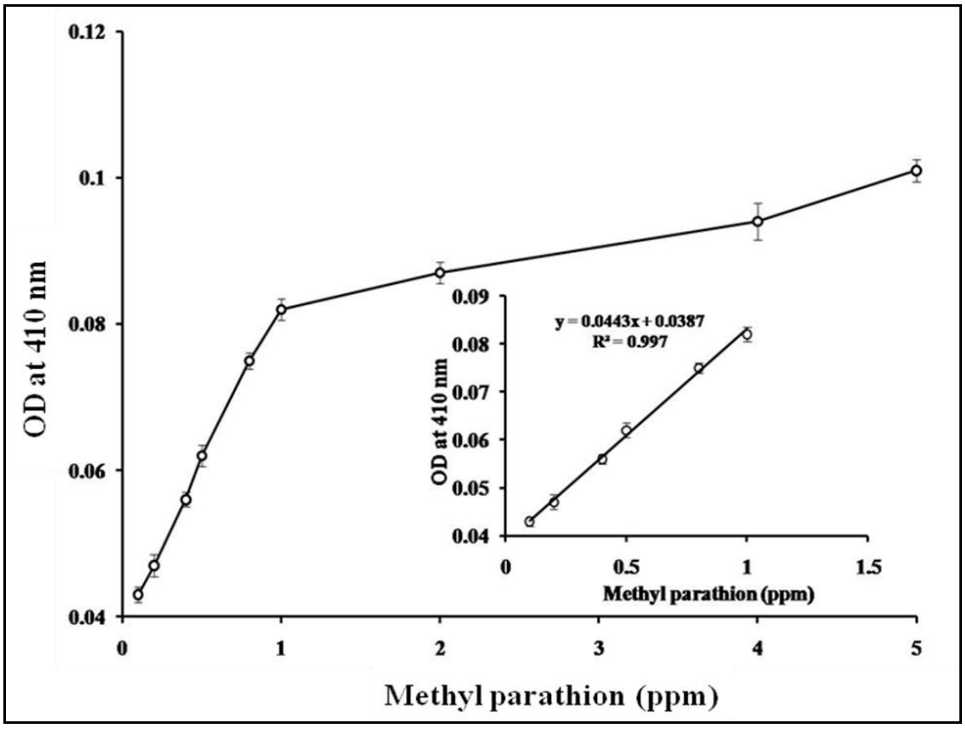

Fig. 3.9. Calibration of the biosensor using MP (0.1-5 ppm) (inset: linearity between 0.1-1 ppm with linear regression equation, y = 0.0443x + 0.0387, R^2 = 0.997 where 'y' represents the absorbance at 410 nm and 'x' the substrate concentration)

3.3.6. Storage stability and reusability study of developed biosensor

The storage stability of the biosensor is presented in Fig. 3.10. The stability of the biosensor was monitored at regular intervals. Developed biosensor showed storage stability upto 180 days with retention of 85 % activity (stored at 4 ^{0}C), while in our previous study; biocomponent was stable only for 18 days. This shows that in present study storage stability has increased by ten times [143]. The possible explanation for increased storage stability could be due to the binding of ^{f}silica NP on microbial cells surface which further act as a protective covering around the cell and reduces the leaching of hydrolytic enzyme [215] which is present in microbial cells. Nassif *et al*. have also reported that silica imparts positive impact on survival of microbes and helps to maintain enzyme activity [137]. This increased storage stability of biosensor will help to improve the practical applicability of the biosensor in many practical/routine applications in various fields like decentralized field testing, screening and rapid detection of multiple samples for a longer period of time. This will also avoid the time consuming preparation of a fresh biosensor.

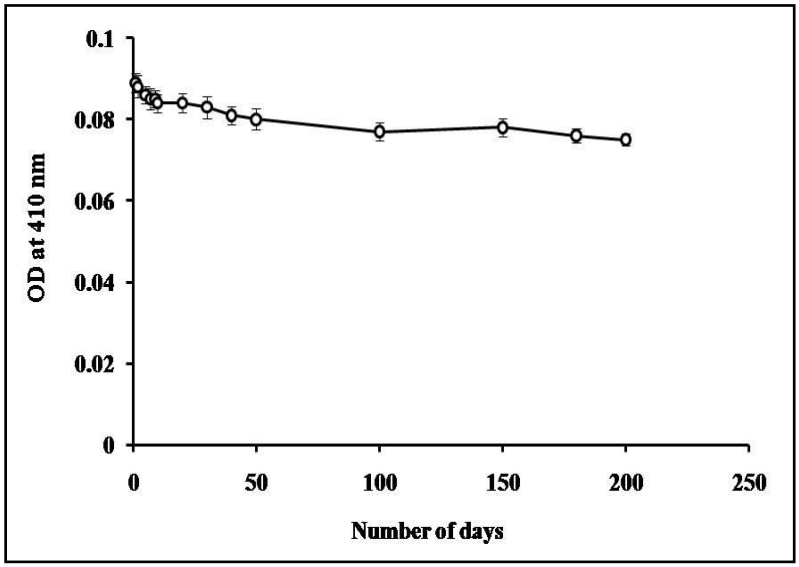

Fig. 3.10. Storage stability of the bio-hybrid-immobilized onto microplate

The reusability of biosensor (stored at 4 ^{0}C) was also carried out (Fig. 3.11). The results showed that 81% of enzyme activity was retained even after 10 repeated cycles.

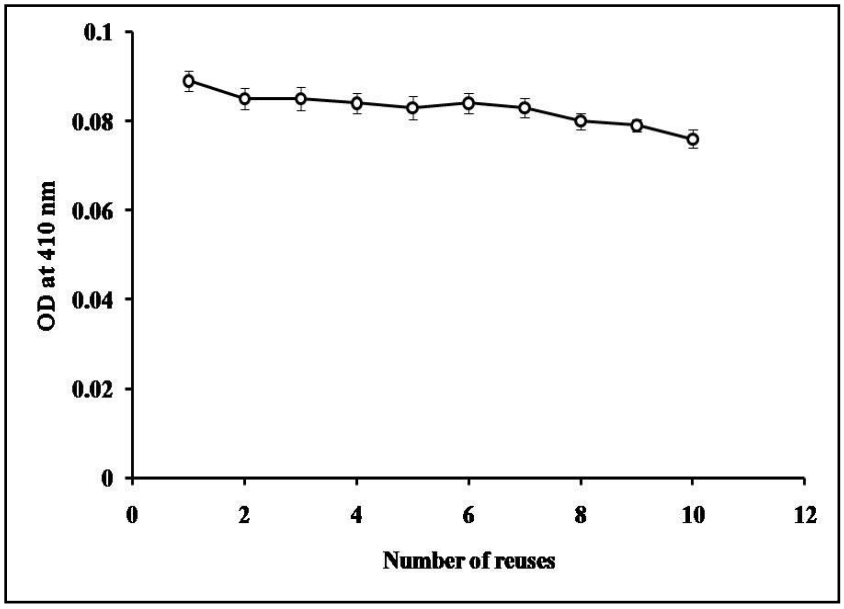

Fig. 3.11. Reusability of the bio-hybrid-immobilized onto microplate

3.3.7. Interference study in presence of different compounds

Interference study was carried out using different organic compounds like sucrose, glucose, carbaryl, malathion and monocrotophos to study the specificity of developed biosensor for MP detection. It was seen (Table 3.1) that glucose and sucrose were not interfering in hydrolyzing the MP. Carbaryl is one of the non-specific compounds which did not interfere during detection of MP. Although malathion and monocrotophos are the substrates of OPH enzyme but in present study, these organophosphate pesticides did not interfere during detection because their hydrolyzed products are not chromophoric like p-nitrophenol (PNP). Basic principle of the

biosensor is to detect the production of PNP by *Sphingomonas* cells which is determined by measuring absorbance at λ_{max} 410 nm (ε_{410} = 16,500 M^{-1} cm^{-1} for PNP).

Table 3.1. Interference study in presence of different compounds

Compounds (1ppm)	**PNP production (%)**	**Interference (%)**
MP only	100	0
MP + Sucrose	98.7	1.3
MP + Glucose	97.4	2.6
MP + Malathion	101.29	-1.29
MP + Monocrotophos	97.8	2.2
MP + Chloropyrifos	98.3	1.7
MP + Carbaryl	97.0	3.0

3.3.8. Analysis of spiked sample with developed biosensor

To study the practical applicability of the proposed biosensor spiked samples were used. Water samples were spiked with different concentrations of MP (0.2, 0.4, 0.5, 0.6, 0.8 and 1 ppm) and then subjected to measurement using developed biosensor. There were 5 replicates for each of the six different concentrations studied. All spiked samples were analyzed at the same time using microplate biosensor. As shown in Fig.3.12, the values of MP concentrations obtained by using the biosensor showed good correlation with that of known spiked concentration values of MP. The straight line fit gave a linear regression equation of $y = 1.0061x + 0.0114$ ($R^2 = 0.9997$), which demonstrated the feasibility of the developed biosensor for stable and sensitive detection of multiple MP samples.

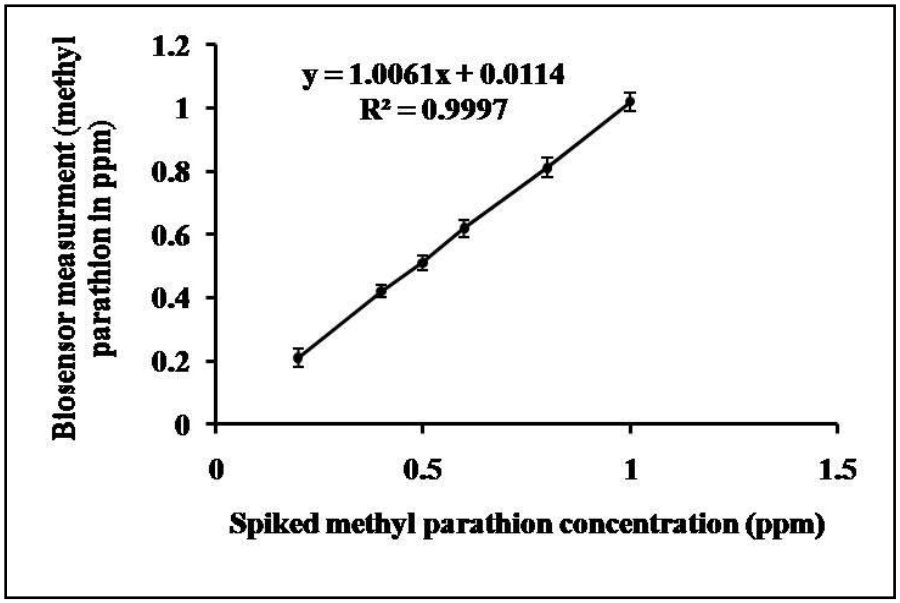

Fig. 3.12. Correlation between the spiked concentrations of MP in water and corresponding data obtained from developed biosensor

To further explore the application of developed biosensor, grape samples were soaked with different concentration of MP, adsorbed MP was extracted in phosphate buffer and the same was used for detection of MP on the developed microplate based biosensor. Results of MP concentration on grapes and the biosensor reading value is mentioned in the table 4.2. This observation showed a good correlation between known spiked concentrations of MP.

Table 3.2. Biosensor measurement of MP in grape samples soaked with different concentrations of MP

MP concentration used for soaking grapes (ppm)	MP concentration adsorbed by grapes after soaking (ppm)*	Biosensor measurement of adsorbed MP (ppm)
10	0.2	0.186±0.013
20	0.8	0.776±0.042
30	1.0	0.963±0.068

* Grape samples were soaked in different concentrations of MP (10, 20, 30 ppm) for 30 min, air dried and extracted as mentioned in section 2.10. Remaining concentration of MP was measured in the spent and washing to know how much MP was adsorbed by grapes.

3.4. Conclusion

Herein, we describe the synthesis of a functional bio-hybrid component by assembling ^{f}silica NP on the surface of *Sphingomonas sp.* cells. Bio-hybrid was further immobilized onto 96 well microplate and immobilization was confirmed by SEM. The detection range of this optical biosensor for the detection of MP is 0.1-1 ppm which is in the range of MRL value of MP and the storage stability is 180 days. Spiked samples of MP were also analyzed using the developed optical biosensor and showed a good correlation with the known spiked concentrations. Present study thus opens a window of interest where *Sphingomonas* cells can be associated with silica

NP to overcome the poor storage stability of enzymes present in cells. This innovative concept leads to the development of a stable and sensitive optical microbial biosensor for detection of MP. The biosensor developed in present study is an alternative to other analytical methods and shows beneficial aspect of application of silica nanoparticles. In this work, it was observed that using microbe as template bio-hybrid was synthesized successfully. The next step is to develop a suitable and efficient method for preparing bio-hybrids of microbial cells and silica NP for application in processing wherein mass scale production of bio-hybrids is required. To achieve this, a bio-hybrid of *Streptococcus lactis* cells and silica NP was synthesized using spray drying technique, in the next chapter.

Chapter-4

Synthesis of silica nanoparticles-*Streptococcus lactis* bio-hybrid for removal of uranium (VI)

4.1.Introduction

The removal of uranium from waste water is of great significance for human health and environment. As discussed in chapter 1, large number of adsorbents have been explored for removal of heavy metals. Among them nanosize silica i.e. silica gel and silica particles have been widely applied for sorption of uranium [145-149]. Nanoparticles offer a number of advantages however, the application of nanoparticles as adsorbent has certain issues regarding the environmental fate of nanoparticles, their harmful impact on human health and some technical limitations like difficulty in separation from aqueous systems.

For bioremediation of heavy metals as well as uranium, a variety of microbial systems have been also used [216-223].Yet, small size with low density, poor mechanical strength and less rigidity of microbial biomass are the bottlenecks [222]. Immobilization of biomass in a suitable support is the most efficient way for improving its mechanical strength and for effective utilization of biomass. Herein, the objective was to develop a stable and functional bio-hybrid material containing silica NP and micro-organisms to achieve the functionalization of material as well as in order to improve its practical applicability for remediation of U (VI) by the combined effect of silica nanoparticles and micro-organisms. Spray dried particles being higher in length scale help in separation once the reaction is over as well as this also helps to overcome the limitations of using silica nanoparticles and micro-organism alone.

Thus, in the present work, self assembled microstructures containing *S. lactis* cells and silica NP were synthesized through one step evaporation induced self assembly process, using a spray dryer. Further, the microstructures were used as a model system for remediation of uranium

wherein presence of cells helped in the functionalization of the support. For the first time, bioremediation of uranium has been carried out with spray dried self assembled microstructures containing *S. lactis* cells and silica nanoparticles. This approach opens a new route of interest in the field of material science for synthesizing functionalized bio-hybrids which finds application as suitable sorbent in the field of bioremediation.

4.2. Materials and methods

4.2.1. Materials

Silica NP (~ 15 nm) was obtained from VISA Chemicals, Mumbai, India. Overnight grown *S. lactis* cells in MRS Broth were used for study. Polyethyleneimine (PEI, average Mw ~ 7.5×10^5) was purchased from Sigma Chemical Co., MO, USA. Microstructures were synthesized using spray dryer LU222, LABULTIMA, India. A stock solution (2000 ppm) of uranium (VI) was prepared by dissolving appropriate amount of UO_2 $(NO_3)_2.6H_2O$ (Merck, Germany) in double-distilled water. 0.1 M HCl or 0.1 M NaOH was used to adjust pH of the solution in the range of 2.0 to 7.0. All chemicals were of analytical grade.

4.2.1.1. MRS Broth composition

MRS Broth contains: 10 g peptone, 10 g beef extract, 5g yeast extract, 20 g destrose, 1g polysorbate-80, 2g ammonium citrate, 5g sodium acetate, 0.1g magnesium sulphate, 0.050 g manganese sulphate and 2g Di potassium phosphate in 1L milli Q water and final pH was 6.5.

4.2.1.2. Preparation of media for growing cells

For preparation of media, 55.15 g of MRS powder was suspended in 1000 ml distilled water. The dissolved media was sterilized by autoclaving at 15 lbs pressure (121°C) for 15 minutes. Sterilized media was allowed to cool down and further used for growing cells.

4.2.1.3. Incubation of cells and recovery from media

1. Using a sterile pipette tip, a single colony was selected from the bacterial grown plate.
2. The colony present on the tip of pipette was transferred into the flask containing MRS broth and swirled.
3. The flask was incubated at 37 ^{0}C for overnight in a shaking incubator.
4. From overnight grown cells, 100 µL was transferred into fresh media and incubated at 37°C for overnight in a shaking incubator.
5. Overnight grown cells were centrifuged at 9000 rpm for 10 min and pellet then washed repeatedly to remove the media.
6. Washed cells were stored at 4 ^{0}C till further use.

4.2.2. Synthesis of non-incinerated and incinerated materials

The pellet of overnight grown *S. lactis* cells was weighed and 6% cell suspension was prepared. The suspension was mixed with 2% colloidal silica NP solution. This mixed suspension of silica NP and cells was used for spray drying and passed through the spray dryer. The spray dryer was operated at 413 K (140 ^{0}C) inlet temperature which resulted in 318 K (45 ^{0}C) outlet temperature. Spray drying leads to the synthesis of dried powder comprising silica NP and cells which was

further named as SDSM (Spray dried Doughnut Shaped Microtructures). In another set of experiment, *S. lactis* cells were treated with 2% polyethyleneimine (PEI) for 30 min with stirring in an incubator shaker. After this, PEI treated cells were harvested by centrifugation and washed three times with distilled water. PEI treated cells along with silica nanoparticles were spray dried (under identical condition as mentioned above) and further named as SSSM (Spray dried spherical Shaped Microtructures). Small quantity of the spray dried powder was incinerated at 673 K for 10 h. Synthesized spray dried incinerated and non-incinerated materials were used for uranium removal. Overall spray drying process is explained in Fig. 4.1.

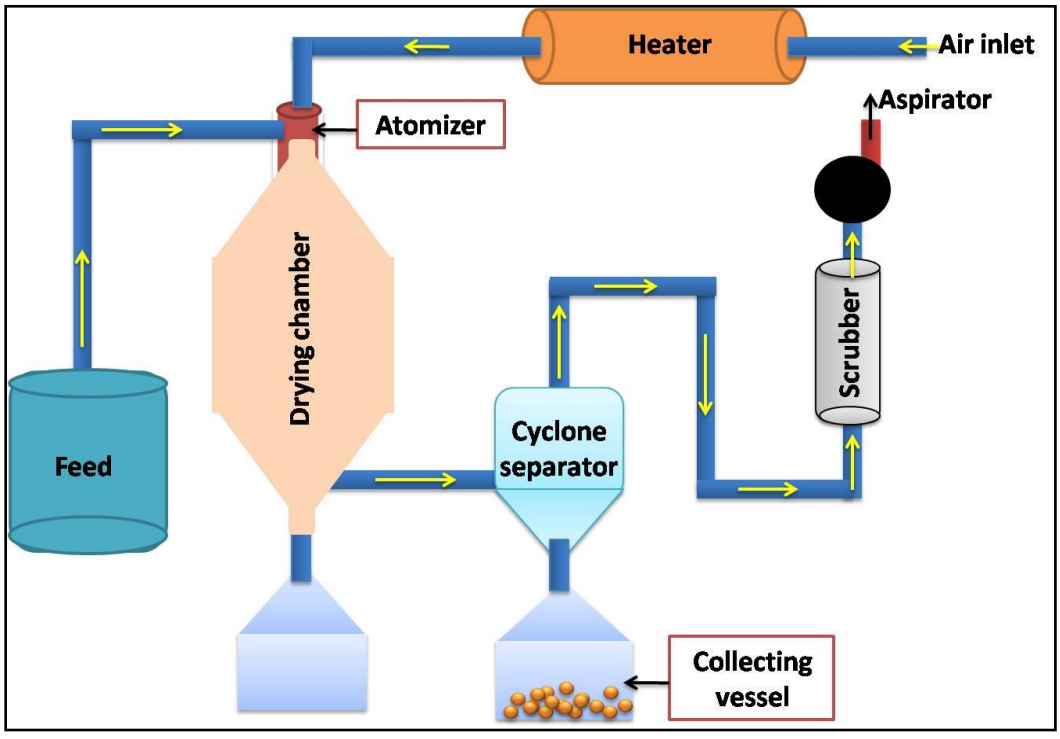

Fig. 4.1. Schematic presentation of synthesis of bio-hybrid using spray dryer

4.2.3. Characterization

SEM protocol

An environmental scanning electron microscope (Quanta 200 ESEM, FEI, USA) was used to characterize the microstructures. For SEM study, a very small quantity of spray dried powder (materials under the study) was applied on a carbon tape and mounted on stubs. The stubs were fitted on the stage of the SEM and further used for SEM analysis (Section 2.2.3.1).

TGA protocol

Thermogravimetric analysis (TGA) of the sorbents under study was performed using Netzsch Thermal analyser (STA 409 pc Luxx). For TGA analysis, the sample was placed in crucible and reinstalled the crucible with the wire basket (stirrup) onto the hang-down wire. The hang-down wire is connected to the microbalance at the top of the instrument. The sample was heated in the furnace under a flow of nitrogen up to 1000 ^{0}C. After this, sample weight was recorded, furnace was allowed to cool and crucible was removed.

FTIR protocol

Fourier transform infrared spectroscopy (FTIR) of the sorbents under study was recorded using Jasco FT-IR 660 plus spectrometer as discussed earlier in Section 2.2.3.2.

4.2.4. Batch adsorption experiments

Batch adsorption experiments were conducted to obtain rate and equilibrium data. The reaction mixture containing U (VI) solution of 50 mg/L concentration and 1 g/L of sorbent (unless otherwise mentioned) was agitated on a rotary shaker (MaxQ 4000, Thermo, USA) operating at

room temperature (298 K) and 150 rpm. From each flask, at regular intervals, aliquots were taken out and centrifuged at 9000 rpm for 5 min (Eppendorf centrifuge, Model-5810R, Germany) to separate the solid sorbent from the solution. The supernatant were analyzed for residual U (VI) concentration. Estimation of uranium (VI) was done by arsenazo (III) method as discussed below. In each set, uranium solution without sorbent was used as a control. Percentage removal of uranium was determined by using the following expression:

$$\text{Percentage removal (\%)} = [(C_0 - C)/C_0] \times 100 \quad (9)$$

Where, C_0 and C (mg/L) are the concentration of the U (VI) in the solution before and after sorption, respectively. All experiments were carried out in triplicate and the mean values with ± standard deviation were plotted.

4.2.5. Kinetics, sorption isotherm and thermodynamic studies

For kinetic studies, uranium solution (pH-5.0) of concentration 50 mg/L was contacted with SDSM (1 g/L) and samples were withdrawn at regular intervals for estimating uranium. Lagergren's pseudo-first and pseudo-second-order equation were used to model the kinetics of uranium sorption. Isotherm study was carried by varying uranium concentration (50-600 mg/L) at fixed sorbent concentration of 1 g/L. Samples were collected after incubation period (120 min), which was sufficient for the reaction to reach equilibrium. In order to examine the relationship between sorbent and aqueous concentration of uranium at equilibrium, Langmuir and Freundlich isotherm models were used to fit the data. U (VI) solution (50 mg/L) was contacted with SDSM (1 g/L) and incubated at different temperatures of 288 K, 298 K, 308 K and 318 K to determine the thermodynamic parameters. U (VI) solution as well as the biomass was incubated at the desired temperature before contact.

4.2.6. Reagents

1. *Standard uranium solution*: A uranium metal stock solution of 2000 mg L^{-1} was prepared by dissolving 422 mg of uranyl nitrate hexahydrate (Merk, Germany) in 100 mL of distilled water at room temperature and later diluted to the desired concentration as required. All other chemicals used were of analytical grade. It was further diluted to achieve a concentration of 50 mg/L.

2. *H_2 SO_4 solution (0.1 N, 500 mL)*: 1.25 mL of concentrated H_2 SO_4 solution was added to 448.75 mL of distilled water.

3. *Concentrated Arsenazo III reagent (0.1%, 500 mL)*: 0.5 g of Arsenazo III was added to 500 of 0.1 N NaOH solution. The pH of the solution was adjusted to 1.5 with the help of concentrated H_2 SO_4 solution.

4. *Dilution of Arsenazo III reagent*: 50 mL of the concentrated reagent was added to 450 mL of 0.1 N H_2 SO_4 solution and used for estimation.

Procedure for uranium (VI) quantification

1. Uranium solution of varying concentrations was prepared by taking the required amount of uranium solution from the diluted stock (50 mg/L) and mixing with distilled water in the test tube. A blank was also prepared which contained 1 mL of distilled water.

2. In all the tubes, 2.5 mL of Arsenazo III was added and mixed well.

3. The absorbance of the sample was measured at 650 nm. After appropriate correction, the absorbance of test samples was recorded.

4. The absorbance against uranium concentration was plotted to get a standard calibration curve.

5. The concentration of the unknown samples was determined using the standard curve.

The uptake of uranium per unit weight of microstructures was calculated using following expression:

$$q_e = [(C_0 - C_e)\, V]/M \quad (10)$$

where, q_e (mg/g) is the amount of U (VI) adsorbed onto unit weight of the adsorbent, C_0 and C_e (mg/L) are the concentrations of the U (VI) in the solution before and after sorption, respectively. V (L) is the volume of the aqueous solution and M (g) is the dry weight of the sorbent.

4.3. Results and discussion

4.3.1. Characterization of the synthesized materials

SEM analysis of the spray dried materials

SEM analysis of spray dried product comprising mixed colloidal suspension of silica nanoparticles-cells (SDSM) and silica nanoparticles-PEI treated cells (SSSM) were carried out. It was observed that SEM micrographs of synthesized microstructures have different morphologies depending on the physico-chemical conditions. As shown in Fig. 4.2a, microstructure comprising silica nanoparticles and *S. lactis* cells are doughnut in shape. In the SEM micrographs presence of cells was seen on the surface of SDSM. Fig. 4.2b showed that after incineration bacterial imprints become more prominent on the surface of SDSM. This may be due to remaining of

carbonaceous substances of bacterial biomass after heating. On the other hand, microstructure comprising of PEI treated cells and silica nanoparticles showed a spherical shape (SSSM) wherein the cells are less prominent in comparison to SDSM (Fig. 4.2c). Fig. 4.2d showed that after incineration, in SSSM also bacterial imprints become prominent. From Fig. 4.2, it was concluded that there is change in the shape of microstructures from doughnut to sphere because of PEI treatment. This transition from doughnut to sphere has been discussed earlier by us [181-182]. The plausible explanation given was most bacteria are known to have a negative charge on their surface because of their cell wall composition. It is well known that silica nanoparticles are negatively charged because of the presence of silanol groups on their surfaces. So, when a mixed suspension of virgin *S. lactis* cells and silica nanoparticles was used for spray drying, the dried grains showed extensive buckling and possessed deformed doughnut morphology. On the other hand, after changing the surface charge of cells by treating with PEI buckling is avoided. Herein, when PEI is coated on *S. lactis*, the negative charge of virgin *S. lactis* gets reduced and attains positive polarity. In such condition, the silica nanoparticles particles which are much smaller than cells form a particle cloud around cells and the air–water interface is mostly exposed to silica nanoparticles and hence the amplitude of buckling gets diminished, during drying process.

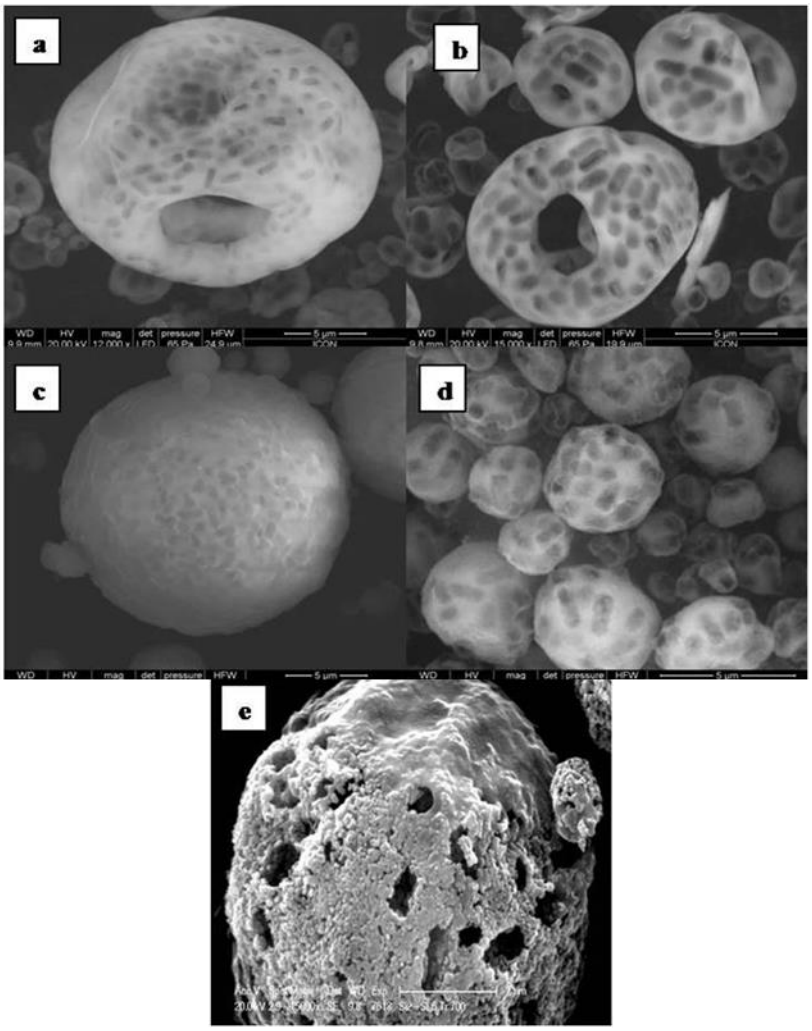

Fig. 4.2. SEM micrographs of microstructures (a) Spray dried doughnut shaped microstructures (SDSM) (b) incinerated SDSM (c) Spray dried spherical shaped microstructures (SSSM) (d) incinerated SSSM and (e) incinerated (973 K) silica microstructure.

4.3.2. Removal of U (VI) by synthesized sorbents

Herein, synthesized microstructures namely SDSM, incinerated SDSM, SSSM, incinerated SSSM, spray dried *S. lactis* cells and 2% spray dried silica nanoparticles were used as sorbent for removal of uranium (VI). The percent uptake of uranium (VI) by these sorbents is presented in Fig. 4.3.

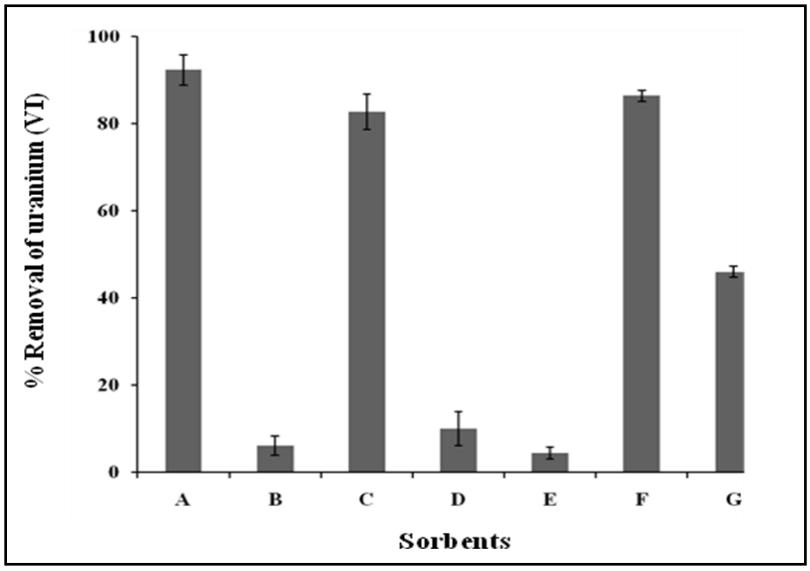

Fig. 4.3. % removal of U (VI) by the different microstructures: A–SDSM, B–incinerated (673 K) SDSM, C–SSSM, D-incinerated (673 K) SSSM, E-incinerated (973 K) SSSM, F-spray dried *S. lactis* cells and G-2% spray dried silica NP. (Experimental conditions: initial U (VI) concentration: 50 mg/L, dose of sorbents: 1 g/L except for spray dried *S. lactis* cells (0.5 g/L), temperature: 298 K, agitation speed: 150 rpm, contact time: 24 h, pH: 5.0) (mean ± SD of three replicates).

For SDSM and incinerated SDSM, the percent uptake of U (VI) was 92 ± 2% and 6 ± 1% respectively after 24 h of contact. In case of uranium uptake by SSSM, incinerated (673 K) SSSM and incinerated (973 K) SSSM, the percent uptake was 82 ± 3%, 10 ± 3% and 4.5 ± 1%, respectively. It was observed that the percent removal was highest for SDSM which may be because these microstructures being doughnut in shape can provide a higher surface area for uranium (VI) uptake. However, SSSM being spherical in shape offer less surface area for sorption of U (VI). Another important aspect is that during the synthesis of doughnuts in the spray drying process, the cells are present more on the outer surface. On the other hand, in case

of spheres, the cells are relatively less on the surface [181] and more are in the core of the sphere. Being inside, these cells are not easily accessible for binding with uranium ions and thus lesser sorption was seen.

As seen in the Fig. 4.3, both SDSM as well as SSSM show a lesser U (VI) uptake after incineration at 673 K and this represents the uptake by the silica microstructure only. Incinerated (673 K) SSSM showed more uptake of U (VI) in comparison to incinerated (673 K) SDSM. The possible reason may be that in SSSM as bacterial cells are present in the interior of the sphere, during incineration at 673 K all the cells are possibly not removed and thus involved in uranium binding. To corroborate this result, SSSM was also incinerated at further higher temperature i.e. 973 K for 10 h and it was observed that the uptake was reduced upto 4.5 ± 1%. To reaffirm this, thermogravimetric analysis (TGA) of SDSM and SSSM was carried out (Fig. 4.4). The mass loss caused till 450 K, is due to the volatilization of physically adsorbed water on microstructures [234]. In the temperature range of 450-670 K, the most significant mass loss which happens is because of the pyrolysis of bacterial component present in SDSM and SSSM. In the temperature range of 700-946 K, mass loss continued in SSSM compared to SDSM due to the presence of some bacterial cells in the interior of SSSM which was involved in binding of uranium ions in incinerated (673 K) SSSM. Further, heating upto 973 K caused pyrolysis of bacterial cells present in the interior of the sphere. Thus, the sorption of U (VI) by incinerated (973 K) SSSM got reduced as compared to incinerated (673 K) SSSM.

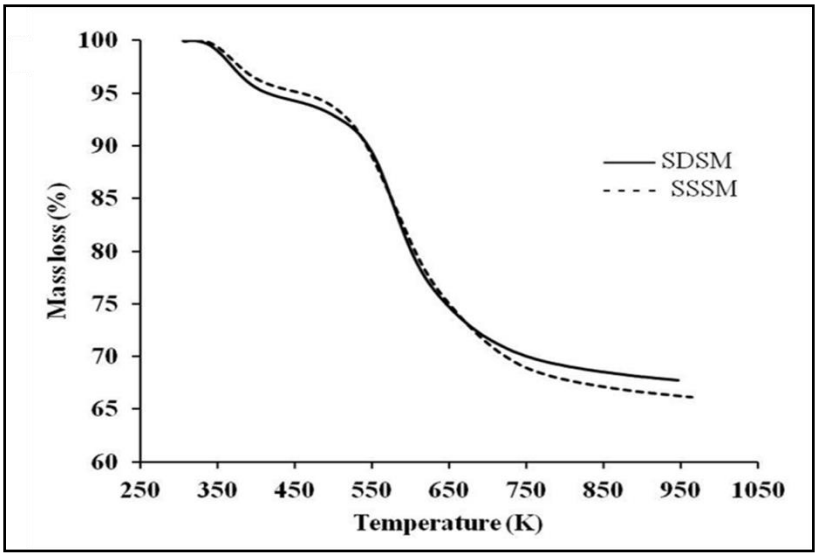

Fig. 4.4. TGA profile of SDSM and SSSM.

Plain spray dried 2% silica showed 46 ± 1% uranium uptake. However, incinerated SSSM and SDSM show much lesser U (VI) sorption as compared to spray dried silica microstructures although they too were representing the sorption by silica microstructures alone. A plausible explanation is that during the incineration, cell debris gets deposited over the silica surface or high temperature affects the silica morphology. As seen in Fig. 4.2e, coalescence of silica was observed when silica microstructures were exposed to high temperature which confirms that incineration at high temperature affects the silica microstructures which further led to reduced U (VI) uptake.

In case of plain spray dried *S. lactis* cells (0.5 g/L) 82 ± 1% uptake was observed. The amount of cells in SDSM and SSSM were 37.5% of its total dry weight and according to this the maximum uptake by the cells should be 61.5%. While the amount of silica in SDSM and SSSM were 62.5% of its total dry weight, as per this, the uptake by the silica should be 29%. So, the total

uptake by both the components in the microstructure should be a sum of both, that is 90% which is almost equal to the experimentally obtained value 92 ± 2% using SDSM. Thus, these results showed that a higher uptake was observed when cells were incorporated in silica microstructure. The similar values for calculated and experimental uptake studies, suggests that the functional groups are easily accessible in the case of SDSM to bind U (VI).

To understand the role of different functional groups in binding with U (VI), FTIR spectroscopy was carried out (Fig. 4.5.). FT-IR spectra for SDSM (metal-free), uranium loaded SDSM, spray dried silica and incinerated SDSM were recorded to elucidate the chemical groups involved in uranium ion binding. Analyzing the IR spectra, certain characteristic peaks can be assigned to the involvement of the functional groups present on the microstructures. The main characteristic bands observed for SDSM (Fig. 4.5A) were as follows: =O stretch at 1600-1700 cm^{-1} for amide I, NH deformation at 1500-1550 cm^{-1} for amide II, C-H stretch at 2890-2940 cm^{-1} and asymmetric vibration of Si-O-Si (1090 cm^{-1}) [222, 225-226]. The broad band centered at 3500-3200 cm^{-1} was assigned to the NH stretch, which overlaps the OH stretch in the same region. Stretching vibration of $-CH_2$ and $-CH_3$ functional groups in some aliphatic compounds, e.g. fatty acids could be detected at 1400-1460 cm^{-1} [226]. In the uranium loaded SDSM (Fig. 4.5B), the distinct peak at 928.56 cm^{-1} and changes in peak position and intensity around 550-1000 cm^{-1} region can be assigned to asymmetric stretching vibration of v_3 UO_2^{2+} and stretching vibration of weekly bonded oxygen ligands with uranium (v U–O_{ligand}). The FTIR spectra of the spray dried silica show absorption bands arising from asymmetric vibration of Si-O-Si (1090 cm^{-1}), asymmetric vibration of Si-OH (950 cm^{-1}), symmetric vibration of Si-O-Si (795 cm^{-1}) and the

band at 1635 cm^{-1} is due to scissor bending vibration of molecular water (Fig. 4.5C) [227]. The FTIR spectra of the incinerated SDSM (Fig. 4.5D) show that the bands at ~ 2900, ~1500, ~ 1400 and ~ 950 cm^{-1} are missing. This is the reason for the lesser uptake of uranium by incinerated SDSM because these wave numbers correspond to the functional groups which could be involved in the uranium (VI) uptake. The overall FTIR spectral analysis supports the involvement of hydroxyl, carboxyl, amide and silanol groups in uranium binding.

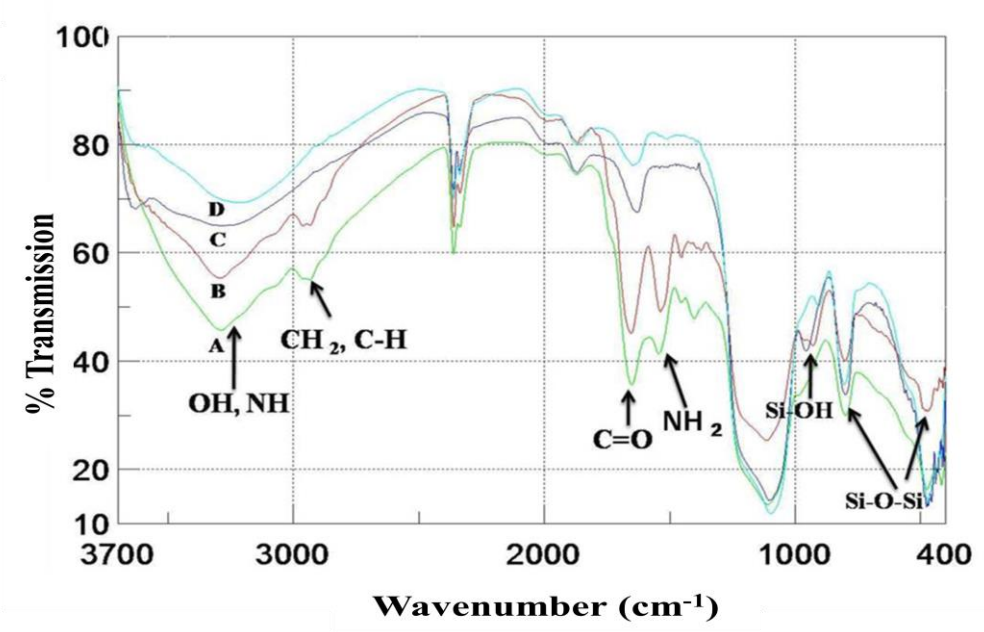

Fig. 4.5. FTIR spectra: (A) SDSM (B) U (VI) exposed SDSM (C) spray dried silica NP and (D) incinerated SDSM.

The process of spray drying and U (VI) sorption on SDSM is shown in Fig 4.6. These results suggests that *S. lactis* cells serve as a means to functionalize the silica microstructures which finds application in U (VI) remediation and silica served both as a sorbent as well as a support

material. As shown, SDSM showed maximum uranium uptake, thus further uranium removal was carried out using SDSM system only.

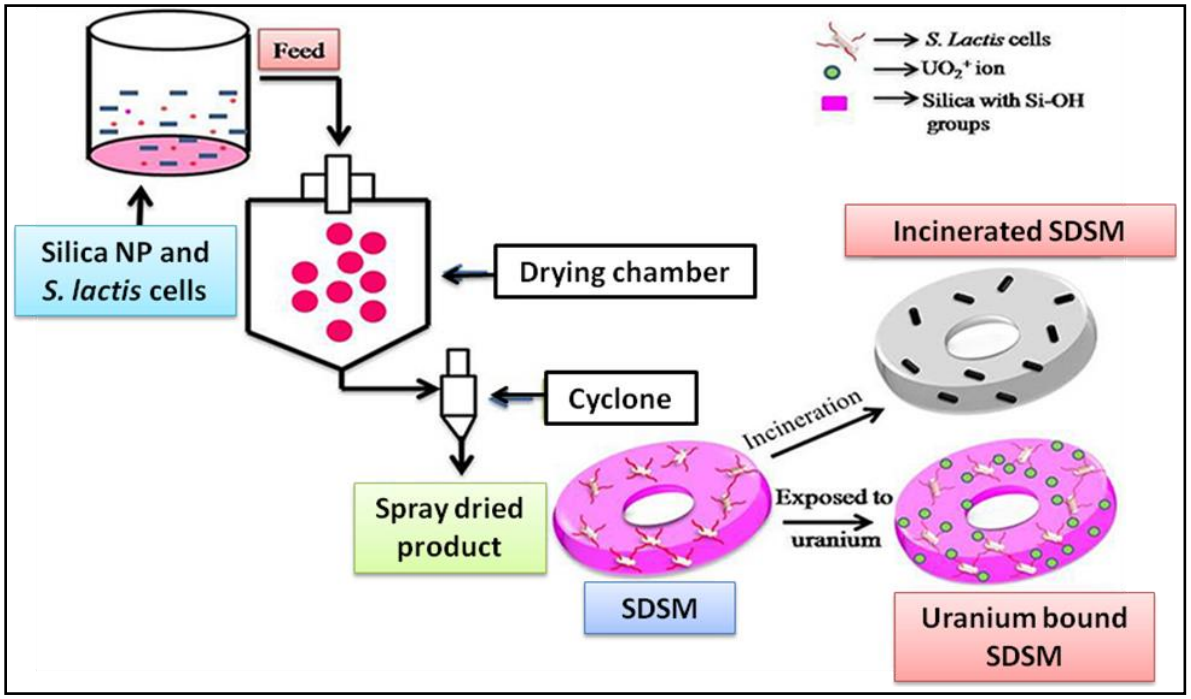

Fig. 4.6. Schematic illustration of spray drying process and U (VI) adsorption on SDSM.

4.3.3. Effect of solution pH on U (VI) removal

The effect of solution pH was studied in the sorption of uranium (VI) using SDSM as sorbent (Fig. 4.7). As seen in Fig. 4.7, adsorption capacity increases with an increase in pH from 2.0 to 5.0 however further increase in pH from 5.0 to 7.0 causes decrease in sorption. Herein, SDSM showed U (VI) uptake at a relatively broad range of pH (3 to 6) with an optimum pH at 5.0. At lower pH (pH-2.0), higher concentration of H^+ ions are present in the solution which competes with uranyl ion for the binding sites [191] and results in a decreased sorption of U (VI). The

functional groups like carboxyl, amide (Fig. 4.5) present on the surface of sorbent are responsible for the optimum uptake at pH 5.0 which have pK_a values in the range of 3-5 [228]. In general, at the pH near the pK_a value of functional groups present on the surface of sorbent, it shows highest availability of functional groups for binding of UO_2^{2+}. At higher pH value, decrease in adsorption of uranium could be due to the formation of uranyl complexes such as UO_2OH^+, $(UO_2)_2(OH)_2^{2+}$ and $(UO_2)_3(OH)^+_5$ [229]. The optimum initial pH was 5.0, and all further experiments were conducted at initial pH 5.0.

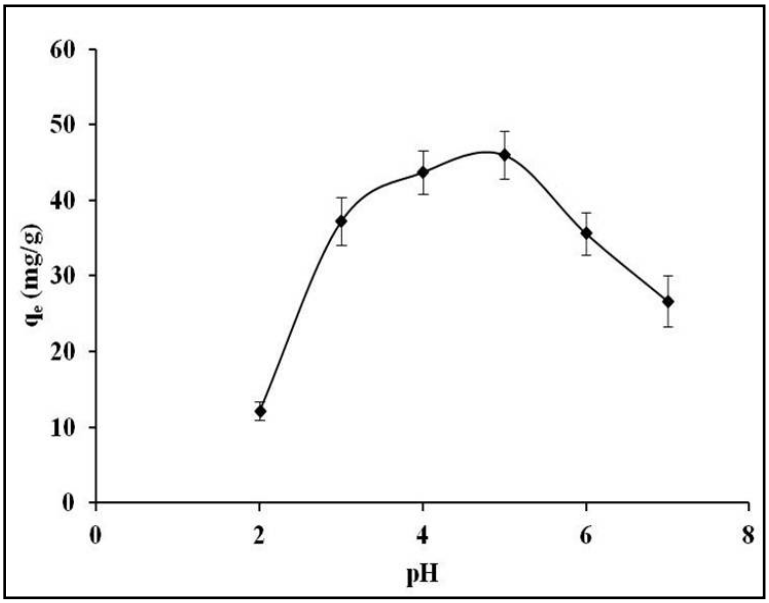

Fig. 4.7. Effect of solution initial pH on U (VI) adsorption capacity of the SDSM (Experimental conditions: initial U (VI) concentration: 50 mg/L, dose of sorbent: 1 g/L, temperature: 298 K, agitation speed: 150 rpm, contact time: 120 min) (mean ± SD of three replicates)

4.3.4. Adsorption kinetics of uranium (VI)

The adsorption profile of uranium (VI) by SDSM with time was shown in Fig. 4.8. In this study, sorption equilibrium is achieved in 120 min. As seen in the figure, sorption happens in two steps, in the first step adsorption is very fast followed by a slow adsorption process. Initially, within 10 min 85% U (VI) uptake occurs. The higher rate of adsorption in the first step may be due to easy availability of functional groups of sorbent for interaction with U (VI). The functional groups present on the surface of the microstructures interact to uranyl ion as soon as they come in contact with each other. As time passes, the availability of binding sites, as well as U (VI) concentration reduces which further leads to reduced rate of biosorption. The fast adsorption which has been observed is considered a good characteristic of a sorbent because it allows short contact time and also allows the use of sorbent materials in column applications [228].

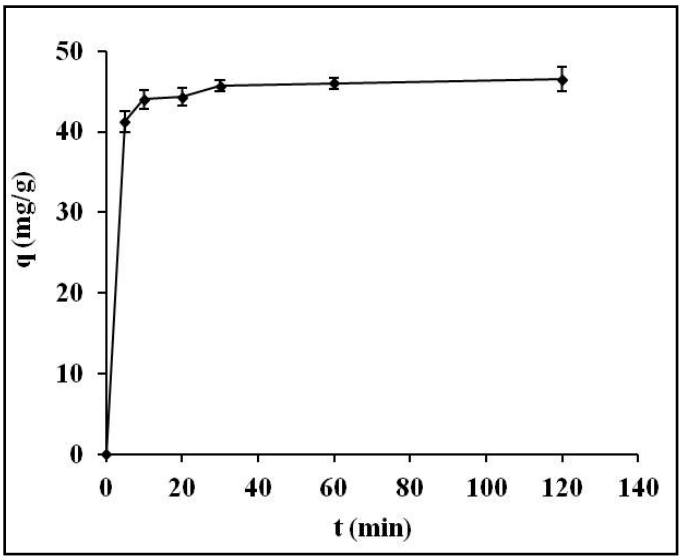

Fig. 4.8. Effect of contact time on U (VI) adsorption capacity of SDSM (Experimental conditions: Initial U (VI) concentration: 50 mg/L, dose of sorbent: 1 g/L, temperature: 298 K, agitation speed: 150 rpm, initial pH: 5.0)

Kinetic analysis of the adsorption process of uranium by SDSM was carried out. Kinetic analysis gives essential information on the sorption mechanism and the rate of sorption. To understand the mechanism of adsorption process, the linearized equation of pseudo-first-order and pseudo-second-order kinetic models were used and the results are mentioned in Fig. 4.9a and Fig. 4.9b. For the pseudo-first-order kinetic model the equation [191] is**:**

$$\log (q_e - q_t) = \log q_e - k_1 t / 2.303 \quad (11)$$

where, q_e and q_t are the amount of heavy metal ion adsorbed on the adsorbent in mg (metal)/g(sorbent) at equilibrium and at time t, respectively. The k_1 is the constant of first-order kinetics. The equation for the pseudo-second-order kinetic model [191] is:

$$t/q_t = 1/ k_2 q_e^2 + t/q_e \quad (12)$$

where, q_e and q_t are the amount of heavy metal ion adsorbed on the adsorbent in mg/g at equilibrium and at time t, respectively. The k_2 is the rate constant of second-order kinetics in g/mg/min. The initial uptake rate h (mg/g/min) is:

$$h = k_2 . q_e^2 \quad (13)$$

The values of q_e, k_1, k_2 and h are calculated and mentioned in Table 4.1. In pseudo second-order kinetics, the calculated q_e values were nearly the same as experimental values, and regression coefficient was found to be 0.99, which also confirms that the uranium (VI) adsorption process of the SDSM follows the pseudo-second-order model. Pseudo-second order model means the reactions in which one parameter is considered to be constant because it is present in very large quantity and the remaining two parameters are determining the reaction kinetics. Herein, the water is in access amount however the sorbent (SDSM) and metal ion are playing important role

in the sorption process. Uranium (VI) sorption onto *Catenella repens* [228] and immobilized *Aspergillus fumigatus* beads [222] shows similar results.

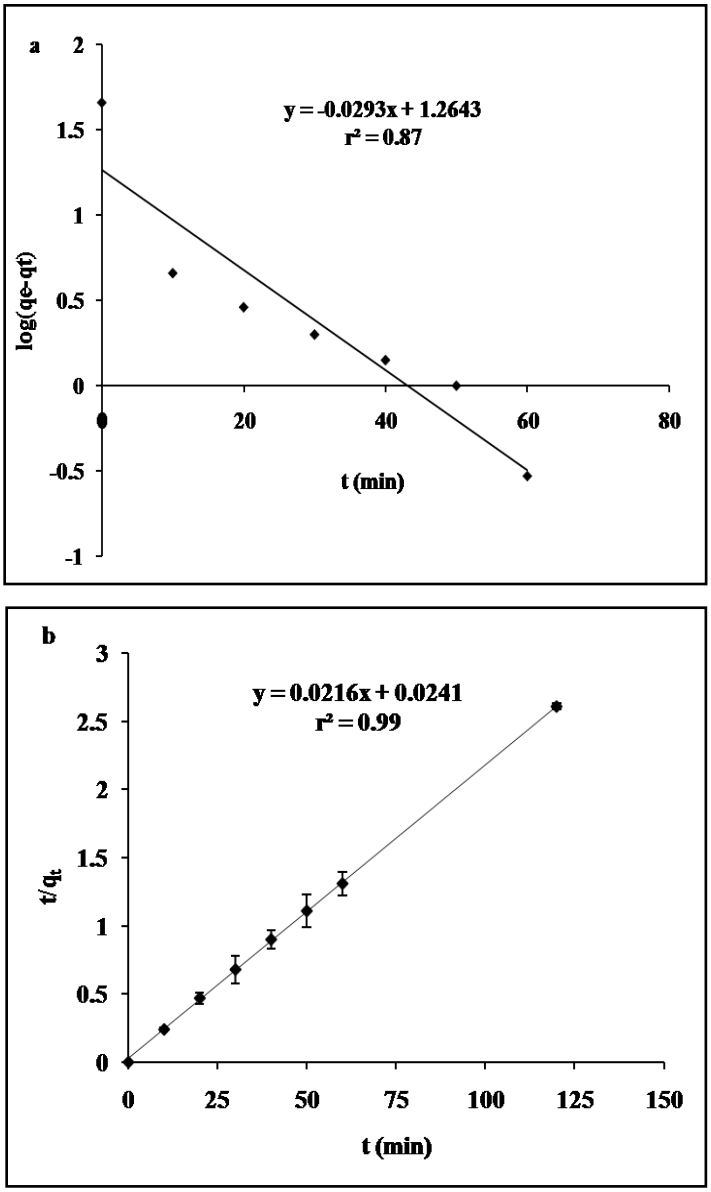

Fig. 4.9. (a) Pseudo first order kinetics and (b) Pseudo second order kinetics plot of U (VI) uptake onto SDSM (Experimental conditions: dose of sorbent: 1 g/L, temperature: 298 K, agitation speed: 150 rpm, contact time: 120 min, initial pH: 5.0)

Table 4.1. Pseudo-first-order, pseudo-second-order and experimental values for uranium (VI) adsorption

Experimental	Pseudo-first-order			Pseudo-second-order			Initial rate
q_e (mg/g)	k_1 (/min)	q_e (mg/g)	r^2	k_1 (g/mg/min)	q_e (mg/g)	r^2	h (mg/g/min)
46.0	0.067	18.37	0.87	0.019	46.3	0.99	40.73

4.3.5. Effect of initial U (VI) concentration on adsorption

The sorption capacity of SDSM at different uranium (VI) concentration is shown in Fig. 4.10. It was observed that initially when U (VI) concentration varies from 50 mg/L to 200 mg/L, there is a sharp increase in the sorption capacity. However, as the concentration was increased above 200 mg/L of U (VI), sorption capacity becomes gradually lesser. Possible reason could be because the sorbent concentration is constant (1 g/L) the number of binding sites are fixed. However, the number of uranyl ions increases with increase in U (VI) concentration. At low U (VI) concentration, saturation of sorbent by uranyl ion could not be obtained because the number of uranyl ion is smaller than the number of binding sites present on the surface of sorbent. Further, increase in the concentration of U (VI) in solution is expected to result in the increase of q_e till the saturation of sorbent is attained. As the binding sites present on the surface of sorbent got saturated with uranyl ions, the availability of binding sites for the U (VI) decreased [228].

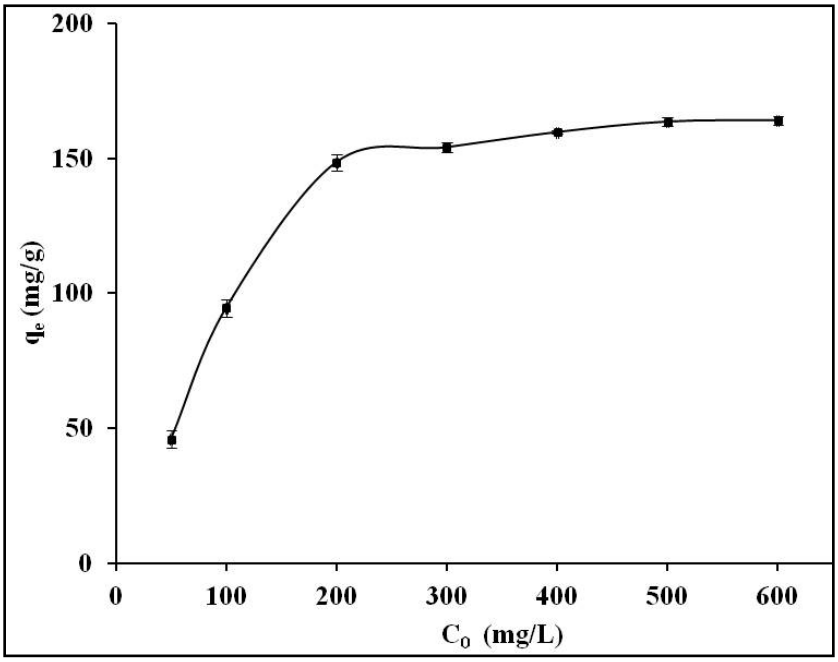

Fig. 2.10. Adsorption effect of varying initial U (VI) concentration (50-600 mg/L) onto SDSM (Dose of sorbent: 1 g/L, temperature: 298 K, agitation speed: 150 rpm, contact time: 120 min, initial pH: 5).

4.3.5. Adsorption isotherm study

For the design and operation of adsorption systems, the correlation of equilibrium adsorption data is important. Two isotherms models (Langmuir and Freundlich), were applied to the obtained adsorption data. In the Langmuir model, it is assumed that all the adsorption sites of the adsorbent have an identical binding energy and each site binds to only a single adsorbate [230]. The Langmuir isotherm is represented as:

$$q_e = (q_m K_L C_e) / (1 + K_L C_e) \quad (14)$$

The linearized Langmuir isotherm is written as:

$$C_e / q_e = 1/(q_m K_L) + C_e / q_m \quad (15)$$

where, q_e is the equilibrium adsorption capacity of adsorbent in mg (metal)/g(sorbent), C_e is the equilibrium concentration of metal ion in mg/L, q_m is the maximum amount of metal adsorbed in mg/g and K_L is the Langmuir constant which is related to sorption energy in L/mg [231]. q_m and K_L were determined from the slope and intercept of the straight-line plot between C_e/q_e versus C_e (Fig. 4.11) and are given in table 4.2. Regression coefficient value (r^2) indicated the best fitting of the data to the Langmuir equation (Table 4.2).

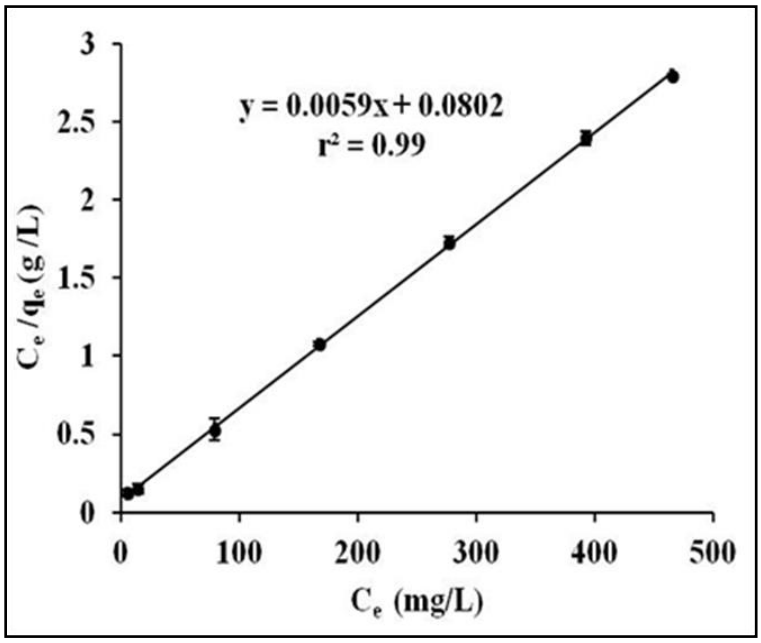

Fig. 4.11. Adsorption isotherm of U (VI) onto SDSM by Langmuir isotherm

The Langmuir isotherm can be expressed in terms of a dimensionless constant called equilibrium parameter, R_L which is defined as:

$$R_L = 1/(1+ K_L C_0) \quad (16)$$

Where, C_0 is the initial metal concentration. The value of R_L indicates the type of isotherm to be favorable ($0 < R_L < 1$), unfavorable ($R_L > 1$), linear ($R_L = 1$), or irreversible ($R_L = 0$) [231].

Fig. 4.12 shows that for the adsorption of U (VI) onto SDSM microstructures $0 < R_L < 1$. Because R_L is larger than zero, the adsorption process is considered favorable.

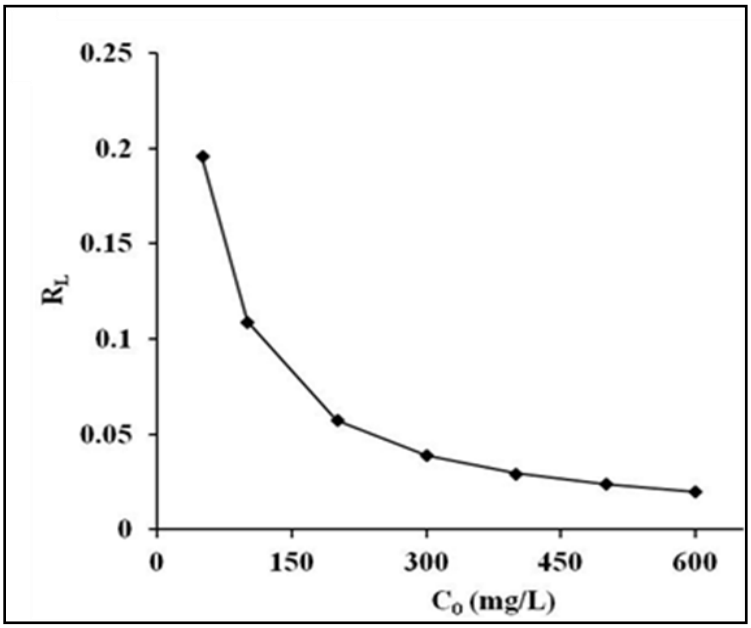

Fig. 4.12. Separation factor for adsorption of U (VI) onto SDSM. (initial U (VI) concentration: 50-600 mg/L, dose of sorbent: 1 g/L, temperature: 298 K, agitation speed: 150 rpm, contact time: 120 min, pH: 5.0).

On the contrary, the Freundlich model is based on a reversible heterogeneous adsorption since it does not restrict to monolayer adsorption capacity [191].

The Freundlich isotherm is written as:

$$q_e = K_F C_e^{1/n} \quad (17)$$

The linearized Freundlich isotherm is represented as:

$$\log q_e = \log K_F + 1/n \log C_e \quad (18)$$

where, q_e is the equilibrium adsorption capacity of the adsorbent in mg/g, C_e is the equilibrium concentration of heavy metal ion in mg/L, K_F [(mg/g)/(mg/L)$^{1/n}$] is the constant related to the adsorption capacity of the sorbent, and n is the constant related to the adsorption intensity [231]. It is generally stated that values of n in the range 2-10 represent good, 1-2 moderately difficult and less than 1 poor adsorption. Freundlich isotherms for the sorption of uranium onto SDSM microstructures are given in the Fig. 4.13. Table 2 shows that the r^2 value of Langmuir and Freundlich isotherm was 0.99 and 0.82, respectively. These values suggested goodness of fit for Langmuir isotherm (Fig. 4.11) compared to Freundlich isotherm, which suggested monolayer sorption of uranium onto the surface of SDSM. K_F and 'n' are calculated from the intercept and slope of the plot log q_e versus log C_e (Fig. 4.13). The value obtained for n (Table 4.2) in the range of $1< n <10$, being suggestive of a beneficial adsorption [228], indicated a beneficial sorption by the SDSM.

The applicability of the Langmuir isotherm for SDSM suggests that the surface of the sorbent is uniform and homogeneous and the sorption process results in the formation of monolayer coverage of U (VI) on SDSM. Similar conclusions were reported on U (VI) sorption by NP10 [159] and ordered nanoporous silica CMPEI/MSU-H [161]. Sorption capacities of different sorbents have been listed in table 4.3, which shows that SDSM is a better sorbent than Si1 silica gel [146], modified silica gel [148], modified MCM-41 [160], *Citrobacter freudii* [223] and others [147, 161] except NP10 [159].

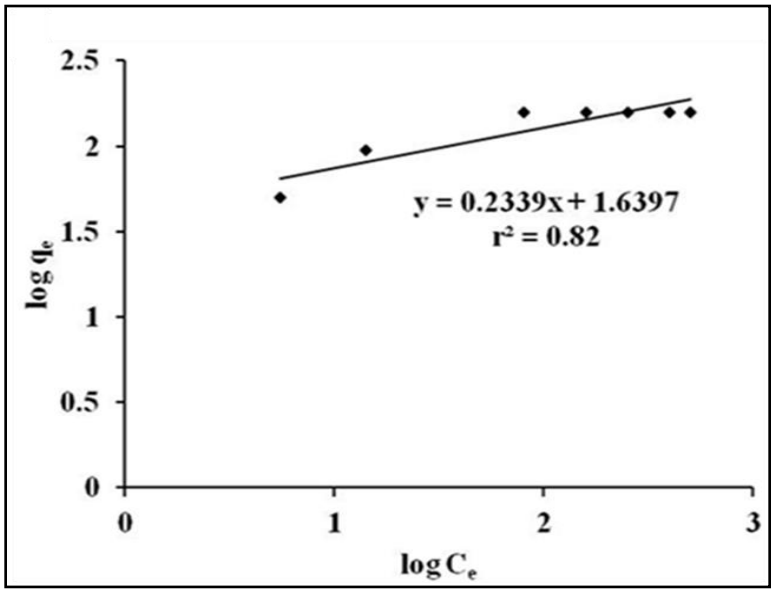

Fig. 4.13. Adsorption isotherm of U (VI) onto SDSM by Freundlisch isotherm

Table 4.2. Langmuir, Freundlich adsorption isotherm constants, correlation coefficients, maximum adsorption capacity and experimental adsorption capacity for uranium (VI) adsorption.

Experimental	Langmuir Isotherm			Freundlich Isotherm		
q (mg/g)	K_L (L/mg)	q_m (mg/g)	r^2	K_F [(mg/g)/(mg/L)$^{1/n}$]	n	r^2
164.0	0.07	169.5	0.99	43.62	4.28	0.82

Table 4.3. Comparison of uranium binding capacities of various sorbents

S. No.	Sorbents	Capacity of sorbent (mg/g)	References
1.	Modified silica gel	64.5	[148]
2.	Modified MCM-41	47	[160]
3.	Catechol – Silica gel	15.94	[147]
4.	NP10	268	[159]
5.	CMPEI/MSU-H	153	[161]
6.	Si1 (silica gel)	59	[146]
7.	*Citrobacter freudii*	48.02	[223]
8.	SDSM	164	Present work

4.3.6. Thermodynamic study of U (VI) sorption

The effect of temperature on adsorption of uranium (VI) using SDSM was investigated in the range of 288 to 318 K (Fig. 4.14). It is found that adsorption capacity (q_e) values increased from 45.2 to 47.1 (mg/g) as temperature is increased from 288 to 318 K. This slight change in the adsorption capacity could be due to increase in collision frequencies at higher temperature leading to more sorption. The slight increase in adsorption capacities (q_e) may reflect the saturation of surface sites of sorbent by the U (VI) at this range of temperatures [191].

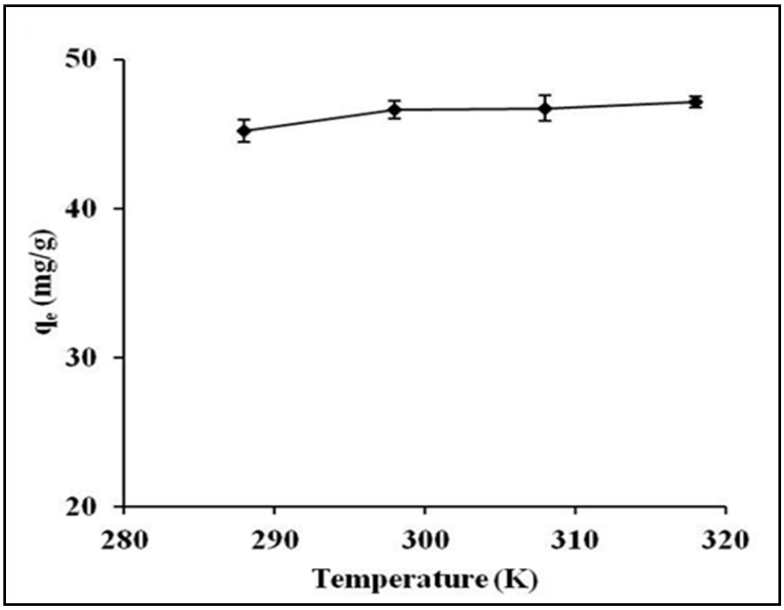

Fig. 4.14. Effect of temperature on U (VI) adsorption capacity of the SDSM

The thermodynamic parameters such as free energy change (ΔG^0), enthalpy change (ΔH^0) and entropy change (ΔS^0) for the sorption of U (VI) on SDSM were determined by the following equation:

$$\Delta G^0 = - RT \ln K \quad (19)$$

$$\ln K = \Delta S^0 / R - \Delta H^0 / RT \quad (20)$$

$$\Delta S^0 = (\Delta H^0 - \Delta G^0) / T \quad (21)$$

Where, R is the universal gas constant, 8.314 J/mol/K, T is temperature (K), and K is the adsorption equilibrium constant. Fig. 4.15 shows the plot of ln K versus 1/T fitted to a straight line Eq. 20. Values of ΔH^0 and ΔS^0 were calculated from the slope and intercept, respectively and are shown in Table 4.4. ΔG^0 values for the adsorption of U (VI) onto SDSM microstructures ranges from - 4.96 to - 6.34 kJ/mol, suggesting a physical adsorption process enhanced by

electrostatic effect [226]. The negative sign of ΔG^0 indicates spontaneous nature of the reaction while positive values of ΔH^0 confirms an endothermic nature of SDSM adsorption. The low value of enthalpy validates that the adsorption of U (VI) on SDSM was a physisorption process [229]. The positive value of ΔS^0 suggests increase in randomness of the system during the sorption process of U (VI). U (VI) sorption by *Citrobacter freudii* bacterium [223] and hydrous silica [232] shows similar results.

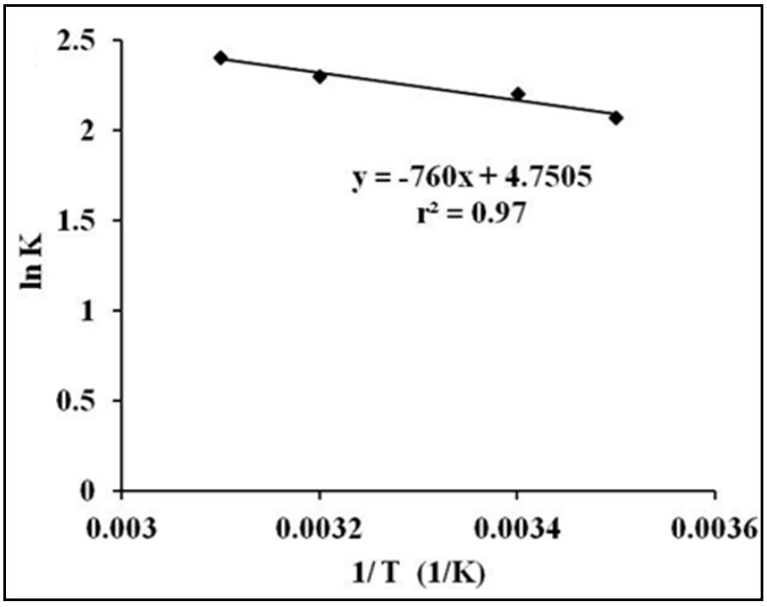

Fig. 4.15. Plot of ln K versus 1/T for the adsorption of U (VI) onto SDSM

Table 4.4. Thermodynamic parameters of uranium (VI) adsorption onto SDSM

ΔH^0 (kJ/mol)	ΔS^0 (kJ/mol/K)	ΔG^0 (kJ/mol)			
6.32	0.04	288 K	298 K	308 K	318 K
		-4.96	-5.46	-5.89	-6.34

4.4. Conclusion

A novel support was developed to overcome the limitations of using silica nanoparticles as such for remediation, by assembling the same, in a higher length scale. The bio-hybrid synthesized from silica nanoparticles and *S. lactis* cells, by the novel and economical method of spray drying, can serve as an alternative to the conventional process of obtaining organically modified silica. Incorporation of microbial cells served to functionalize the synthesized bio-hybrid using a single step of spray drying and overcome the requirement of chemical modification which is a costlier and time consuming process. SDSM emerged as suitable sorbent for uranium (VI) removal and more than 85 ± 2% of total uptake was observed in 10 min. The maximum sorption capacity (q_{max}) was 169.5 mg/g at pH 5.0. U (VI) adsorption data followed pseudo second order kinetic model and showed a better fit for Langmuir isotherm model. Thermodynamic parameters indicated that the sorption process was feasible and could occur spontaneously. Herein, spray drying emerged as an efficient, scalable and one step technique for synthesis of functionalized bio-hybrids. In view of this, in the next chapter spray drying has been used for the synthesis of another bio-hybrid comprising silica NP-sodium alginate. Also the impact of silica NP on association with biopolymer was studied in terms of drug release rate and efficacy of entrapped drug on lung cancer cells.

Chapter-5

Synthesis and application of silica nanoparticles-sodium alginate bio-hybrid as doxorubicin drug carrier

5.1. Introduction

The synthesis of new drug delivery carrier is important for high drug loading capacity and controlled drug release kinetics [233]. Silica based materials like mesoporous silica have been widely used as drug carrier because it exhibits several advantages such as high surface area, ordered structure, controllable pore size and various surface functionalities as discussed in chapter 1 [162-171, 234]. Mesoporous silica nanoparticles have been synthesized through sol-gel method in the presence of structure-directing agents (templates) in laboratory conditions [173, 233]. However, for its application as drug carrier in industry, there is a need to synthesize drug carrier in large scale. Another limitation of functionalized mesoporous silica based carrier is because of functionalization wherein the surface properties of carrier are altered and causes immunogenicity [173]. The poor penetration capability of nanosystems within the tumor mass, due to the presence of a collagen-rich extracellular matrix is one of the major issues which hamper the diffusion of nanocarriers [173].

On the other hand, polymeric additives like organic polymers are widely used in the pharmaceutical industry. The advantage is that they are able to penetrate the parts of the body which remain poorly accessible to other drug carriers. Additionally, due to the higher vascular permeability, as compared to free drugs, they can preferentially accumulate in tumors, thus, reducing side effects. Yet, due to low stability and low drug loading capacity its application is limited. Many of the polymer-based drug carriers like sodium alginate are very unstable in water and premature release of loaded drug is often a problem. Sodium alginate (a natural polysaccharide) is an abundant biopolymer which has high biocompatibility and biodegradability [233]. It is widely used in the food industry because it is generally regarded as safe by the US

Food and Drug Administration (GRN 328) [233, 235-237] Alginate based microparticles or microcapsules have been successfully synthesized and used as drug carriers. However, its sensitivity towards chelating agents discourages its application.

To overcome the limitations associated with mesoporous silica nanoparticles and biopolymers as drug carrier, silica based bio-hybrids could be a solution. Bio-hybrid exhibits advance properties which are not present in the individual component and impart dual functionality. Several methods like emulsion polymerization, intercalative polymerization, sol-gel method and hybrid latex polymerization were developed for the production of hybrids microspheres [238-240]. However, in all these methods, surfactants and organic solvents are used which are not desired when material is going to be used as drug carrier. Thus, there is an urgent need to devise simple, low cost and efficient methods for development of bio-hybrids as a drug carrier.

In this work, a bio-hybrid of silica nanoparticles-sodium alginate and other carriers were synthesized using spray drying technique for entrapment of doxorubicin hydrochloride. Synthesized carriers were characterized. Further, bio-hybrid along with other carriers were used for release study of the loaded drug. Cytotoxicity effect of doxorubicin loaded in bio-hybrid was also studied.

5.2. Materials and methods

5.2.1. Materials

LUDOX HS-40 colloidal silica (40 wt% suspension in H_2O, pH-9.8) was obtained from Aldrich Co., MO, USA. Sodium alginate was purchased from Sigma-Aldrich Co., MO, USA. Doxorubicin hydrochloride was purchased from Sigma-Aldrich Co., MO, USA. Microstructures

were synthesized using spray dryer LU222, LABULTIMA, India. All chemicals were of analytical grade.

5.2.2. Synthesis of the bio-hybrid and other drug carriers

The cationic anticancer agent, Doxorubicin (Dox), was used as a drug model to estimate the drug loading and release behavior of Dox from the bio-hybrid. Doxorubicin drug carriers were synthesized using spray dryer (as discussed previously). A mixed suspension of 1% silica NP-2% sodium alginate, plain 1% silica NP and plain 2% sodium alginate with and without 0.1 mg/mL doxorubicin were used as feed in the spray dryer. Synthesized products were stored at 4 ^{0}C and used for further studies. The overall spray drying process was discussed in section 4.2.2.

5.2.3. Characterization

SEM Protocol

An environmental scanning electron microscope (Quanta 200 ESEM, FEI, USA) was used to characterize the microstructures. The SEM protocol was discussed earlier in Section 2.2.3.1.

Fourier Transform Infrared Spectroscopy (FTIR) protocol

Developed bio-hybrid was characterized through FTIR. FTIR spectra of the materials under study were recorded using Jasco FT-IR 660 plus spectrometer. FTIR protocol was discussed earlier in Section 2.2.3.2.

5.2.4. In vitro drug release profile

In order to study the in-vitro drug release, Dox-loaded bio-hybrid and other drug carriers were suspended in PBS (pH 7.4) at concentration of 1 mg/mL. The solution was kept in a shaking

incubator at 37 ^{0}C with constant agitation (100 rpm). At regular time intervals, 200 µL of the release medium was withdrawn, centrifuged (10 min at 10000 rpm) and subjected to measurement. The amount of doxorubicin released was determined by measuring fluorescence emission at 585 nm (excitation wavelength: 490 nm) using microplate reader against the standard plot prepared under similar conditions. Each sample was performed in triplicate. A curve of cumulative percent released versus time was plotted. Data were presented as mean ± SD from at least three independent experiments.

5.2.5. Drug loading efficiency (LE)

Drug loading efficiency (LE) was determined from the calibration curve of Dox. The LE was calculated based on the following equation:

$$\% \text{ LE} = (W_{drug}/W_0)*100 \quad (22)$$

where, W_{drug} is the weight of loaded drug and W_0 is the initial weight of drug. The experiments were carried out three times, from which average values were obtained.

5.2.6. Cell culture

A-549 lung carcinoma cell lines were maintained in Dulbecco`s Modified Eagle Media (DMEM) supplemented with 10% (v/v) fetal calf serum (FBS). All cells were cultured at 37 ^{0}C in a 5% CO_2 humidified incubator.

5.2.7. Intracellular uptake of Dox entrapped in bio-hybrid and other carriers

The intracellular uptake of Dox was visualized by flow cytometry. A-549 cells were seeded into 96-well plates (1×10^4 cells/well) and incubated with free Dox (1 µM) and Dox entrapped in spray dried silica, sodium alginate and bio-hybrid (containing 1 µM of Dox) for 4 h. The quantification of Dox incorporation by cells was measured by Flow cytometer.

5.2.8. Cytotoxicity assay

For cytotoxicity experiments, A-549 lung carcinoma cells were harvested and $1x10^4$ cells were seeded per well in 96 well microplate for 4 h. Different concentrations of bio-hybrid without Dox (5, 10, 20, 50, 100 µg/ml) was added to the cells and incubated for next 36 hr at 37 ^{0}C in a 5% CO_2 humidified incubator. The cytotoxicity activity was measured by amethylthiazolyldiphenyl-tet-razolium bromide (MTT) assay.

In another set of experiment, cells were incubated with different concentrations of (100 nM, 200 nM and 500 nM) free Dox and Dox loaded spray dried silica NP, sodium alginate and bio-hybrids for 36 h and cytotoxicity activity was measured by MTT assay as described below.

MTT assay

MTT assay is widely used in vitro assay for measurement of cell viability. Metabolically active cells have ability to reduce yellow tetrazolium MTT (3-(4, 5-dimethylthiazolyl-2)-2, 5-diphenyltetrazolium bromide) into purple formazan by the action of dehydrogenase enzymes which is present in mitochondira. The resulting formazan was solubilized and quantified by spectrophotometer.

Reagent:

SDS – 10% solution

MTT reagent

Basic protocol

1. The cells were seeded in 96 well plates ($1x10^4$ cells/well) and incubated for 6 h.

2. Further, 10 µL of MTT Reagent was added and incubated 4 h (until purple precipitate was visualized).
3. After this, 100 µL (10%) SDS was added to solubilize the formazan crystal formed by the reduction of MTT.
4. Plates were incubated overnight at room temperature in the dark.
5. Absorbance was recorded at 570 nm.

5.2.9. Statistical analysis

Comparisons between groups were conducted using analysis of unpaired t-tests. $P < 0.05$ was considered to be statistically significant.

5.3.Results and discussion

5.3.1. Characterization of drug carriers

Synthesized bio-hybrids were characterized through SEM and FTIR techniques.

(a) SEM analysis

Fig. 5.1, shows the SEM micrographs of spray dried 1% silica NP with doxorubicin, spray dried 2% sodium alginate with doxorubicin and bio-hybrid of 1% silica NP-2% sodium alginate with doxorubicin. As shown in Fig. 5.1a, spray dried plain silica with doxorubicin shows smooth doughnut shaped microstructures and size varies from 0.5 µm to 1 µm. Spray dried sodium alginate with doxorubicin shows smooth doughnut and size varies between 0.2 µm to 3 µm (Fig. 5.1b). On the other hand, bio-hybrid of silica NP-sodium alginate with doxorubicin showed irregular doughnut shaped multi-buckled microstructures in the size range 1 µm to 2 µm (Fig. 5.1c). The possible explanation may be that herein silica NP and sodium alginate both are

negatively charged thus there is possibility that repulsive forces are high. However, hydrogen bonds formed between carboxyl/hydroxyl group of alginate and silanol group of silica NP also play an important role (Fig. 5.2). In bio-hybrid, Dox being positively charged minimizes the repulsive forces upto some extent.

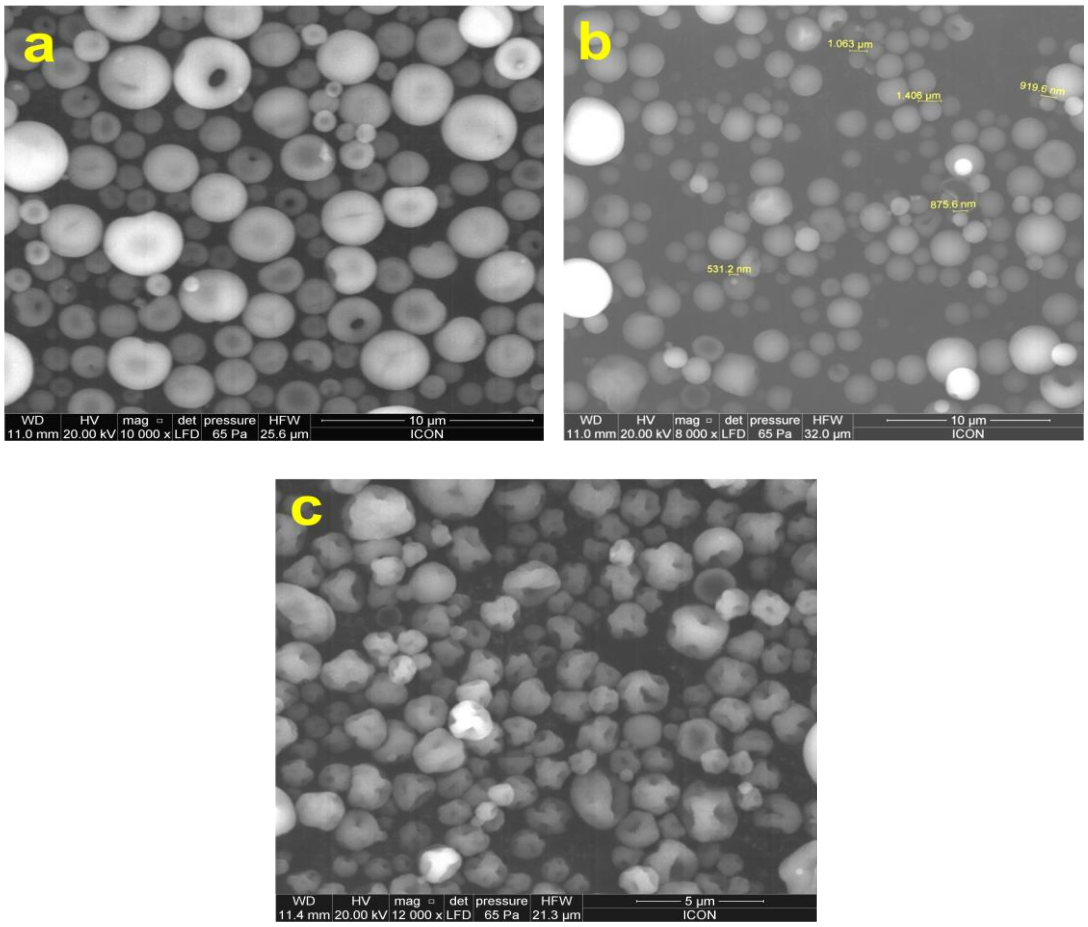

Fig. 5.1. SEM micrographs of (a) spray dried 1% silica NP with doxorubicin (b) spray dried 2% sodium alginate with doxorubicin and (c) bio-hybrid of 1% silica NP- 2% sodium alginate with doxorubicin.

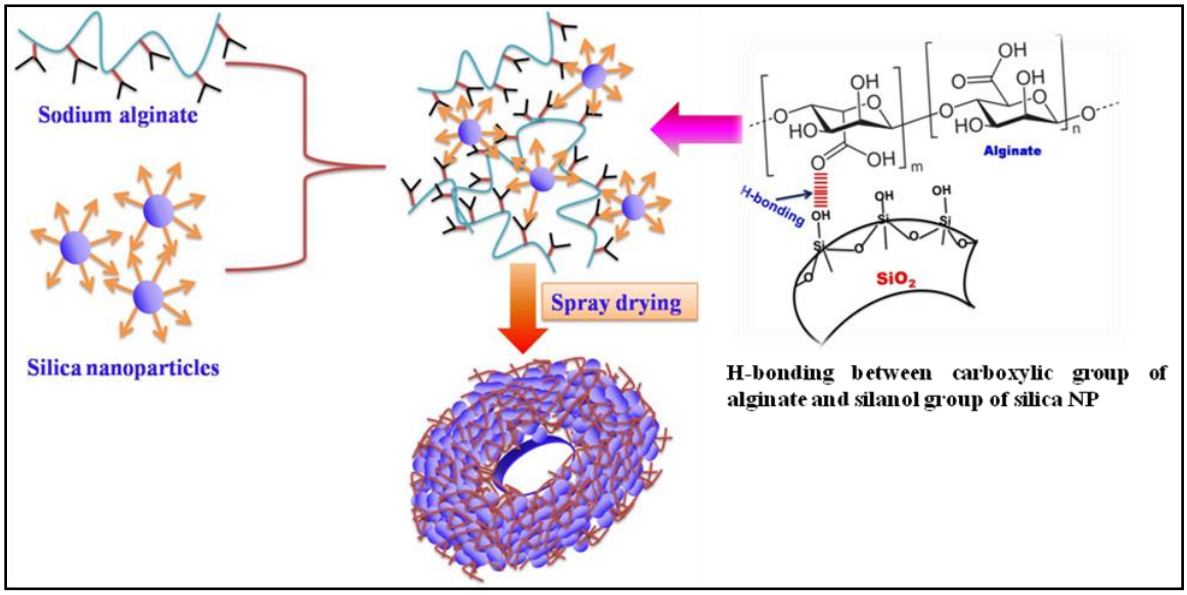

Fig. 5.2. Schematic presentation of interaction between silica NP and sodium alginate

(b) FTIR study

The Fourier transform infrared (FTIR) spectra of the spray dried silica nanoparticles, spray dried sodium alginate and Dox loaded bio-hybrid were recorded and compared (Fig. 5.3). The FTIR spectra of the silica showed absorption bands arising from asymmetric vibration of Si-O-Si (1102 cm^{-1}), asymmetric vibration of Si-OH (960 cm^{-1}), symmetric vibration of Si-O-Si (795 cm^{-1}) and the band at 1630 cm^{-1} is due to scissor bending vibration of molecular water [183, 141]. FTIR spectrum of sodium alginate showed important absorption bands corresponds to hydroxyl, and carboxylic functional groups. Stretching vibrations of O–H bonds of alginate appeared in the range of 3000–3600 cm^{-1}. Stretching vibrations of aliphatic C–H were observed at 2920–2850 cm^{-1}. Bands observed at 1605 and 1413 cm^{-1} were attributed to asymmetric and symmetric stretching vibrations of carboxylate ion, respectively. The bands at 1036 cm^{-1} and 945 cm^{-1} were

attributed to the C–O stretching vibration of pyranosyl ring and the C–O stretching with contributions from C–C–H and C–O–H deformation [242].

In case of Dox loaded bio-hybrids, there is shift in the band in the region 3000–3600 cm^{-1} which corresponds to –OH group stretching and shows the formation of hydrogen bonds. There are shift in the bands 1605 cm^{-1} and 1413 cm^{-1} which corresponds to asymmetric and symmetric stretching vibration of COO^- groups. Band arising from asymmetric vibration of Si-O-Si (1102 cm^{-1}) also shifted to 1120 cm^{-1}. However, the changes in asymmetric vibration of Si-OH (958 cm^{-1}) could not be figured out due to overlapping bands of sodium alginate in the same region. Overall, FTIR analysis showed the involvement of carboxyl and hydroxyl group of alginate and silanol groups of silica NP.

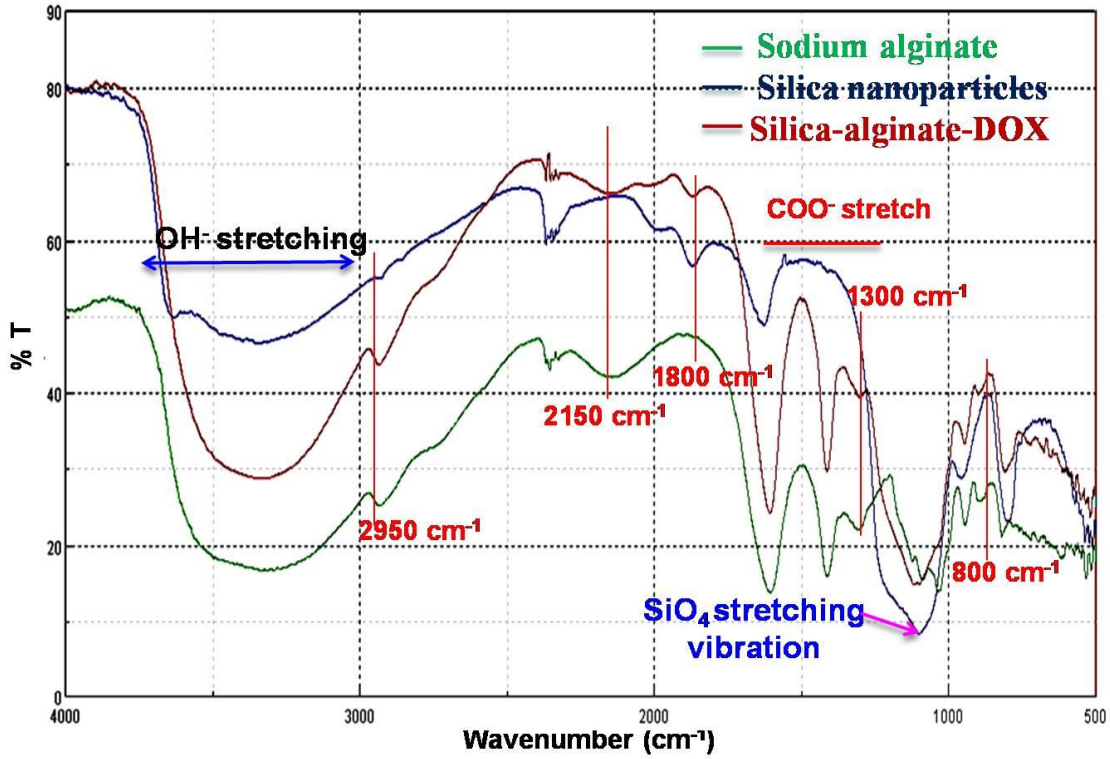

Fig. 5.3. FTIR spectra of spray dried silica NP, spray dried sodium alginate and Dox loaded bio-hybrid.

5.3.2. In-vitro Dox release study

As show in Fig. 5.4, spray dried silica NP and alginate showed a biphasic release of Dox. In the first phase, a burst release of Dox was observed. Spray dried silica shows much faster (91% release in 1 h) release of Dox than alginate (69% release in 2 h). The fast drug release from spray dried silica particles could be due to the high surface area and hydrophilicity of silica nanoparticles [234]. However, the interaction between carboxyl group of alginate and amino/hydroxyl group of Dox has slowed down the release of drug in spray dried alginate microparticles in comparison to spray dried silica.

Synthesized bio-hybrid shows a continuous and slow release of Dox over a period of 30 h. There is possibility of ionic interaction between carboxylic group of alginate and amine group of Dox as well as cumulative effect of hydrogen bonding between silanol group of silica and hydroxyl group of alginate as well as hydroxyl group of Dox and silanol group of silica/hydroxyl group of alginate which could be responsible for slow release of drug from the bio-hybrid. Overall, the compact structure of the silica matrix in presence of alginate biopolymer slows down the release of drug which can be beneficial to maintain an effective drug concentration in the blood for a longer time [243-245].

In vitro release profile of Dox loaded in bio-hybrid was studied at two different pH (Fig. 5.5). The release rate of Dox at pH 5.5 (in cancer cells) was significantly higher ($p < 0.01$) than that at pH 7.4 (physiological pH) and could be caused by weakening of hydrogen bonds between Dox and bio-hybrid. Noncovalent attachment of Dox to alginate involves hydrogen bonds between –

COOH of alginate and –OH of Dox and between –OH of alginate or Si-OH of silica and –OH of Dox. The degree of hydrogen bond interactions between Dox and bio-hybrid is a function of the pH value. The H^+ in solution would compete with the hydrogen bond-forming group and weaken the hydrogen bond interactions at pH 5.5 which will further lead to greater release of Dox [243]. On the other hand, the high release rate at acidic conditions may be caused by the amine ($–NH_2$) groups of Dox getting protonated resulting in partial dissociation of bond interaction between Dox and bio-hybrid. The high drug loading and the pH-sensitive release of Dox suggest that bio-hybrid is a promising delivery vehicle for the anticancer drug.

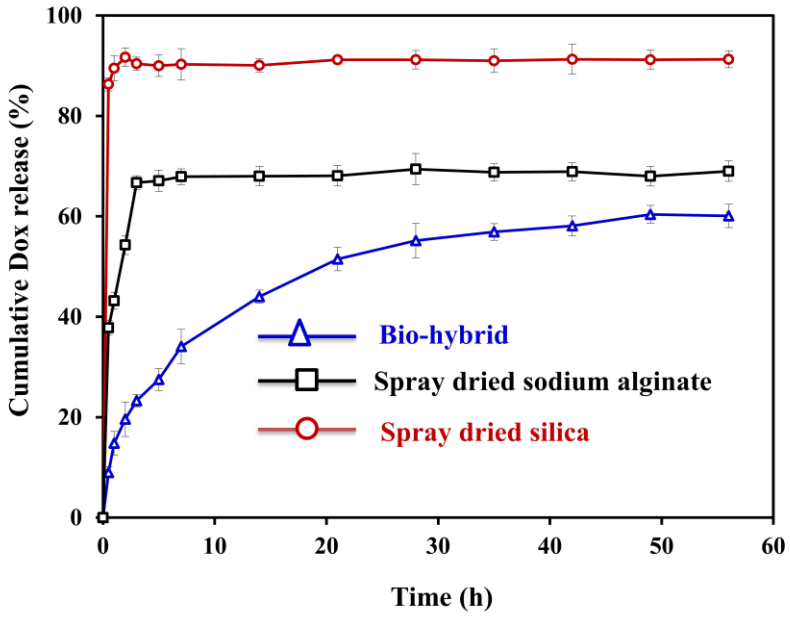

Fig. 5.4. Release profile of Dox loaded in spray dried silica NP, spray dried sodium alginate and bio-hybrid.

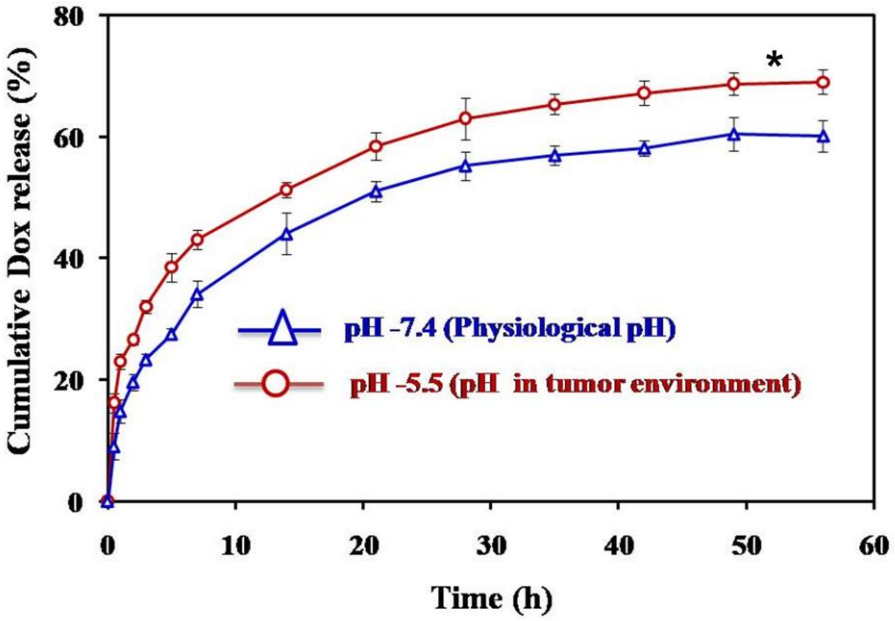

Fig. 5.5. pH dependent release profile of Dox loaded in bio-hybrid at 37 ^{0}C. (*p<0.01)

5.3.3. Cellular uptake of free and loaded Dox

The cellular uptake behavior of free and entrapped Dox was investigated by flow cytometry (Fig. 5.6). A-549 cell lines were treated with free Dox and Dox loaded in silica NP, sodium alginate and bio-hybrid at the corresponding Dox concentration of 1 μM for 4 h. Cells were harvested, washed with PBS and percentage positive cells for the presence of DOX were quantified using flow cytometry. As shown in Fig. 5.6 Dox was delivered into 54%, 40%, 75% and 99% of cells in case of free Dox, Dox loaded in silica NPs, sodium alginate and bio-hybrid, respectively. Figure 5.7 showed average of percentage positive cells from three independent experiments. Cells treated with Dox entrapped in spray dried sodium alginate and bio-hybrid induced efficient cellular uptake of Dox. Noticeably, bio-hybrid have higher delivery efficiency than free Dox (p <

0.01), indicating that the combined effect of silica NP and sodium alginate could significantly enhance the cellular uptake of Dox [246-247].

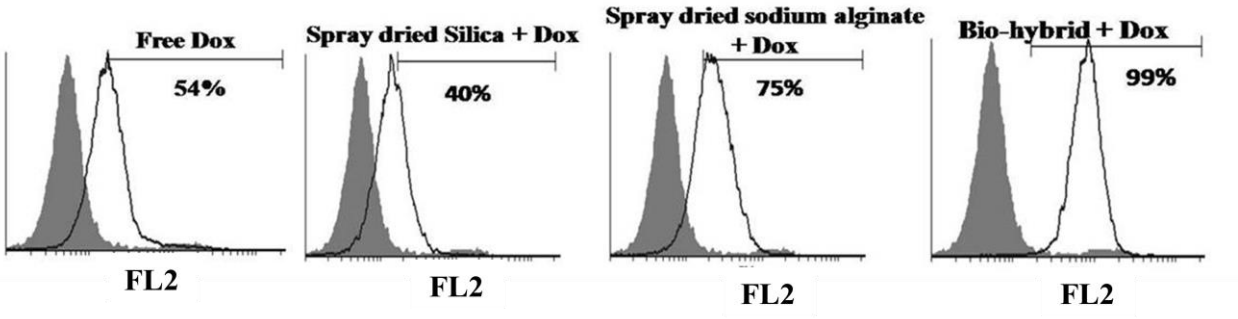

Fig. 5.6. Flow cytometry analysis of A-549 cells after 4 h incubation with free Dox and Dox entrapped in spray dried silica nanoparticles, sodium alginate and bio-hybrid.

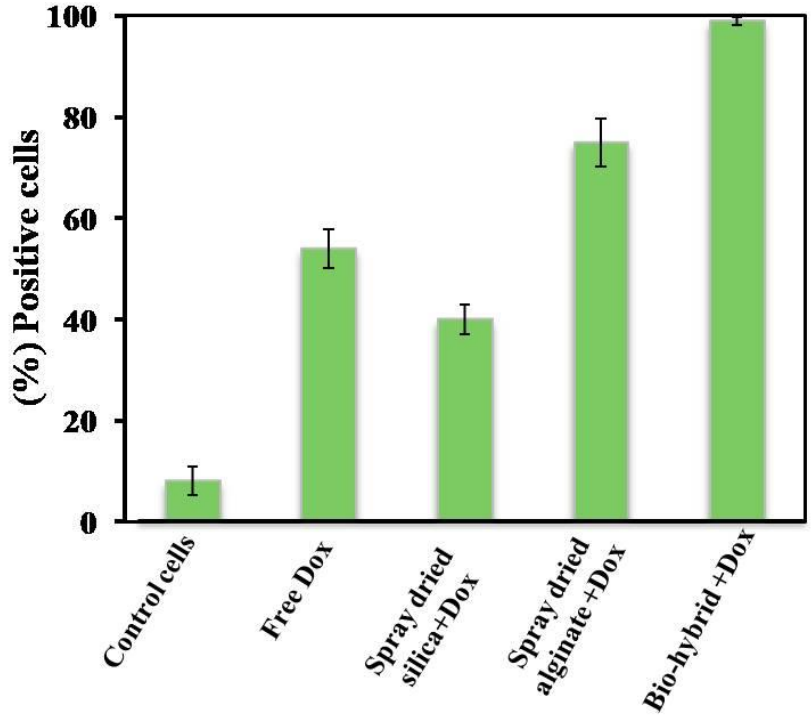

Fig. 5.7. Percent positive cells with Dox expression analyzed through flow cytometry.

5.3.4. In vitro cytotoxicity of Dox loaded bio-hybrid

Cytotoxicity of plain bio-hybrid without Dox was studied (Fig. 5.8). The study showed that as the concentration of bio-hybrid was increased from 5 to 20 μg/mL, there was no significant cell cytotoxicity observed. However, at concentration 50 μg/mL significant cell killing was observed. This observation suggests that bio-hybrid in a concentration of up to 20 μg/mL is safe for primary cells in in vitro conditions. Thus, for further studies, the concentration of bio-hybrid less than 20 μg/mL was used.

In order to quantify the effects of Dox entrapped in silica NP, sodium alginate and bio-hybrid compared to free Dox, a MTT assay were performed using A-549 cells. Cells were incubated with different concentration of free Dox (100 nM, 200 nM and 500 nM) along with spray dried silica with Dox, spray dried alginate with Dox and bio-hybrid with Dox. The corresponding entrapped Dox concentration was same as free Dox. Cells were incubated for 36 hr and cell viability was assessed by MTT assay. As shown in Fig. 5.9, Dox entrapped in bio-hybrid showed dose dependant cell cytotoxicity as cell viability was decreased with the increase in Dox concentration. Compare to free Dox, there was significant decrease in cell viability with bio-hybrid-Dox in all concentration and at 500 nM concentration 50% cell death was observed (IC_{50}) with bio-hybrid-Dox. This could have resulted because of the slow and continuous release of Dox from the bio-hybrid which finally improves the bioavailability of entrapped Dox at cellular level.

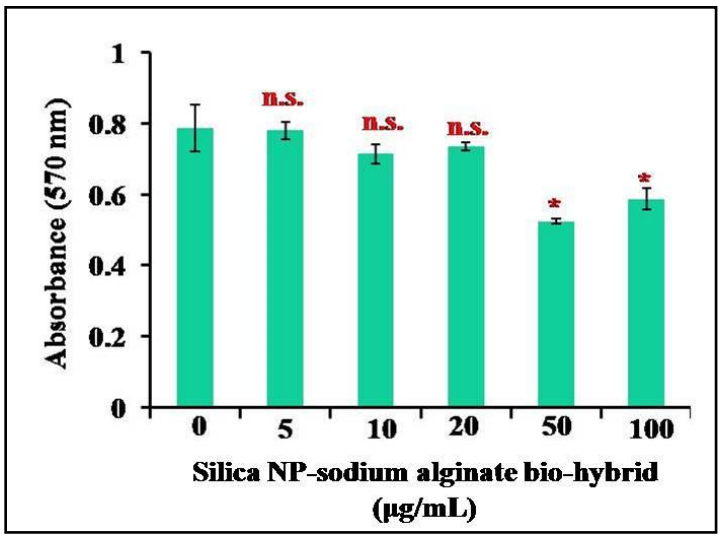

Fig. 5.8. Cytotoxicity study of plain bio-hybrid without Dox in mouse lymphocyte cells.

(*p<0.01, n.s.-not significant)

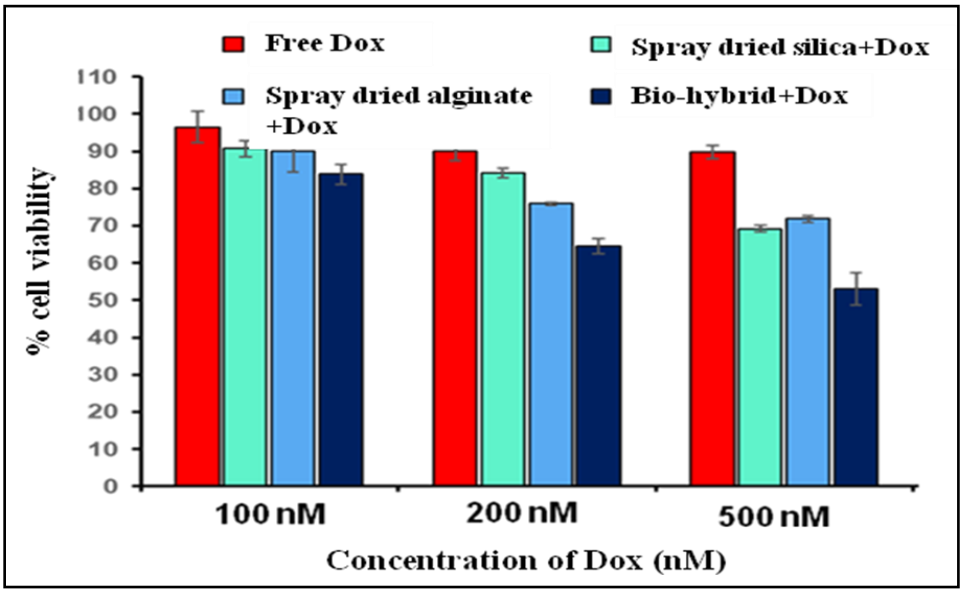

Fig. 5.9. In vitro cell cytotoxicity study of free Dox and Dox entrapped in spray dried silica nanoparticles, sodium alginate and bio-hybrid at Dox concentration of 100, 200 and 500 nM against A-549 cells after 36 h incubation using MTT assay.

5.4. Conclusion

In this study, an efficient, simple and facile method was developed to synthesize doxorubicin loaded bio-hybrids of silica nanoparticles and sodium alginate in large scale. The antitumor drugs Dox were entrapped in different carriers during evaporation induced self assembly process. The slow and continuous release behavior of Dox from bio-hybrid helps to maintain an effective drug concentration for a longer time. The intracellular uptake study and *in vitro* cytotoxicity results showed that the presence of silica NP along with sodium alginate provided an opportunity to locally enhance the intracellular drug concentration and their cytotoxicity to cancer cell lines. Thus, Dox loaded bio-hybrid developed through spray drying has emerged as efficient drug carrier and has potential as a Dox delivery system for cancer therapy.

Chapter-6

Future perspectives

- Other available biological fibrous structures can be explored for assembly of nanoparticles in order to synthesize dendritic support system which will find applications in various areas of biotechnology.

- Suitable microbial cells which are efficient for removal of metals can be associated with silica nanoparticles in order to enhance metal removal capacity of the bio-hybrids.

- Multi-functional bio-hybrids can be designed for better remediation of metal/organic pollutants in a continuous system.

- Since the biodegradability of pure silica is relatively slow due to the stable cross-linked framework, the accumulation of silica nanoparticles in organs is an obstacle which hampers its clinical application. In order to improve the biosafety, biosilica based carriers can be synthesized.

- pH sensitive biodegradable silica based bio-hybrids as nanocarrier can be synthesized for its effective utilization in pharma industry.

- Multimodal/multifunctional bio-hybrid which are highly sensitive, stable, biocompatible and targetable can be designed which will enable sensing of the target using multiple sensing modalities.

- To address the problem associated with low penetration ability of silica nanoparticles, silica NP can be associated with targeting ligands along with bio-component which are capable of interacting with receptors over-expressed on tumor cells.

- Silica based bio-hybrid can be developed which act as targeted drug delivery systems to improve the probability and accuracy of tumor recognition.

- In future, novel bio-hybrids with improved properties and multifunctionality can be synthesized which will have applications in biotechnology.

References

1. H. Buyukgungor, L. Gurel, The role of biotechnology on the treatment of wastes, African J Biotechnol 2009, 8, 7253.

2. Z.T. Yu-Qung, S. Mei-Lin, Z. Wei-De, D. Yu-Zhen, M. Yue, Z. Wen-Ling, Immobilization of L-asparaginase of the microparticles of the natural silk serum protein and its characters, Biomaterials, 2004, 25, 3151.

3. E.G. Griffin, J.M. Nelson, The influence of certain substances on the activity of invertase, J Amer Chem Soc 1916**,** 38**,** 722.

4. A. A. Homaei, R. Sariri, F. Vianello, R. Stevanato, Enzyme immobilization: an update, J Chem Biol, 2013, 6:185–205. DOI 10.1007/s12154-013-0102-9

5. M. Hartmann, Ordered mesoporous materials for bioadsorption and biocatalysis. Chem Mater, 2005, 17, 4577.

6. A.I. Kallenberg, F.V. Rantwijk, R.A. Sheldon, Immobilization of penicillin G acylase: the key to optimum performance. Adv Synth Catal, 2005, 347, 905.

7. C. Pierre, The sol–gel encapsulation of enzymes. Biocatal Biotransfor, 2004, 22,145.

8. M.M.M. Elnashar, The art of immobilization using biopolymers, biomaterials and nanobiotechnology, Biotechnology of Biopolymers, 2011, ISBN 978-953-307-179-4, 1.

9. T. Tosa, T. Mori, N. Fuse, I. Chibata, Studies on continuous enzyme reactions Part V Kinetics and industrial application of aminoacylase column for continuous optical resolution of acyl-dl amino acids, Biotechnol Bioeng, 1967, 9, 603.

10. L. Cao, R.D. Schmid RD, Carrier-bound Immobilized Enzymes: Principles, Application and Design. 2005, WILEY-VCH Verlag GmbH & Co. Weinheim

11. G.F. Bickerstaff, Impact of genetic technology on enzyme technology, Genet Eng Biotechnol, 1995, 15, 13.

12. A. Riaz, S. Qader, A. Anwar, S. Iqbal, Immobilization of a Thermostable á-amylase on calcium alginate beads from *Bacillus Subtilis* KIBGE-HAR, Aust J Basic & Appl Sci, 2009, 3, 2883.

13. A. Groboillot, D.K. Boadi, D. Poncelot, R.J. Neufled, Immobilization of cells for application in the food industry, Crit Rev Biotechnol, 1994, 14, 75.

14. J.S. Patil, M.V. Kamalapur, S.C. Marapur, D.V. Kadam, Ionotropic gelation and polyelectrolyte complexation: The novel techniques to design hydrogel particulate sustained, modulated drug delivery system: A Review, Digest J Nanomat Biostruct, 1994, 5, 241.

15. B. Menaa B, M. Herrero, V. Rives, M. Lavrenko, D.K. Eggers, Favorable influence of hydrophobic surfaces on protein structure in porous organically-modified silica glasses, Biomaterials, 2008b, 29, 2710.

16. B. Menaa, Y. Miyagawa, M. Takahashi, M. Herrero, V. Rives, F. Menaa, D.K. Eggers, Bioencapsulation of apomyoglobin in nanoporous organosilica sol-gel glasses: influence of the siloxane network on the conformation and stability of a model protein, Biopolymers, 2009, 91, 895.

17. B. Menaa, F. Menaa, C. Aiolfi-Guimaraes, O. Sharts, Silica-based nanoporous sol-gel glasses: from bioencapsulation to protein folding studies, Internatl J Nanotechnol, 2010, 7, 1.

18. T. Xie, A. Wang, L. Huang, H. Li, Z. Chen, Q. Wang, X. Yin, Review: Recent advance in the support and technology used in enzyme immobilization, Afr J Biotechnol, 2009, 8, 4724.

19. A.M. Girelli, E. Mattei, Application of immobilized enzyme reactor in on-line high performance liquid chromatography: a review, J Chromatogr B, 2005, 819, 3.

20. G.F. Bickerstaff, Impact of genetic technology on enzyme technology, Genet Eng Biotechnol, 1995, 15, 13.

21. J. Zdarta, A. S. Meyer, T. Jesionowski, M. Pinelo, A general overview of support materials for enzyme immobilization: characteristics, properties, practical utility, Catalysts, 2018, 8, 92.

22. O. Kirk, M.W. Christensen, Lipases from Candida antarctica: Unique biocatalysts from a unique origin, Org Process Res Dev, 2002, 6, 446.

23. A. Basso, P. Braiuca, S. Cantone, C. Ebert, P. Linda, P. Spizzo, P. Caimi, U. Hanefeld, G. Degrassi, L. Gardossi, In silico analysis of enzyme surface and glycosylation effect as a tool for efficient covalent immobilisation of CalB and PGA on Sepabeads, Adv Synth Catal, 2007, 349, 877.

24. P.C. Ashly, M.J. Joseph, P.V. Mohanan, Activity of diastase *a*-amylase immobilized on polyanilines (PANIs), Food Chem, 2011, 127, 1808.

25. M.C. Jimenez Hamann, B.A. Saville, Enhancement of tyrosinase stability by immobilization on Nylon 66, Food Bioprod Process Trans Inst Chem Eng C, 1996, 74, 47.
26. W. Wang, W. Zhou, J. Li, D. Hao, Z. Su, G. Ma, Comparison of covalent and physical immobilization of lipase in gigaporous polymeric microspheres, Bioprocess Biosys Eng, 2015, 38, 2107.
27. J. Vartiainen, M. Rättö, S. Paulussen, Antimicrobial activity of glucose oxidase-immobilized plasma-activated polypropylene films, Packag Technol Sci, 2005, 18, 243.
28. D. Alsafadi, F. Paradisi, Covalent immobilization of alcohol dehydrogenase (ADH_2) from *Haloferaxvol canii*: How to maximize activity and optimize performance of halophilic enzymes, Mol Biotechnol, 2014, 56, 240.
29. D. Mislovicova, J. Masarova, A. Vikartovska, P. Germeiner, E. Michalkova E, Biospecific immobilization of mannan–penicillin G acylase neoglycoenzyme on Concanavalin A-bead cellulose, J Biotechnol, 2004), 110, 11.
30. L.E. Shi, Z.X. Tang, Y. Yi, J.S. Chen, W.Y. Xiong, G.Q. Ying, Immobilization of nuclease p1 on chitosan micro-spheres, Chem Biochem Eng Q, 2011, 25, 83.
31. T. Coradin, N. Nassif, J. Livage, Silica-alginate composites for microencapsulation, Appl Microbiol Biotechnol, 2003, 61, 429.
32. S.S. Betigeri, S.H. Neau, Immobilization of lipase using hydrophilic polymers in the form of hydrogel beads, Biomaterials, 2002, 51, 3627.
33. E.P.S. Ceniceros, A. Ilyina, J.C.C. Esquivel, D.R. Menchaca, J.C.F. Espinoza, O.E.M. Rodriguez, Entrapment of enzymes in natural polymer extracted from residue of food industry: preparation methods, partial characterisation and possible application, Becth Mock, 2003, 44, 84.
34. K. Kurita, Controlled functionalization of the polysaccharide chitin, Prog Polym Sci, 2001, 26, 1921.
35. N. Peter, Applications and environmental aspects of chitin and chitosan, J Macromol Sci, 1995, 32, 629.
36. M. Namdeo, S.K. Bajpai, Immobilization of a-amylase onto cellulose-coated magnetite (CCM) nanoparticles and preliminary starch degradation study, J Mol Catal B-Enzym, 2009, 59,134.

37. K. Labus, A. Turek, J. Liesiene, J. Bryjak, Efficient Agaricus bisporus tyrosinase immobilization on cellulose-based carriers, Biochem Eng J, 2011, 56, 232.
38. X.J. Huang, P.C. Chen, F. Huang, Y. Ou, M.R. Chen, Z.K. Xu, Immobilization of Candida rugosa lipase on electrospun cellulose nanofiber membrane, J Mol Catal B-Enzym, 2011, 70, 95.
39. M.P. Klein, C.W. Scheeren, A.S.G. Lorenzoni, J.D.J. Frazzon, P.F. Hertz, Ionic liquid-cellulose film for enzyme immobilization, Process Biochem, 2011, 46, 1375.
40. S.E. Cahyaningrum, N. Herdyastusi, D.K. Maharani, Immobilization of glucose isomerase in surface-modified chitosan gel beads, Res J Pharm Biol Chem Sci, 2014, 5, 104.
41. E.T. Hwang, M.B. Gu, Enzyme stabilization by nano/microsized hybrid materials, Eng Life Sci, 2013, 13, 49.
42. L. Gomez, H.L. Ramırez, A. Neira-Carrillo, R. Villalonga, Polyelectrolyte complex formation mediated immobilization of chitosan–invertase neoglycoconjugate on pectin-coated chitin, Bioproc Biosyst Eng, 2006, 28, 387.
43. R. Satar, M. Matto, Q. Husain, Studies on calcium alginate– pectin gel entrapped concanavalin A–bitter gourd (*Momordica charantia*) peroxidase complex, J Sci Ind Res India, 2008, 67, 609.
44. M.L. Foresti, G. Valle, R. Bonetto, M.L. Ferreira, L.E. Briand, FTIR, SEM and fractal dimension characterization of lipase B from *Candida antarctica* immobilized onto titania at selected conditions, Appl Surf Sci, 2010, 256, 1624.
45. R. Reshmi, G. Sanjay, S. Sugunan, Immobilization of *a*-amylase on zirconia: A heterogeneous biocatalyst for starch hydrolysis, Catal Commun, 2007, 8, 393.
46. Z. Yang, S. Si, C. Zhang, Study on the activity and stability of urease immobilized ontonanoporous alumina membranes, Micropor Mesopor Mater, 2008, 111, 359.
47. A.E. David, N.S. Wang, V.C. Yang, A.J. Yang, Chemically surface modified gel (CSMG): an excellent enzyme-immobilization matrix for industrial processes, J Biotechnol, 2006, 125, 395.
48. P. Zucca, E. Sanjust, Inorganic materials as supports for covalent enzyme immobilization: methods and mechanisms, Molecules, 2014, 19, 14139.

49. L.T. Zhuravlev, The surface chemistry of amorphous silica. Zhuravlev model, Colloids Surf Physicochem Eng Asp, 2000, 173, 1.
50. V.Y. Davydov, V.Y. Adsorption on Silica Surfaces; Papirer, E., Ed.; CRC Press, Taylor & Francis Group: Santa Barbara, CA, USA, 2000, 90, 63.
51. C.T.G. Knight, R.J. Balec, S.D. Kinrade, The structure of silicate anions in aqueous alkaline solutions, Angew Chem Int Ed 2007, 46, 8148.
52. A. Rimola, D. Costa, M. Sodupe, J.-F. Lambert, P. Ugliengo, Silica surface features and their role in the adsorption of biomolecules: Computational modeling and experiments, Chem Rev, 2013, 113, 4216.
53. H.E. Bergna, W.O. Roberts, Colloidal science in colloidal silica fundamentals and applications; CRC Press: Boca Raton, 2006, 575.
54. E.D.E.R. Hyde, A. Seyfaee, F. Neville, R. Moreno-Atanasio, Colloidal silica particle synthesis and future industrial manufacturing pathways: A Review, Ind Eng Chem Res, 2016, 55, 8891.
55. W. Xie, L. Hu, X. Yang, Basic ionic liquid supported on mesoporous SBA-15 silica as an efficient heterogeneous catalyst for biodiesel production, Ind Eng Chem Res, 2015, 54, 1505.
56. R.B. Nasir Baig, R.S. Varma, Magnetic silica-supported palladium catalyst: synthesis of allyl aryl ether in water, Ind Eng Chem Res, 2014, 53, 18625.
57. L. Chen, J. Hu, Z. Qi, Y. Fang, R. Richards, Gold nanoparticles intercalated into the walls of mesoporous silica as a versatile redox ratalyst, Ind Eng Chem Res, 2011, 50, 13642.
58. K. Wang, P. Liu, Y. Ye, J. Li, W. Zhao, X. Huang, Fabrication of a novel laccase biosensor based on silica nanoparticles modified with phytic acid for sensitive detection of dopamine, Sens Actuators B, 2014, 197, 292.
59. W. Zhao, Y. Fang, Q. Zhu, K. Wang, M. Liu, X. Huang, J. Shen, A novel glucose biosensor based on phosphonic acid- functionalized silica nanoparticles for sensitive detection of glucose in real samples, Electrochim Acta, 2013, 89, 278.
60. F. Ma, L. Zhou, J. Tang, S. Wei, Y. Zhou, J. Zhou, F. Wang, J. Shen, A facile method for haemoglobin encapsulation in silica nanoparticles and applications in biosensors, Micropor Mesopor Mater, 2012, 160, 106.

61. O. Choi, B.C. Kim, J.H. An, K. Min, Y.H. Kim, Y. Um, M.K. Oh, B.I. Sang, A biosensor based on the self-entrapment of glucose oxidase within biomimetic silica nanoparticles Induced by a fusion enzyme, Enzyme Microb Technol, 2011, 49, 441.
62. M. Geszke-Moritz, M. Moritz, APTES-modified mesoporous silicas as the carriers for poorly water-soluble drug. Modeling of Diflunisal Adsorption and Release, Appl Surf Sci, 2016, 368, 348.
63. A. Wang, Y. Yang, Y. Qi, W. Qi, J. Fei, H. Ma, J. Zhao, W. Cui, J. Li, Fabrication of mesoporous silica nanoparticle with well- defined multicompartment structure as efficient drug carrier for cancer therapy in vitro and in vivo, ACS Appl Mater Interfaces, 2016, 8, 8900.
64. S.K. Rajanna, D. Kumar, M. Vinjamur, M. Mukhopadhyay, Silica aerogel microparticles from rice husk ash for drug delivery, Ind Eng Chem Res, 2015, 54, 949.
65. X. Hao, X. Hu, C. Zhang, S. Chen, Z. Li, X. Yang, H. Liu, G. Jia, D. Liu, K. Ge, X.-J. Liang, J. Zhang, Hybrid mesoporous silica-based drug carrier nanostructures with improved degradability by hydroxyapatite, ACS Nano, 2015, 9, 9614.
66. F. Tang, L. Li, D. Chen, Mesoporous silica nanoparticles: synthesis, biocompatibility and drug Delivery, Adv Mater, 2012, 24, 1504.
67. L. J. Zhu, L. P. Zhu, J.H. Jiang, Z. Yi, Y.F. Zhao, B.K. Zhu, Y.Y. Xu, Hydrophilic and anti-fouling polyethersulfone ultrafiltration membranes with poly(2-hydroxyethyl methacrylate) grafted silica nanoparticles as additive, J Membr Sci, 2014, 451, 157.
68. H. Wu, J. Mansouri, V. Chen, Silica nanoparticles as carriers of antifouling ligands for PVDF ultrafiltration membranes, J Membr Sci, 2013, 433, 135.
69. K. Jo, M. Ishizuka, K. Shimabayashi, T. Ando, Development of new mineral oil-based antifoams containing size-controlled hydrophobic silica particles for gloss paints. J Oleo Sci, 2014, 63, 1303.
70. M. Puig, L. Cabedo, J.J. Gracenea, A. Jiménez-Morales, J. Gámez-Pérez, J.J. Suay, Adhesion enhancement of powder coatings on galvanised steel by addition of organo-modified silica particles, Prog Org Coat, 2014, 77, 1309.

71. I.A. Rahman, V. Padavettan, Synthesis of silica nanoparticles by sol-gel: size-dependent properties, surface modifications and applications in silica-polymer nanocomposites − A Review, J Nanomater, 2012, 2012, 1.

72. D. Boldridge, Morphological characterization of fumed silica aggregates, Aerosol Sci Technol, 2010, 44, 182.

73. O. Taikum, R. Friehmelt, M. Scholz, The last 100 years of fumed silica in rubber reinforcement, Rubber World, 2010, 242, 35.

74. S. Prasertsri, N. Rattanasom, Fumed and precipitated silica reinforced natural rubber composites prepared from latex System: mechanical and dynamic properties, Polym Test, 2012, 31, 593.

75. E. Wagner, H. Brünner, Aerosil, Herstellung, Eigenschaften und Verhalten in Organischen Flüssigkeiten, Angew Chem, 1960, 72, 744.

76. S.S. Idrus, H. Ismail, S. Palaniandy, Study of the effect of different shapes of ultrafine silica as fillers in natural rubber compounds, Polym Test, 2011, 30, 251.

77. S. Pattanawanidchai, S. Loykulnant, P. Sae-oui, N. Maneevas, C. Sirisinha, Development of eco-friendly coupling agent for precipitated silica filled natural rubber compounds, Polym Test, 2014, 34, 58.

78. Z. Sun, C. Bai, S. Zheng, X. Yang, R.L. Frost, A comparative study of different porous silica minerals supported TiO_2 catalysts, Appl Catal A, 2013, 458, 103.

79. J.K. Kim, J.K. Park, H.K. Kim, Synthesis and characterization of nanoporous silica support for enzyme immobilization, Colloids Surf A, 2004, 241, 113.

80. A.K. Mülller, J. Ruppel, C.P. Drexel, I. Zimmermann, Precipitated silica as flow regulator, Eur J Pharm Sci, 2008, 34, 303.

81. A. Katiyar, S. Yadav, P.G. Smirniotis, N.G. Pinto, Synthesis of ordered large pore SBA-15 spherical particles for adsorption of biomolecules, J. Chroma A, 2006, 1122 (1–2), 13.

82. T. Yanagisawa, T. Shimizu, K. Kuroda, C. Kato, The preparation of alkyltrimethylammonium-kanemite complexes and their conversion to microporous materials, Bulletin Chem Soc Japan, 1990, 63 (4), 988.

83. J.S. Beck, J.C. Vartuli, W.J. Roth, M.E. Leonowicz, C.T. Kresge, K.D. Schmitt, C.T.W. Chu, D.H. Olson, E.W. Sheppard, A new family of mesoporous molecular sieves prepared with liquid crystal templates, J Am Chem Soc, 1992, 114 (27), 10834.

84. B.G. Trewyn, I.I. Slowing, S. Giri, H.T. Chen, V.S. Lin, Synthesis and functionalization of a mesoporous silica nanoparticle based on the sol–gel process and applications in controlled release, Acc Chem Res, 2007, 40 (9), 846.

85. D. Zhao, J. Feng, Q. Huo, N. Melosh, G.H. Fredrickson, B.F. Chmelka, G.D. Stucky, Triblock copolymer syntheses of mesoporous silica with periodic 50 to 300 angstrom pores, Science, 1998, 279 (5350), 548.

86. G. Valenti, R. Rampazzo, S. Bonacchi, L. Petrizza, M. Marcaccio, M. Montalti, L. Prodi, F. Paolucci, Variable doping induces mechanism swapping in electrogenerated chemiluminescence of Ru(bpy)32^{+} core−shell silica nanoparticles, J Am Chem Soc, 2016, 138 (49), 15935.

87. R.-A. Mitran, D. Berger, C. Munteanu, C. Matei, Evaluation of different mesoporous silica supports for energy storage in shape-stabilized phase change materials with dual thermal responses, J Phys Chem C, 2015, 119 (27), 15177.

88. E. Brunner, P. Richthammer, H. Ehrlich, S. Paasch, P. Simon, S. Ueberlein, K.H. van Pée, Chitin-based organic networks: an intergral part of cell wall biosilica in the diatom *Thalassiosira pseudonana*, Angew Chem Int Ed, 2009, 48, 9724.

89. C.A. Durkin, T. Mock, E.V. Armbrust, Chitin in diatom and its association with cell wall, Eukaryotic Cell, 2009, 8, 1038.

90. S. Wenzl, R. Hett, P. Richthammer, M. Sumper, Silacidins: highly acidic phosphopeptides from diatom shells assist in silica precipitation in vitr, Angew Chem Int Ed, 2008, 47, 1729.

91. N. Kroger, Prescribing diatom morphology: toward genetic engineering of biological nanomaterials, Curr Opin Chem Biol, 2007, 11, 662.

92. C.C. Perry, D. Belton, K. Shafran, Studies of biosilicas; structural aspects, chemical principles, model studies and the future, Prog Mol Subcell Biol, 2003, 33, 269.

93. K. Shimizu, J. Cha, G.D. Stucky, D.E. Morse, Silicatein α: cathepsin L-like protein in sponge biosilica, Proc. Natl. Acad. Sci. U. S. A., 1998, 95, 6234.

94. L.L. Hench, J.K. West, The sol-gel process, Chem Rev, 1990, 90(1), 33.

95. A.B.D. Nandiyanto, S.-G. Kim, F. Iskandar, K. Okuyama, Synthesis of silica nanoparticles with nanometer-size controllable mesopores and outer diameters, Micropor Mesopor Mat, 2009, 120 (3), 447.

96. A.M. Siouffi, Silica gel-based monoliths prepared by the sol-gel method: facts and figures, J Chroma A, 2003, 1000(1-2), 801.

97. R.K. Iler, Chemistry of silica-solubility, polymerization, Colloid and Surface Properties and Biochemistry, 1979, New York: John Wiley & Sons.

98. R. Aelion, A. Loebel, F. Eirich, Hydrolysis of ethyl silicate, J Am Chem Soc, 1950. 72(12), 5705.

99. C.J. Brinker, G.W. Scherer, Sol-gel-glass: I. gelation and gel structure. J Non-Crystal Solids, 1985. 70(3), 301.

100. W. Stöber, A. Fink, E. Bohn, Controlled growth of monodisperse silica spheres in the micron size range, J Colloid Inter Sci, 1968, 26 (1), 62.

101. E.J. Mezey, Pigments and Reinforcing Agents. In Vapor Deposition; C.F. Powell, J.H. Oxley, J.M. Blocher, Eds., John Wiley and Sons: New York, 1966

102. Evonik Industries. Basic characteristics of AEROSIL fumed silica; technical bulletin fine particles 11 [Online]. http://www.aerosil.com/sites/lists/IM/Documents/TB-11-Basic-Characteristicsof- AEROSIL-Fumed-Silica-EN.pdf (accessed July 26, 2016).

103. Cabot Corporation. General Guide: CAB-O-SIL Fumed silica and spectral fumed alumina [Online], Cabot Corporation: MA, 2011. http://cdn.inoxia.co.uk/documents/product-documents/ CabOSil-guide.pdf (accessed Mar 22, 2016).

104. J. Huang, K. Zhang, K. Wang, Z. Xie, B. Ladewig, H. Wang, Fabrication of polyethersulfone-mesoporous silica nanocomposite ultrafiltration membranes with antifouling properties, J Membr Sci, 2012, 423−424, 362.

105. C. Drummond, R. McCann, S.V. Patwardhan, A feasibility study of the biologically inspired green manufacturing of precipitated silica, Chem Eng J, 2014, 244, 483.

106. N.N. Greenwood, A. Earnshaw, Chemistry of the Elements (2nd ed.), Butterworth-Heinemann, 1997, ISBN 978-0-08-037941-8.

107. A.B.D. Nandiyanto, F. Iskandar, K. Okuyama, Nano-sized polymer particle-facilitated preparation of mesoporous silica particles using a spray method, Chem Lett, 2008, 37 (10), 1040.

108. B.G. Trewyn, A.J. Nieweg, Y. Zhao, L. Yannan, S.-Y.Victor, Biocompatible mesoporous silica nanoparticles with different morphologies for animal cell membrane penetration, Chem Eng J, 2007, 137 (1), 23.

109. N. Poulsen, A. Scheffel, V.C. Sheppard, P.M. Chesley, N. Kroger, Pentalysine clusters mediate silica targeting of silaffins in *Thalassiosira pseudonana*, J Biol Chem, 2013, 288, 20100.

110. M. Hildebrand, G. Holton, D.C. Joy, M.J. Doktycz, D.P. Allison, Diverse and conserved nano- and mesoscale structures of diatom silica revealed by atomic force microscopy, J Microsc, 2009, 235, 172.

111. M. Hildebrand, S. Kim, D. Shi, K. Scott, S. Subramaniam, 3D Imaging of diatoms with ion-abrasion scanning electron microscopy, J Struct Biol, 2009, 166, 316.

112. J. Aleman, A.V. Chadwick, J. He, M. Hess, K. Horie, R.G. Jones, P. Kratochvil, I. Meisel, I. Mita, G. Moad, Definitions of terms relating to the structure and processing of sols, gels, networks, and inorganic-organic hybrid materials, Pure Appl Chem, 2007, 79, 1801.

113. G. Kickelbick, Hybrid materials – past, present and future, hybrid mater, 2014, 1, 39.

114. J. Li, H. Wu, Y. Liang, Z. Jiang, Y. Jiang, L. Zhang, Facile fabrication of organic-inorganic hybrid beads by aminated alginate enabled gelation and biomimetic mineralization, J Biomater Sci-Polym E, 2013, 24, 119.

115. A. Jedrzak, T. Rebis, L. Klapiszewski, J. Zdarta, G. Milczarek, T. Jesionowski, Carbon paste electrode based on functional GOx/silica-lignin systemto prepare an amperometric glucose biosensor, Sens Actuators B, 2018, 256, 176.

116. J. Wen, G.L. Wilkes, Organic/inorganic hybrid network materials by the sol-gel approach, Chem Mater, 1996. 8(8), 1667.

117. D. Tian, P. Dubois, R. Jérôme, Biodegradable and biocompatible inorganic–organic hybrid materials. I. Synthesis and characterization, J Polym Sci A: Poly Chem, 1997, 35(11), 2295.

118. C.J. Brinker, G.W. Scherrer, Sol-Gel Science, 1990, San Diego: Academic Press.

119. Y. Yang, H. Yang, M. Yang, Y. Liu, G. Shen, R. Yu, Amperometric glucose biosensor based on a surface treated nanoporous ZrO2/Chitosan composite film as immobilization matrix, Anal Chim Acta, 2004, 525(2), 213.

120. D. Avnir, S. Braun, O. Lev, M. Ottolenghi, Enzymes and other proteins entrapped in sol-gel Materials, Chem Mater, 1994, 6, 1605.

121. S.F. Kim, R. B. John, L.W. James, Encapsulation of sulfate-reducing bacteria in a silica host, J Mater Chem, 2000, 10, 1099.

122. J.R. Premkumar, O. Lev, R. Rosen, S. Belkin, Encapsulation of luminous recombinant *E. coli* in sol-gel silicate films, Adv MateR, 2001, 13 (23), 1773.

123. A. Popat, S.B. Hartono, F. Stahr, J. Liu, S.Z. Qiao, G.Q. Lu, Mesoporous silica nanoparticles for bioadsorption, enzyme immobilization and delivery carriers, Nanoscale, 2011, 3, 2801.

124. J.F. Diaz, K.J. Balkus, Jr, Enzyme immobilization in MCM-41 molecular sieve, J Mol Catal B: Enzym, 1996, 2, 115.

125. D. Zhao, J. Feng, Q. Huo, N. Melosh, G.H. Frederickson, B.F. Chmelka, G.D. Stucky, Triblock copolymer syntheses of mesoporous silica with periodic 50 to 300 angstrom pores, Science, 1998, 279, 548.

126. J. Sun, H. Zhang, R. Tian, D. Ma, X. Bao, D.S. Su, H. Zou, Stimuli-responsive blue fluorescent supramolecular polymers based on a pillar [5] arene tetramer, Chem Commun, 2006, 1322.

127. J. Liu, C. Li, Q. Yang, J. Yang, C. Li, Morphological and structural evolution of mesoporous silicas in a mild buffer solution and lysozyme adsorption, Langmuir, 2007, 23, 7255.

128. C. Lei, Y. Shin, J. Liu, E. J. Ackerman, Entrapping enzyme in a functionalized nanoporous support, J Am Chem Soc, 2002, 124, 11242.

129. A.S.M. Chong, X.S. Zhao, Design of large-pore mesoporous materials for immobilization of penicillin G acylase biocatalyst, Catal Today, 2004, 93–95, 293.

130. S.B. Hartono, S.Z. Qiao, J. Liu, K. Jack, B.P. Ladewig, Z. Hao, G.Q.M. Lu, Functionalized mesoporous silica with very large pores for cellulase immobilization, J Phys Chem C, 2010, 114, 8353.

131. X.-Y. Yang, Z.-Q. Li, B. Liu, A. Klein-Hofmann, G. Tian, Y.-F. Feng, Y. Ding, D. Su, F.-S. Xiao, “Fish-in-Net” Encapsulation of Enzymes in Macroporous Cages as Stable, Reusable, and Active Heterogeneous Biocatalysts, Adv Mater, 2006, 18, 410.
132. I. Gill, A. Ballesteros, Encapsulation of biologicals within silicate, siloxane and hybrid sol-gel polymers: an efficient and generic Approach, J Am Chem Soc, 1998, 120, 8587.
133. C.D. Bakul, B. Dunn, J.S. Valentine, J.I. Zink, Sol-gel encapsulation methods for biosensors, Anal Chem, 1994, 66 (22),1120.
134. J. Wang, Sol–gel materials for electrochemical biosensors, Anal Chim Acta, 1999, 399, 21.
135. A. Coiffier, T. Coradin, C. Roux, O.M.M. Bouvet, J. Livage, Sol–gel encapsulation of bacteria: a comparison between alkoxide and aqueous routes, J Mater Chem, 2001, 11, 2039.
136. E.J.A. POPE, *Saccharomyces cerevisiae*-silica gel biocomposites, J Sol-Gel Sci Technol,1995, 4, 225.
137. N. Nassif, O. Bouvet, R.M. Noelle, C. Roux, T. Coradin, J. Livage, Living bacteria in silica gels, Nat Mater, 2002, 1 (1), 42.
138. O.N. Ponamoreva, O.A. Kamanina, V.A. Alferov, A.V. Machulin, T.V. Rogova, V.A. Arlyapov, S.V. Alferov, N.E. Suzina, E.P. Ivanova, Yeast based self organized hybrid bio-silica sol–gels for the design of biosensors, Biosens Bioelectro., 2015, 67, 321.
139. Y. Diana, J. Volponi, S. Chhabra, C.J. Brinker, A. Mulchandani, A.K. Singh, Aqueous sol–gel encapsulation of genetically engineered *Moraxella* spp. cells for the detection of organophosphates, Biosens Bioelectron, 2005, 20, 1433.
140. A. Mulchandani, S. Pan, W. Chen, Fiber-optic enzyme biosensor for direct determination of organophosphate nerve agents, Biotechnol Prog 1999, 15, 130.
141. K.R. Roger, Y. Wang, A. Mulchandani, P. Mulchandani, W. Chen, Organophosphorus hydrolase-based fluorescence assay for organophosphate pesticides, Biotechnol Prog, 1999, 15, 517.
142. J. Kumar, S.K. Jha, S.F. D’Souza, Optical microbial biosensor for detection of methyl parathion pesticide using *Flavobacterium* sp. whole cells adsorbed on glass fiber filters as disposable biocomponent, Biosens Bioelectron, 2006, 21, 2100.

143. J. Kumar, S.F. D'Souza, An optical microbial biosensor for detection of methyl parathion using *Sphingomonas sp.* immobilized on microplate as a reusable biocomponent, Biosens Bioelectron, 2010, 26, 1292.
144. J. Kumar, S.F. D'Souza, Immobilization of microbial cells on inner epidermis of onion bulb scale for biosensor application, Biosens Bioelectron, 2011b, 26 (11) 4399.
145. P. Michard, E. Guibal, T. Vincent, P.L. Cloirec, Sorption and desorption of uranyl ions by silica gel: pH, particle size and porosity effects, Micropor Mater,1996, 5 309.
146 T. Reicha, H. Molla, T. Arnolda, M.A. Deneckea, C. Henniga, G. Geipela, G. Bernharda, H. Nitschea, P.G. Allenb, J.J. Bucherb, N.M. Edelsteinb, D.K. Shuh, An EXAFS study of uranium(VI) sorption onto silica gel and ferrihydrite, J. Electron Spectrosc Relat Phenom, 1998, 96, 237.
147. P. Metilda, J.M. Gladis, T.P. Rao, Catechol functionalized aminopropyl silica gel: Synthesis, characterization and preconcentrative separation of uranium(VI) from thorium(IV), Radiochim Acta, 2005, 93, 219.
148. P.G. Krishna, J.M. Gladis, K.S. Rao, T.P. Rao, G.R.K. Naidu, Synthesis of xanthate functionalized silica gel and its application for the preconcentration and separation of uranium(VI) from inorganic components, J Radioanal Nucl Chem, 2005, 266 (2), 251.
149. U. Gabriel, L. Charlet, C.W. Schlapfer, J.C. Vial, A. Brachmann, G. Geipel, Uranyl Surface Speciation on Silica Particles Studied by Time-Resolved Laser-Induced Fluorescence Spectroscopy, J Colloid Interface Sci, 2001, 239, 358.
150. I. Sierra, D. Perez-Quintanilla, Heavy metal complexation on hybrid mesoporous silicas: an approach to analytical applications, Chem Soc Rev., 2013, 42, 3792.
151. X. Feng, G.E. Fryxell, L.Q. Wang, A.Y. Kim, J. Liu, K.M. Kemner, Functionalized monolayers on ordered mesoporous supports, Science, 1997, 276, 923.
152. L. Mercier, T.J. Pinnavaia, Access in mesoporous materials: advantages of a uniform pore structure in the design of a heavy metal ion adsorbent for environmental remediation, Adv Mater, 1997, 9, 500.
153. J. Liu, X. Feng, G.E. Fryxell, L.Q. Wang, A.Y. Kim, M. Gong, Hybrid mesoporous materials with functionalized monolayers, Adv Mater, 1998, 10, 161.

154. L. Mercier, T.J. Pinnavaia, Heavy metal ion adsorbents formed by the grafting of a thiol functionality to mesoporous silica molecular sieves: factors affecting Hg(II) uptake, Environ Sci Technol., 1998, 32, 2749.

155. E. Dana, Adsorption of heavy metals on functionalized-mesoporous silica: A review Micropor Mesopor Mater, 2017, 247, 145.

156. J. Aguado, J.M. Arsuaga, A. Arencibia, Influence of synthesis conditions on mercury adsorption capacity of propylthiol functionalized SBA-15 obtained by co-condensation, Micropor Mesopor Mater, 2008, 109, 513.

157. A. Walcarius, L. Mercier, Mesoporous organosilica adsorbents: nanoengineered materials for removal of organic and inorganic pollutants, J Mater Chem, 2010, 20, 4478.

158. M. Najafi, Y. Yousefi, A.A. Rafati, Sep Purif Technol, 2012, 85,193.

159. L.-Y. Yuan, Y.-L. Liu, W.-Q. Shi, Y.-L. Lv, J.-H. Lan, Y.-L. Zhao, Z.-F. Chai, High performance of phosphonate-functionalized mesoporous silica for U(VI) sorption from aqueous solution, Dalton Trans, 2011, 40, 7446.

160. S.R. Yousefia, S.J. Ahmadib, F. Shemirania, M.R. Jamalic, M. Salavati-Niasari, Simultaneous extraction and preconcentration of uranium and thorium in aqueous samples by new modified mesoporous silica prior to inductively coupled plasma optical emission spectrometry determination, Talanta, 2009, 80, 212.

161. H.I. Lee, J.H. Kim, J.M. Kim, S. Kim, J.-N. Park, J.S. Hwang, J.-W. Yeon, Y. Jung, J Nanosci Nanotechnol, 2010, 10, 217.

162. L. Wang, W. Zhao, W. Tan, Bioconjugated silica nanoparticles: development and applications, Nano Res, 2008, 1 (99), 115.

163. M. Vallet-Regi, A. Rámila, R.P. del Real, J. Pérez-Pariente, A new property of MCM-41: drug delivery system, Chem Mater, 2001, 13, 308.

164. K.S. Butler, P.N. Durfee, C. Theron, CE. Ashley, E.C. Carnes, C.J. Brinker, Protocells: modular mesoporous silica nanoparticle-supported lipid bilayers for drug delivery, Small, 2016, 12, 2173.

165. Y. Yang, C. Yu, Advances in silica based nanoparticles for targeted cancer therapy, Nanomedicine, 2016, 12, 317.

166. S. Baek, R.K. Singh, D. Khanal, K.D. Patel, E.-J. Lee, K.W. Leong, W. Chrzanowski, H.-W. Kim, Smart multifunctional drug delivery towards anticancer therapy harmonized in mesoporous nanoparticles, Nanoscale, 2015, 7, 14191.

167. S. Alberti, G.J.A.A. Soler-Illia, O. Azzaroni, Gated supramolecular chemistry in hybrid mesoporous silica nanoarchitectures: Controlled delivery and molecular transport in response to chemical, physical and biological stimuli, Chem Commun, 2015, 51, 6050.

168. Y. Wang, Q. Zhao, N. Han, L. Bai, J. Li, J. Liu, E. Che, L. Hu, Q. Zhang, T. Jiang, Mesoporous silica nanoparticles in drug delivery and biomedical applications, Nanomedicine, 2015, 11, 313.

169. I. Roy, T.Y. Ohulchanskyy, H.E. Pudavar, E.J. Bergey, A.R. Oseroff, J. Morgan, T.J. Dougherty, P.N. Prasad, Ceramic-based nanoparticles entrapping water-insoluble photosensitizing anticancer drugs: A novel drug-carrier system for photodynamic therapy, J Am Chem Soc, 2003, 125, 7860.

170. C.Y. Lai, B.G. Trewyn, D.M. Jeftinija, K. Jeftinija, S. Xu, S. Jeftinija, V.S.A. Lin, Mesoporous silica nanospherebased carrier system with chemically removable CdS nanoparticle caps for stimuli-responsive controlled release of neurotransmitters and drug molecules, J Am Chem Soc, 2003, 125, 4451.

171. K.-N. Yang, C.-Q. Zhang, W. Wang, P.C. Wang, J.-P. Zhou, X.-J. Liang, pH-responsive mesoporous silica nanoparticles employed in controlled drug delivery systems for cancer treatment, Cancer Biol Med, 2014, 11, 34.

172. Y. Tian, A. Glogowska, W. Zhong, T. Klonisch, M. Xing, Polymeric mesoporous silica nanoparticles as a pH-responsive switch to control doxorubicin intracellular delivery, J Mater Chem B, 2013, 1, 5264.

173. M. Vallet-Regí, M. Colilla, I. Izquierdo-Barba, M. Manzano, Mesoporous silica nanoparticles for drug delivery: current insights, Molecules, 2018, 23(47), 1-19.

174. J.S. Melo, S.F. D'souza, G.B. Nadkarni, *Ocimum basilicum* seeds as a pellicular support for immobilizing enzymes, Biotechnol Lett, 1986, 8 (12), 885.

175. J.S. Melo, S.F. D'souza, Immobilization of invertase through its carbohydrate moiety on *Ocimum basilicum* seed, Appl Biochem Biotechnol, 32 (1992) 159-170.

176. J.S. Melo, S.F. D'Souza, Removal of chromium by mucilaginous seeds of *Ocimum basilicum*, Bioresour Technol, 2004, 92, 151.

177. M. Biswal, K. Bhardwaj, P.K. Singh, P. Singh, P. Yadav, A. Prabhune, C. Rode, S. Ogale, Nanoparticle-loaded multifunctional natural seed gel bits for efficient water purification, RSC Adv, 2013, 3, 2288.

178. F. Hoffmann, M. Cornelius, J. Morell, M. Froba, Silica-based mesoporous organic–inorganic hybrid materials, Angew Chem Int Ed, 2006, 45, 3216.

179. D. Sen, S. Mazumder, J.S. Melo, A. Khan, S. Bhattyacharya, S.F. D'Souza, Evaporation driven self-assembly of a colloidal dispersion during spray drying: volume fraction dependent morphological transition, Langmuir, 2009, 25, 6690.

180. V. Polshettiwar, D. Cha, X. Zhang, J.M. Basset, High-surface-area silica nanospheres (KCC-1) with a fibrous morphology, Angew Chem Int Ed, 2010, 49, 9652.

181. D. Sen, J.S. Melo, J. Bahadur, S. Mazumder, S. Bhattacharya, S.F. D'Souza, H. Frielinghaus, G. Goerigk, R. Loidl, Arrest of morphological transformation during evaporation-induced self-assembly of mixed colloids in micrometric droplets by charge tuning, Soft Matter, 2011, 7, 5423.

182. J.S. Melo, D. Sen, S. Mazumder, S.F. D'Souza, Spray drying as a novel technique for obtaining microbial imprinted microspheres and its application in filtration, Soft Matter, 2013, 9, 805.

183. A. Mishra, J.S. Melo, D. Sen, S.F. D'Souza, Evaporation induced self assembled microstructures of silica nanoparticles and *Streptococcus lactis* cells as sorbent for uranium (VI), J Colloid Interface Sci, 2014, 414, 33.

184. P.G. Cadena, R.A.S. Jeronimo, J.M. Melo, R.A. Silva, J.L. Lima Filho, M.C.B. Pimentel, Covalent immobilization of invertase on polyurethane, plast-film and ferromagnetic Dacron, Bioresour Technol, 2010, 101, 1595.

185. A.R. Nesic, M.J. Kokunesoski, S.M. Ilic, M.V. Gordic, S.B. Ostojic, D.M. Micic, S.J. Velickovic, Biocomposite membranes of highly methylated pectin and mesoporous silica SBA-15, Composites: Part B, 2014, 64, 162.

186. J.S. Pedersen, Determination of size distributions from small angle scattering data for systems with effective hard-sphere interactions, J Appl Crystallogr, 1994, 27, 595.

187. S. Liang, X. Guo, N. Feng, Q. Tian. Isotherms, kinetics and thermodynamic studies of adsorption of Cu_2 from aqueous solutions by Mg^{2+}/K^+ type orange peel adsorbents, J Hazard Mater, 2010, 174, 756.
188. N. Carlsson, H. Gustafsson, C. Thorn, L. Olsson, K. Holmberg, B. Åkerman, Enzymes immobilized in mesoporous silica: a physical–chemical perspective, Adv Colloid Interface Sci, 2014, 205, 339.
189. Y. Wang, F. Caruso, Mesoporous silica spheres as supports for enzyme immobilization and encapsulation, Chem Mater, 2005, 17, 953.
190. G.A. Petkova, K. Záruba, V. Kral, Synthesis of silica particles and their application as supports for alcohol dehydrogenases and cofactor immobilizations: conformational changes that lead to switch in enzyme stereoselectivity, Biochim Biophys Acta, 2012, 1824, 792.
191. J. Song, H. Kong, J. Jang, Adsorption of heavy metal ions from aqueous solution by polyrhodanine-encapsulated magnetic nanoparticles, J Colloid Interface Sci, 2011, 359, 505.
192. G. Bayramoglu, S. Akgol, A. Bulut, A. Denizli, M.Y. Arıca, Covalent immobilisation of invertase onto a reactive film composed of 2-hydroxyethyl methacrylate and glycidyl methacrylate: properties and application in a continuous flow system, Biochem Eng J, 2003, 14 (2), 117.
193. S.F. D'Souza, J.S. Melo, Immobilization of bakers yeast on jute fabric through adhesion using polyethylenimine: application in an annular column reactor for the inversion of sucrose, Process Biochem, 2001, 36, 677.
194. Y.E.T. Chen, K.G. Kang, K.L. Neoh, Covalent immobilization of invertase onto the surface-modified polyaniline from graft copolymerization with acrylic acid, Eur Polym J, 2000, 36 (10), 2095.
195. T. Bahar, A. Tuncel, Immobilization of invertase onto crosslinked poly(pchloromethylstyrene) beads, J Appl Polym Sci, 2002, 83, 1268.
196. M.Y. Arıca, G. Bayramoglu, Invertase reversibly immobilized onto polyethylenimine-grafted poly(GMA–MMA) beads for sucrose hydrolysis, J Mole Catal B Enzym, 2006, 38, 131.

197. M.Y. Arica, G. Bayramoglu, N. Bıcak, Characterization of immobilized tyrosinase onto spacer-arm attached glycidyl methacrylate based reactive microbead, Process Biochem, 2004, 39, 2007.

198. S. Akgol, Y. Kacar, A. Denizli, M.Y. Arıca, Hydrolysis of sucrose by invertase immobilized onto novel magnetic polyvinylalcohol microspheres, Food Chem, 2001, 74 (3), 281.

199. T. Danisman, S. Tan, Y. Kacar, A. Ergene, Covalent immobilization of invertase on microporous pHEMA-GMA membrane. Food Chem, 2004, 85 (3), 461.

200. J.J. Karimpil, J.S. Melo, S.F. D'Souza, Hen egg white as a feeder protein for lipase immobilization, J Mol Catal B Enzym, 2011, 71, 113.

201. FAO/WHO 1986, Codex Maximum Limits for pesticide residues. Codex Alimentarius Commission CAC/Vol. XIII. 3rd ed. Rome, Food and Agriculture Organization of the United Nations.

202. FSSAI 2011, Food safety and standards (contaminants, toxins and residues) regulations:http://www.fssai.gov.in/Portals/0/Pdf/Food%20safety%20and%20standards%20%28contaminats,%20toxins%20and%20residues%29%20regulation,%202011.pdf

203. FSSAI 2016. Fixation of MRLs for Pesticide Residues in Processed Foods: Modalities http://fssai.gov.in/Portals/0/Pdf/Fixation_MRLs_Pesticide_Residues_Processed_foods_03_02_2016.pdf

204. A. Mulchandani, W. Chen, P. Mulchandani, J. Wang, K.R. Rogers, Biosensors for direct determination of organophosphate pesticides, Biosens Bioelectron, 2001, 16, 225.

205. W. Lan, G. Chen, F. Cui, F. Tan, R. Liu, M. Yushupujiang, Development of a novel optical biosensor for detection of organophoshorus resticides based on methyl parathion hydrolase immobilized by metal-chelate affinity, Sensors, 2012, 12 (7), 8477206.

206. S. Chen, J. Huang, D. Dua, J. Li, H. Tu, D. Liu, A. Zhang, Methyl parathion hydrolase based nanocomposite biosensors for highly sensitive and selective determination of methyl parathion, Biosens Bioelectron, 2011, 26 (11), 4320.

207. J. Kumar, J.S. Melo, Microbial biosensors for methyl parathion: From single to multiple samples analysis, Advances in Biosensors Research, Nova Science Publishers, 2015, 89-112, ISBN: 978-1-63463-652-0.

208. J. Kumar, S.F. D'Souza, Microbial biosensor for detection of methyl parathion using screen printed carbon electrode and cyclic voltammetry, Biosens Bioelectron, 2011a, 26 (11) 4289.

209. A.S. Saini, J. Kumar, J.S. Melo, Microplate based optical biosensor for L-Dopa using tyrosinase from Amorphophallus campanulatus, Anal Chim Acta, 2014, 849, 50.

210. A.P.F. Turner, I. Karube, G.S. Wilson, (Eds.), Biosensors fundamentals and applications. Oxford University Press, Oxford, UK, 1987.

211. J.S. Melo, S.F. D'Souza, Simultaneous filtration and immobilization of cells from a flowing suspension using a bioreactor containing polyethylenimine coated cotton threads: Application in the continuous inversion of concentrated sucrose syrups, World J Microbiol Biotechnol, 1999, 15 (1), 17.

212. J. Kumar, S.F. D'Souza, Inner epidermis of onion bulb scale: As natural support for immobilization of glucose oxidase and its application in dissolved oxygen based biosensor, Biosens Bioelectron, 2009, 24, 1792.

213. J.J. Karimpil, J.S. Melo, S.F. D'Souza, Immobilization of lipase on cotton cloth using the layer-by-layer self-assembly technique, Int J Biol Macromol, 2012, 50 (1) 300.

214. J. A. Ryan, The evolution of cell culture surfaces, Biofiles, 2008, 3 (8), 21.

215. C.E. Hamm, R. Merkel, O. Springer, P. Jurkojc, C. Maier, K. Prechtel, V. Smetacek, Architecture and material properties of diatom shells provide effective mechanical protection, Nature, 2003, 421 (6925), 841.

216. P. Sar, S.K. Kazy, S.F. D'Souza, Radionuclide remediation using a bacterial biosorbent, Int Biodeter Biodegr, 2004, 54, 193.

217. K.C. Bhainsa, S.F. D'Souza, Biosorption of uranium(VI) by Aspergillus fumigates, Biotechnol Tech, 1999, 13, 695.

218. P. Sar, S.F. D'Souza, Biosorptive uranium uptake by a Pseudomonas strain: characterization and equilibrium studies, J Chem Technol Biot, 2001, 76, 1286.

219. P. Sar, S.F. D'Souza, Biosorption of thorium (IV) by a Pseudomonas biomass, Biotechnol Lett, 2002, 24, 239.

220. S.K. Kazy, S.F. D'Souza, P. Sar, Uranium and thorium sequestration by a *Pseudomonas* sp., Mechanism and chemical characterization, J Hazard Mater, 2009, 163, 65.

221. M.L. Merroun, J. Raff, A. Rossberg, C. Hennig, T. Reich, S. Selenska-Pobell, Complexation of uranium by cells and S-layer sheets of *Bacillus sphaericus* JG-A12, Appl Environ Microbiol, 2005, 71(9), 5532.

222. J.-S. Wang, X.-J. Hu, Y.-G. Liu, S.-B. Xie, Z.-L. Bao, Biosorption of uranium (VI) by immobilized Aspergillus fumigatus beads, J Environ Radioactiv, 2010, 101, 504.

223. S. Xie, J. Yang, C. Chen, X. Zhang, Q. Wang, C. Zhang, Study on biosorption kinetics and thermodynamics of uranium by *Citrobacter freudii*, J Environ Radioact, 2008, 99, 126.

224. Y. Yao, S. Miao, S. Yu, L.P. Ma, H. Sun, S. Wang, Formation and characterization of natural polysaccharide hollow nanocapsules via template layer-by-layer self-assembly, J Colloid Interface Sci, 2012, 379, 20.

225. E.-J. Lee, D.-S. Shin, H -E. Kim, H.-W. Kim, Y.-H. Koh, J.-H. Jang, Membrane of hybrid chitosan–silica xerogel for guided bone regeneration, Biomaterials, 2009, 30, 743.

226. Z. Filip, S. Hermann, K. Demnerova, FT-IR Spectroscopic characteristics of differently cultivated *Escherichia coli*, Czech J Food Sci, 2008, 26, 458.

227. A. Beganskiene,V. Sirutkaitis, M. Kurtinaitiene, R. Juskenas, A. Kareiva, FTIR, TEM and NMR Iinvestigations of Stöber Silica Nanoparticles, J Mater Sci, 2004, 10, 1392.

228. S.V. Bhat, J.S. Melo, B.B. Chaugule, S.F. D'Souza, Biosorption characterstics of uranium(VI) from aqueous medium onto *Catenella repens*, a red alga, J Hazard Mater, 2008, 158, 628.

229. S. Saxena, M. Prasad, S.F. D'Souza, Radiionuclide sorption onto low-cost mineral adsorbent, Ind Eng Chem Res, 2006, 45, 9122.

230. I. Langmuir, The adsorption of gasses on plane surfaces of glass, mica and platinum, J Am Chem Soc, 1981, 40, 1361.

231. Z. Ghasemi, A. Seif, T.S. Ahmadi, B. Zargar, F. Rashidi, G.M. Rouzbahani, Thermodynamic and kinetic studies for the adsorption of Hg(II) by nano-TiO_2 from aqueous solution, Adv Powder Technol, 2012, 23, 148.

232. P.N. Pathak, G.R. Choppin, Kinetics and thermodynamics of U(VI)(VI) sorption on hydrous silica, Radiochim. Acta, 2007, 98, 507.

233. Y.-T. Liao, C.-H. Liu, J. Yu, K. C-W Wu, Liver cancer cells: targeting and prolonged-release drug carriers consisting of mesoporous silica nanoparticles and alginate microspheres, International Journal of Nanomedicine, 2014, 9, 2767.

234. L. Hu, C. Sun, A. Song, D. Chang, X. Zheng, Y. Gao, T. Jiang, S. Wang, Alginate encapsulated mesoporous silica nanospheres as a sustained drug delivery system for the poorly water-soluble drug indomethacin, Asian J Pharma Scien, 2014, 9, 183.

235. M. George, T.E. Abraham, Polyionic hydrocolloids for the intestinal delivery of protein drugs: alginate and chitosan – a review. J Control Release, 2006, 114(1), 1.

236. H.H. Tonnesen, J. Karlsen, Alginate in drug delivery systems. Drug Dev Ind Pharm, 2002, 28(6), 621.

237. P. Rajesh, G. Khuller, Alginate as a drug delivery carrier. In: Yarema KJ, editor. Handbook of carbohydrate engineering. Boca Raton, FL: CRC Press; 2005, 799.

238. X. Ma, B. Zhou, Study on $CaCO_3$/PMMA nanocomposite microspheres by soapless emulsion polymerization, Colloid Surf A: Physicochem Eng Aspects, 2008, 312(2–3), 190.

239. Y. Yang, X. Kong, C. Kan, C. Sun, Encapsulation of calcium carbonate by styrene polymerization. Polym Adv Technol, 1999, 10, 54.

240. I. Tissot, C. Novat, F. Lefebvre, E. Bourgeat-Lami, Hybrid latex particles coated with silica. Macromolecules, 2001, 34, 5737.

241.A. Mishra, J. Kumar, J.S. Melo, An optical microplate biosensor for the detection of methyl parathion pesticide using a biohybrid of *Sphingomonas sp.* cells-silica nanoparticles, Biosens Bioelectron, 2017, 87.

242. H. Daemi, M. Barikani, Synthesis and characterization of calcium alginate nanoparticles, sodium homopolymannuronate salt and its calcium nanoparticles, Scientia Iranica F, 2012, 19 (6), 2023.

243. S. Jianga, L. Hua, Z. Guo, L. Sun, One-pot green synthesis of doxorubicin loaded-silica nanoparticles for in vivo cancer therapy, Mater Sci Eng C, 2018, 90, 257.

244. X. He, L. Hai, J. Su, K. Wang, X. Wu, One-pot synthesis of sustained-released doxorubicin silica nanoparticles for aptamer targeted delivery to tumor cells, Nano, 2011, 3, 2936.

245. L.F. Dalmolin, N.M. Khalil, R.M. Mainardes, Delivery of vanillin by poly(lactic-acid) nanoparticles: development, characterization and in vitro evaluation of antioxidant activity, Mater Sci Eng C Mater Biol Appl, 2016, 62, 1.
246. M. Li, Z. Tang, D. Zhang, H. Sun, H. Liu, Y. Zhang, Doxorubicin-loaded polysaccharide nanoparticles suppress the growth of murine colorectal carcinoma and inhibit the metastasis of murine mammary carcinoma in rodent models, Biomaterials, 2015, 51, 161.
247. P. Kortesuo, M. Ahola, I. Kangasniemi, U.A. Yli, J. Kiesvaara, Silica xerogel as an implantable carrier for controlled drug delivery–evaluation of drug distribution and tissue effects after implantation, Biomaterials, 2000, 21, 193.

Reprints of Publication